Cyclophilin A and serine proteases –

Targets of neuronal cell death upstream of mitochondrial demise

Dissertation

zur

Erlangung des Doktorgrades

der Naturwissenschaften

(Dr. rer. nat.)

dem

Fachbereich Pharmazie der

Philipps-Universität Marburg

vorgelegt von

Christina Reuther

aus Prien am Chiemsee

Marburg/Lahn 2014

Erstgutachter: Prof. Dr. Carsten Culmsee

Zweitgutachter: Prof. Dr. Nikolaus Plesnila

Eingereicht am 14.05.2014

Tag der mündlichen Prüfung am 25.06.2014

Hochschulkennziffer: 1180

Meinen Eltern und Großeltern

ERKLÄRUNG

Ich versichere, dass ich meine Dissertation

„Cyclophilin A and serine proteases – Targets of neuronal cell death upstream of mitochondrial demise“

selbständig ohne unerlaubte Hilfe angefertigt und mich dabei keiner anderen als der von mir ausdrücklich bezeichneten Quellen bedient habe. Alle vollständig oder sinngemäß übernommenen Zitate als solche gekennzeichnet.

Die Dissertation wurde in der jetzigen oder einer ähnlichen Form noch bei keiner anderen Hochschule eingereicht und hat noch keinen sonstigen Prüfungszwecken gedient.

Marburg, den 14.05.2014

.....

(Christina Reuther)

Table of contents

1. Introduction

1.1. Cell death pathways in neurons

Programmed cell death (PCD) is a highly conserved cell death mechanism essential for various physiological processes such as maintenance of embryonic development, tissue homeostasis and removal of injured cells. Many studies detected the paradigm of PCD in neurodegenerative diseases such as Alzheimer's disease (AD), Parkinson's disease (PD) or Huntington's disease (HD) and after acute brain damage, e.g. caused by cerebral ischemia or traumatic brain injury [1–3]. The term PCD is a very broad expression and consists of various classifications of different modes of cell death [4]. The best characterized type of PCD is apoptosis, which was first described by Kerr et al. and occurs during tissue development and regulates the replacement of senescent and impaired cells. Typical hallmarks associated with apoptosis are DNA condensation (pyknosis) and fragmentation, membrane blebbing and the formation of apoptotic bodies [5]. However, today the term apoptosis can also be subdivided into different categories, related to cell death stimuli and biochemical features, namely 'extrinsic apoptosis' and caspase-dependent or caspase-independent 'intrinsic apoptosis' [4]. Extrinsic apoptosis bypasses the mitochondria and is induced by extracellular stress stimuli, which bind to transmembrane receptors and thereby initiate the ensuing cell death cascade. Various ligands mediate extrinsic apoptosis, such as FAS/CD95 ligand (FASL), tumor necrosis factor α (TNFα) and TNF-related apoptosis inducing ligand (TRAIL), by binding to their corresponding death receptors FAS/CD95, TNFα receptor 1 (TNFR1) and TRAIL receptor (TRAILR) 1-2 [6,7] (reviewed in [8]). Ligand binding induces the generation and stabilization of death receptor oligomers, which leads to conformational changes at the cytosolic tail of the receptors resulting in the formation of death domains (DD). This leads to the recruitment of different adaptor proteins, such as Fas-associated death domain (FADD) or TNF receptor-associated death domain (TRADD), connecting the receptor signaling to the apoptotic machinery [9]. FADD contains a death effector domain (DED) which facilitates the subsequent binding of DED of procaspase-8 (-10). The assembly of activated receptor, FADD and the procaspases is commonly known as death-inducing signaling complex (DISC), which is a platform for caspase activation [10,11]. Caspase-8 (-10) activation can directly trigger the caspase cascade by proteolytic maturation of the effector

caspase caspase-3, which accordingly releases the caspase-activated deoxyribonuclease (CAD) from its inhibitor (ICAD) and translocates to the nucleus where it induces DNA fragmentation and cell death [12–14]. Another important function of activated caspase-8 is the cleavage of the pro-apoptotic B-cell-lymphoma-2 (Bcl2) protein Bid (Bcl2 interacting domain death antagonist) to its active form (truncated Bid, tBid), which links the extrinsic to the intrinsic apoptotic pathway, where mitochondria engage the central role of the apoptotic process [4,15].

In neurons, the intrinsic apoptotic pathway occurs triggered by neurotrophic factor withdrawal, increased oxidative stress or overactivation of glutamate receptors. These apoptotic stimuli are linked to mitochondrial damage and are associated with diverse neurological disorders [2,16,17]. They trigger an intricate series of molecular and biochemical mechanisms leading to impaired neurological function. These complex mechanisms involve the activation of calcium/calmodulin-dependent kinases (CaMKs) and mitogen-activated protein kinases (MAPKs), such as extracellular signal-regulated kinase (ERK), p38, and c-Jun N-terminal kinase (JNK), leading to altered gene expression which is important for cell survival or damaging mechanisms. Transcription factors like the tumor suppressor p53 contribute to the recruitment of pro-apoptotic Bcl2 family proteins, Bcl2-associated x protein (Bax) and Bcl2 antagonist killer 1 (Bak), to the mitochondria where they induce mitochondrial outer membrane (MOM) permeabilization and as a result pore formation. The generation of large permeability transition pores (PTP) results in the release of pro-apoptotic proteins from the mitochondrial intermembrane space (IMS) to the cytosol, such as cytochrom c (Cytc), apoptosis-inducing-factor (AIF), endonuclease G (EndoG), high temperature acquired protein A2 (Omi/HrtA2) or second mitochondria-derived activator of caspases (Smac/Diablo). The release of Cytc leads to the apoptosome formation which includes the apoptosis-protease activating factor (Apaf1) and dATP leading to the recruitment and activation of caspase-9, which in turn activates caspase-3. X-chromosomal linked inhibitor of apoptosis (XIAP) and other inhibitors of apoptosis (IAP), which are known to be potent direct inhibitors of caspases, are inactivated by Omi/HtrA2 and Smac/Diablo, leading to cell death [18–23].

Emerging evidence suggests that besides the well-established caspase-dependent pathway of PCD, the caspase-independent pathway plays an important role, especially in the adult brain. This intrinsic cell death pathway is mediated by

mitochondrial alterations including energy depletion, ROS formation and opening of the PTP, resulting in the release of AIF and EndoG from the mitochondrial IMS, followed by their translocation to the nucleus where they induce large scale chromatin condensation and DNA fragmentation [24–26]. Triggers of such caspase-independent cell death pathways in neurons are for instance glucose deprivation or reduced oxygen levels which occur e.g. after cerebral ischemia. This leads to energy depletion and ensuing to the depolarization of membranes resulting in the activation of voltage-dependent Ca^{2+}-channels. Excitatory amino acids are released into the extracellular space which activate ionotropic glutamate receptors like N-methyl-D-aspartate- (NMDA), 2-amin-3-(3-hydroxy-5-methylisoxazol-4-yl) propionate (AMPA) or kainate receptors. This receptor overactivation leads to an elevated Ca^{2+}-influx followed by mitochondrial dysfunction and the subsequent release of pro-apoptotic factors from the mitochondrial IMS [27]. All these mechanisms place mitochondria in the center of apoptotic cell death pathways, which are the underlying cause for neuronal dysfunction and death in many neurodegenerative disorders.

1.2. Mitochondria in neuronal cell death

Mitochondria are semi-autonomous organelles containing their own mitochondrial DNA (mtDNA), RNA and protein synthesis machinery. Depending on different physiological conditions, mitochondrial fission and fusion processes can lead to elongated, tubular-like mitochondria, which build an interconnected network, or to small spheres which are associated with enhanced mitochondrial fission. Recent evidence suggests that mitochondrial fission and fusion processes are linked to mitochondrial distribution, to mitochondrial metabolism and mitochondrial function [28]. Mitochondria consist of an outer membrane (MOM), the IMS, the mitochondrial inner membrane (MIM), where the complexes I, III, IV and V of the electron transport chain (ETC) are localized, and the matrix, where the tricarboxylic acid cycle (TCA cycle) takes place to provide reducing equivalents ($NADH/H^+$ and $FADH_2$) for oxidative phosphorylation (Oxphos) and subsequent ATP production. The most prominent role of mitochondria is the generation of energy in form of ATP. Electrons donated from the reducing equivalents are transported through the ETC to finally reduce ½ O_2 to hydrogen peroxide (H_2O_2). The released energy is used to pump protons into the IMS through complex I, III and IV, thereby creating an electrochemical gradient which is

coupled to ATP synthesis by complex V. The mitochondrial oxygen consumption rate is hence increased when a lot of ATP is produced [28–31]. Besides the ability to generate ATP, mitochondria are the major source of endogenous ROS levels, which include superoxide (O_2^-), H_2O_2 and hydroxyl free radical ($^{\cdot}OH$) [29,32]. The hydroxyl radical is highly reactive and can induce DNA, protein and lipid damage [33]. These toxic by-products of Oxphos are neutralized by the antioxidant defense, which contains besides non-enzymatic antioxidants like ascorbic acid or tocopherols, antioxidant enzymes, such as superoxide dismutases, catalases and glutathione peroxidases [34]. The imbalance of ROS generation and detoxifying mechanisms can cause mitochondrial membrane permeabilization and the impairment of the MMP, because in this case mitochondria are subjected directly to large amounts of ROS and might therefore be particular susceptible for oxidative stress [33]. In addition to elevated ROS levels, mitochondrial dysfunction can be caused by increased Ca^{2+}-levels or the activation of pro-apoptotic Bcl2 family members [35]. The Bcl2 family is subdivided in two groups on the basis of their pro- or anti-apoptotic function. Anti-apoptotic Bcl2-like proteins are for instance Bcl2, Bcl_{xL} or Mcl1, while pro-apoptotic 'multi-domain' proteins include Bax and Bak, and 'BH3-only' proteins include Bid, Bad and Bim [36]. From the pro-apoptotic family members, Bax and Bak are the main mediators of MOM permeabilization in response to many apoptotic stimuli, as cells lacking Bax and Bak fail to undergo MOM permeabilization and apoptosis [37]. At least two of the BH3-only proteins, namely Bid and Bim, are able to activate Bax and Bak. The active form of Bid (tBid) promotes the oligomerization of Bax and Bak at the MOM and thereby induces Cytc release and cell death. Similar evidence exists for Bim-mediated Bax/Bak activation and subsequent MOM permeabilization [38]. However, Bid is also capable of mediating mitochondrial demise independent of Bax and Bak through pore formation in the mitochondrial membrane due to tBid oligomerization [39].

Especially in neurons, which are rarely renewed, mitochondrial abnormalities cause severe neuronal dysfunction. Defects in mitochondrial function are linked to a variety of neurodegenerative diseases, such as PD, AD or amyotrophic lateral sclerosis (ALS). Also dominant optic atrophy (DOA) which is an optic neuropathy characterized by optic nerves degeneration and Charcot-Marie-Tooth 2A disease (CMT2A) which is a peripheral sensorimotor neuropathy characterized by motor deficits are consequences of elevated mitochondrial fission or attenuation of mitochondrial fusion

[30,40,41]. The impairment of the mitochondrial network, which may occur by excessive mitochondrial fission and a lack of fusion, leads to the loss of mtDNA, respiratory defects, and the generation of detrimental ROS levels [42]. Numerous proteins mediate mitochondrial fission and fusion processes and defects in this regulation are associated with mitochondrial dysfunction and afore mentioned diseases. Mitochondrial fission is mainly mediated by dynamin-related protein 1 (Drp1) and mitochondrial fission 1 protein (Fis1) [43,44], while mitochondrial fusion is under control of mitofusin 1 and 2 (Mfn1, Mfn2) and optical atrophy 1 (Opa1) [45]. Mutations in human Drp1 can cause early infant mortality, and mutations in Mfn2 and Opa1 can cause CMT2A or DOA, respectively [46].

Mitochondrial organization and distribution in cells corresponds in some extent to the cytoplasmic tubular network as the interaction of the cytoskeleton and the mitochondria was demonstrated [47]. Furthermore, the actin cytoskeleton is involved in the movement and positioning of mitochondria and in mitochondrial fission [48]. As mentioned above, Drp1 is one of the major regulators of mitochondrial fission and its activity and translocation to the mitochondria is under control of different triggers. For instance, the work of De Vos et al. revealed that the F-actin cytoskeleton is involved in the recruitment of Drp1 to the mitochondria. Disruption of the F-actin network attenuated the redistribution of Drp1 to the mitochondria and thereby prevented mitochondrial fission [49]. Mitochondrial shape changes due to Drp1 redistribution from the cytosol to the mitochondria are controlled by the phosphorylation status of Drp1 at two different serine residues. Phosphorylation at Ser616 by cyclin-dependent kinase 1 (Cdk1) promotes mitochondrial fission [50] whereas dephosphorylation of Drp1 at Ser637 by the Ca^{2+}-dependent phosphates calcineurin regulates the translocation to the mitochondria and promotes mitochondrial fission leading to cell death [51,52]. A polypeptide antagonist of calcineurin was discovered as a potent inhibitor of Drp1-dependent mitochondrial fragmentation. The polypeptide PPD1, which corresponds to the peptidyl-prolyl isomerase domain of FKBP52, inhibits calcineurin activation and thus dephosphorylation of Drp1 at Ser637 and thereby prevents cell death at the level of mitochondria [53]. These findings depict a pivotal role of calcineurin and the F-actin cytoskeleton for the activation/redistribution of Drp1 and the subsequent mitochondrial fragmentation. In this study, the interaction of Drp1 and actin, the translocation to the mitochondria and the involvement of calcineurin in

conditions of glutamate-induced cell death in HT22 cells were a major focus of investigation.

1.2.1. The role of AIF in life and death of neurons

AIF is a flavoprotein which is encoded in the nucleus and synthesized in the cytoplasm as a ~67 kDa precursor protein. Murine AIF is organized in three domains: (i) an amino-terminal mitochondrial localization sequence (MLS) of 100 amino acids (aa), (ii) a spacer sequence (aa 101-121), a FAD-binding domain (aa 122-262 and 400-477), a NADH-binding domain (aa 263-399) with two nuclear leading sequences (NLS) and (iii) a carboxy-terminal which consist of 136 amino acids. After the import of AIF in the mitochondrial IMS, MLS is proteolytically removed resulting in the ~62 kDa mature form, which changes its configuration incorporating FAD and anchoring in the MIM [54–57]. Upon induction of apoptosis AIF is cleaved into a ~57 kDa truncated protein (tAIF), which translocates to the nucleus and induces DNA fragmentation and large scale (~50 bp) chromatin condensation. The interaction of AIF with DNA is sequence-independent but is due to a strong positive electrostatic potential [58,59]. Since AIF lacks nuclease activity to degrade DNA [60], the particular mechanism of DNA fragmentation is still elusive. However, recent reports suggested that proteins which exhibit nuclease activity are involved in AIF-mediated DNA fragmentation. For example, in human cells cyclophilin A (CypA) was discovered as a direct binding partner of AIF, which exhibits a latent, Ca^{2+}-dependent nuclease activity [61,62]. Since both proteins alone are not able to induce DNA degradation it has been proposed that the direct interaction of AIF and CypA is necessary to induce chromatinolysis [62]. More recent findings showed, however, that the histone H2AX is a further essential component of the AIF/CypA-containing DNA-degrading complex. H2AX is a member of the histone H2A family and is a sensitive marker for DNA double strand breaks (DSBs). The phosphorylation of H2AX at Ser139 residue following DSBs is the critical step for the interaction with AIF and the formation of the DNA-degrading complex [63,64].

While in some models of cell death the mitochondrial AIF release is caspase-dependent [65], AIF release occurs in a caspase-independent manner in several important paradigms of PCD. For instance, DNA damage is linked to mitochondrial AIF release through activation of p53 [24] or via Poly (ADP-Ribose) Polymerase 1 (PARP1)-mediated pathways (Parthanatos) [66–68]. DNA strand breaks

trigger the activation of PARP1 which leads to the depletion of mitochondrial nicotinamide adenine dinucleotide (NAD+) and ATP, and subsequently to cell death, which could be prevented by PARP1 inhibitors or genetic knockout of PARP1 [66]. Further, it was demonstrated that proteases, such as the Ca^{2+}-activated calpain I, induce AIF truncation and the subsequent release from isolated mitochondria [69]. In addition, the pro-apoptotic protein Bid was associated with mitochondrial AIF release after glutamate toxicity in neural cells [70–72]. Further, *in vivo* lethal AIF translocation from the mitochondria to the nucleus was observed, for instance, in models of neonatal cerebral hypoxia/ischemia [73], TBI [74], epilepsy [75] or transient focal cerebral ischemia [76].

All these findings depict AIF as an important mediator of caspase-independent neuronal PCD pathways. Targeting the mitochondrial release of AIF may therefore serve as a therapeutic target to prevent diseases where the translocation of AIF to the nucleus induces neuronal dysfunction and cell death. Recent findings revealed that neuronal cells depleted of AIF by siRNA were resistant to oxygen glucose deprivation (OGD) and glutamate-induced cell death [70,77]. Moreover, harlequin mice (Hq), carrying a mutation that mediates an 80% reduction of AIF expression in all tissues including the brain, were protected against hypoxia/ischemia [78], focal cerebral ischemia [76,79] and global cerebral ischemia [80]. However, it seems that AIF's redox function is essential for cell survival, as it plays a major role in the maintenance of the ETC function, the control of ROS generation and mitochondrial integrity, regulated by the NADH-oxidase domain [57,81]. This becomes apparent in paradigms of long term AIF depletion, as for example Hq mice develop ataxia, blindness and loss of cerebellar neurons. Such AIF-deficiency is accompanied by increased ROS levels and a loss in complex I function, which underlines the pro-survival function of AIF [77,82–84]. Therefore, AIF plays apparently a central role controlling physiological functions of mitochondria that are essential for cellular homeostasis and maintenance as well as in mitochondrial cell death pathways that are mediated by the translocation of AIF to the nucleus. However, upstream mechanisms of AIF function and the lethal translocation to the nucleus are largely unknown. Since some proteases are associated with upstream mechanisms of mitochondrial demise and the mitochondrial AIF release the involvement of trypsin-like serine proteases in paradigms of PCD associated with mitochondrial damage are in the main focus of the second part of this work.

1.3. Proteases in paradigms of programmed cell death

Endopeptidases, which represent about 2% of all proteases, are classified due to their catalytic active-site residue. The main representatives are metalloproteinases (34%), serine proteases (30%) and cysteine proteases (26%). Serine and cysteine proteases are named after their nucleophile amino acid in their catalytic triad. Proteases mediate the cleavage of peptide bonds in other proteins and thereby determine protein folding and hence control many diverse physiological processes, such as digestion, blood coagulation, tissue homeostasis, immune response, neuronal outgrowth, embryonic development, apoptosis and ageing. However, a deregulation of proteases by genetic mutations can cause a variety of hereditary diseases, such as haemophilia A or AD, and activation of proteases is linked to many forms of cell death [85].

1.3.1. Caspases

The finding of the human protease interleukin-1β converting enzyme (ICE or caspase-1), resulted in the discovery of several other ICE-like proteases, which were renamed ‘cysteine aspartate-specific proteases’, and in short ‘caspases’. Caspases exist as zymogens within cells and have to be activated by proteolytic autoactivation, transactivation or by other endopeptidases. This activation is mediated by the release of the pro-domain and the subsequent separation of the small and large subunit, which form subsequently an active tetrameric enzyme [86,87]. Caspases are important mediators of apoptosis and in this paradigm they can be classified as ‘initiator caspases’ (caspase-2, -8, -9, -10), which are activated early in apoptotic pathways and exhibit DED or caspase recruitment domains (CARD) and ‘executioner caspases’ (caspase-3, -6, -7), which are activated at later time points and execute apoptosis [87].

As described before, the initiator caspase-8 (and -10) [88] are involved in the extrinsic apoptotic pathway and are recruited by adaptor proteins like FADD via their DED, building the DISC [10]. The recruitment of pro-caspase-8 and the subsequent activation can be antagonized by the anti-apoptotic cellular FLICE inhibitory protein (cFLIP) which binds to FADD via its DED [89]. After its activation, caspase-8 mediates Bid cleavage, which links the extrinsic to the intrinsic apoptotic pathway, or directly activates caspase-3 independently of mitochondrial involvement. The second initiator

caspase, caspase-9, is recruited by the CARD domain of Apaf1, which together with Cytc and dATP builds a proteasome protein complex and activates pro-caspase-9 [90]. Little is known about the role of caspase-2 in apoptotic cell death pathways. Recent findings suggest, however, that the activation of pro-caspase-2 occurs upon nerve growth factor deprivation and DNA damage, but is independent of Apaf1 [91,92].

The executioner caspases-3, -6 and -7 are activated by functional initiator caspases and execute apoptosis by cleaving downstream substrates such as ICAD, IAPs, Rho-associated kinase (ROCK) or PARP [93,94]. Caspase-6 has been less intensively studied, however, due to its structural properties and its cleavage downstream of the initiator caspases it is regarded as an executioner caspase [90]. The typical caspase-dependent DNA laddering which results in ~180 bp fragments is mediated by the activation of CAD through executioner caspases, resulting in cell death [12].

1.3.2. Non-caspase proteases

Since the inhibition of caspases with broad-range inhibitors such as z-VAD-fmk does not necessarily prevent cell death, growing evidence suggests that other proteases are also mediators of apoptotic cell death pathways [95]. One representative for a non-caspase mediator of cell death is the cytosolic neutral cysteine protease calpain, which is Ca^{2+}-dependent and consists of two isoforms, m- and µ-calpain [96]. Since calpains contribute to the impairment of synaptic transmission in AD [97] and to the pathology of spinal cord injury [98], they came into the focus of research in apoptotic mechanisms. A large variety of proteins and transcription factors which are linked to apoptotic cell death mechanisms such as p53, c-jun and c-fos, were identified as calpain substrates. Furthermore, calpain-cleaved Bid and calpain-activated Bax have been implicated in mitochondrial permeabilization and the subsequent release of Cytc and AIF, which can also be directly cleaved by calpains, from the mitochondrial IMS [69,99,100].

Another group of non-caspase proteases are known as cathepsins which include a group of ‘lysosomal proteolytic enzymes’, irrespective of their enzyme class. Therefore, apart from cysteine proteases (cathepsin B, C, F, H, K, L, S, W and X) also serine proteases (cathepsin A and G) and aspartic proteases (cathepsin E and D) are included by this term [101]. Cathepsins are involved in many physiological processes, however, in the last years they were associated with apoptotic cell death

pathways [102,103]. To exert their apoptogenic function cathepsins have to be released from lysosomes, which requires lysosomal destabilization or permeabilization. Possible mechanisms of lysosomal disruption and the subsequent release of cathepsins into the cytosol involve the activation of phospholipase A2 [104], elevated ROS levels [105] or TNFα-mediated apoptosis [106], respectively. The major mediators of apoptosis within this protease family are reported to be cathepsins B, L and D [101]. After being released into the cytosol different substrates are activated. Cathepsin L participates in caspase-3 activation, cathepsin B induces the cleavage of Bid and the activation of pro-caspases-1 and -11 [107], while cathepsin D triggers Bax activation which, in turn, mediates mitochondrial AIF release [108].

1.3.3. Serine proteases

Serine proteases represent approximately one-third of all known proteases and due to their structure they can be divided into two classes: trypsin-like (also termed chymotrypsin-like) and subtilisin-like serine proteases. The class of trypsin-like serine proteases can be further categorized based on their substrate specificity as trypsin-like, chymotrypsin-like or elastase-like serine proteases [85,109]. The mammalian serine proteases trypsin, chymotrypsin and elastase are the best characterized among all serine proteases. The catalytic triad of serine proteases consists of three essential amino acids, histidine (His57), aspartate (Asp102) and serine (Ser195), which are closely related to each other due to protein folding (Figure 1) [110].

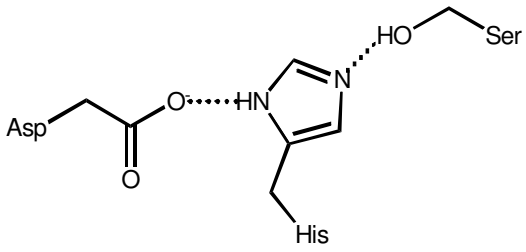

Figure 1: Catalytic triad of serine proteases

Serine proteases exhibit a catalytic triad with three essential amino acid residues involved in the cleavage of peptide bonds: histidin 57, aspartate 102, and serine 195.

Activation of serine protease cascades are involved in many physiological conditions including digestion, blood clotting and development and plasticity of the nervous system [111]. However, serine proteases were also related to PCD pathways as introducing them in tumor cells led to cell death with characteristics of apoptosis [112]. The major representatives of serine proteases involved in apoptosis are granzyme B and the mitochondrial serine protease high temperature required protein A2 (Omi/HtrA2). Granzyme B is found in cytoplasmic granules of cytotoxic T lymphocytes (CTLs) and natural killer (NK) cells and can be released by exocytosis [113]. The central nervous system (CNS) exhibits the lowest number of CTLs of any tissue, however, in neuroinflammatory and neurodegenerative disorders like AD and after traumatic and ischemic brain injury the amount of $CD8^+$ CTLs is enriched [114,115]. Furthermore, motor neuron dysfunction in amyotrophic lateral sclerosis (ALS) is linked to increased invasion of CTLs in the spinal cord [116]. After the release of granzyme B from CTLs it is endocytosed by target cells and mediates apoptosis by cleaving/activating downstream substrates, such as pro-caspase-3, Bid, ICAD or PARP [117]. Moreover, pro-apoptotic proteins, namely Bid, PARP and caspase-3, where identified as interaction partners of granzyme B in a model of ischemic/reperfusion injury [118].

The second serine protease associated with neurodegenerative disorders is Omi/HtrA2 [119,120]. Like other pro-apoptotic factors such as AIF, EndoG, Smac/Diablo or Cytc, Omi/HtrA2 is released from the mitochondria during apoptosis induced by DNA damage, death receptor activation or several other apoptotic stimuli [120]. After being released into the cytoplasm Omi/HtrA2 binds to the inhibitor of apoptosis proteins (IAPs), thus deactivating them and indirectly promoting the activation of caspases [121,122]. Furthermore, Omi/HtrA2 is able to induce apoptosis in a caspase-independent manner due to its protease activity [123]. Since the specific Omi/HtrA2 inhibitor Ucf-101 showed protective effects *in vitro* and also in *in vivo* models of ischemia/reperfusion, serine proteases represent promising targets to prevent neurological dysfunction [124–126].

In addition to granzyme B and Omi/HtrA2 the serine proteases trypsin and chymotrypsin are also related to apoptotic cell death pathways [112]. Recently chymotrypsin B was linked to apoptosis via cleavage of Bid and thus inducing Cytc release from the mitochondria [127]. Furthermore, the serine protease trypsin directly

increases intracellular ROS levels arising from the mitochondria and contributing to cytotoxicity. As the protease-induced ROS increase and subsequent cell death was attenuated by catalase treatment, a decomposer of H_2O_2, and accelerated by aminotriazole (a catalase inhibitor) treatment, Aoshiba and colleagues revealed a direct influence of serine proteases on the generation of intracellular ROS levels thereby mediating cell death [128]. The protective potential of the two serine protease inhibitors Nα-Tosyl-L-lysinchlormethylketon hydrochlorid (TLCK) and Np-Tosyl-L-phenylalanine chloromethyl ketone (TPCK) in sympathetic and hippocampal neurons underlines the importance of trypsin- and chymotrypsin-like serine proteases in neuronal cell death [129,130]. Proteins involved in downstream mechanisms of serine protease activation are for instance the degradation of the anti-apoptotic protein Bcl-2, the up-regulation/activation of pro-apoptotic proteins such as Bid and Bax, and the activation of caspases, all leading to cell death [131–133]. Another target of TLCK is the tumor suppressor protein p53. p53 plays an essential role in cell-cycle progression or apoptosis, which is influenced by many factors, such as cell type or stress stimuli [134,135], e.g. oxidative stress induces the accumulation of p53 [136]. It was reported by different groups that the accumulation of p53 was prevented by TLCK and the ensuing cell viability was increased [131,137]. Chymotrypsin-like serine proteases are also involved in another paradigm of PCD, the CD47-mediated PCD pathway. This type of cell death is characterized by F-actin network disruption, redistribution of Drp1 to the mitochondria, the impairment of the ETC and the exposure of phosphatidylserine on the outer leaflet of the plasma membrane [138]. F-actin disruption and the following cascade are mediated by chymotrypsin-like serine proteases as TPCK was able to prevent all these events in chronic lymphocytic leukemia cells [138]. All these findings contribute to the rising importance of serine proteases in cell death mechanisms. In this work trypsin-like serine proteases were in the focus of interest in glutamate-induced oxidative stress and associated intrinsic pathways of cell death in HT22 cells. Figure 2 exhibits a possible cell death mechanism induced by activated trypsin-like serine proteases.

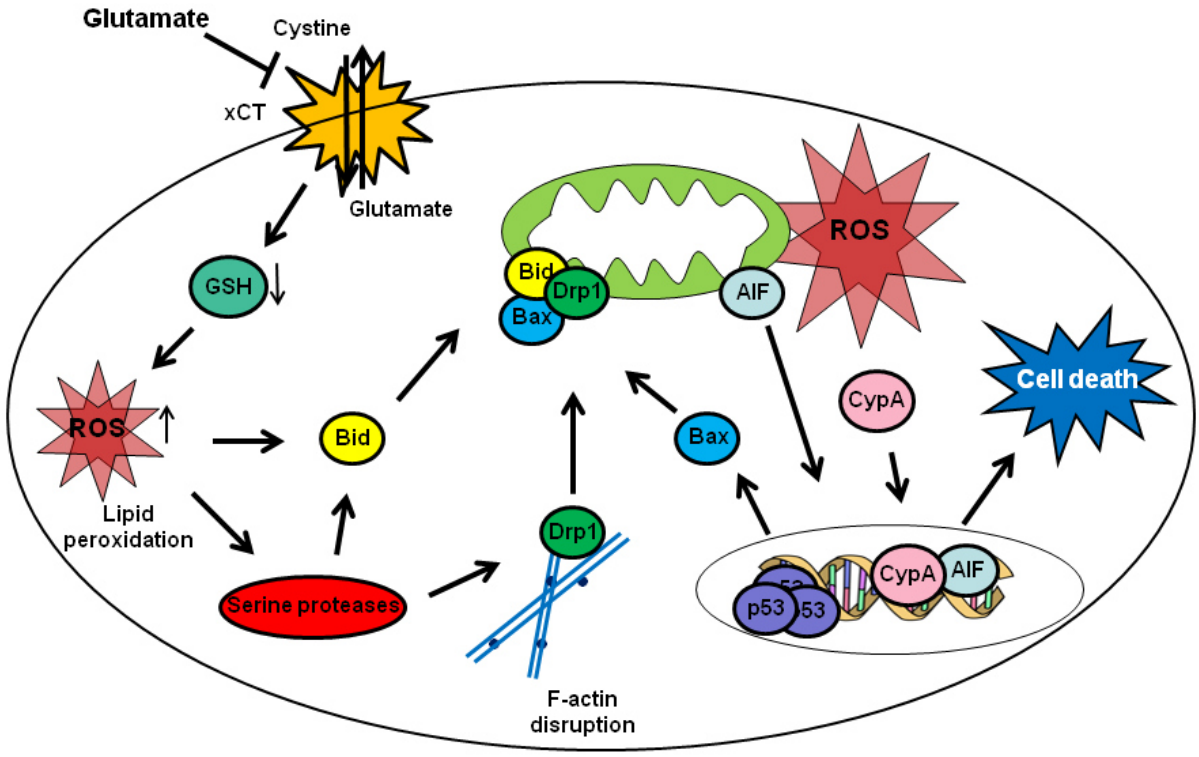

Figure 2: Serine proteases in glutamate-induced cell death in HT22 cells

Glutamate-induced increases in ROS may trigger the activation of serine proteases, which in turn activate Bid and lead to the disruption of the F-actin cytoskeleton. Subsequently, Drp1 redistributes to the mitochondria, where it associates with Bid and Bax. The ternary complex of Bid, Bax and Drp1 promotes mitochondrial fission, the release of AIF from the mitochondria and cell death.

1.4. The family of Peptidyl-prolyl cis-trans isomerases

Peptidyl-prolyl cis-trans isomerases (PPIases) catalyze cis-trans isomerization of peptide bonds at proline residues and thereby facilitate protein folding of other proteins. PPIases were first discovered as the intracellular receptors for the immunosuppressive drugs cyclosporine A (CsA), FK506 (tacrolimus) and sirolimus (earlier rapamycin), respectively. Today three classes of PPIases are characterized: (i) the cyclophilins (ii) FK506-binding proteins (FKBPs) and (iii) the parvulins [139]. While all three classes exhibit isomerase activity, cyclophilins and FKBPs constitute the class of immunophilins, because of their ability to build immunosuppressive complexes with the before mentioned drugs, however, parvulins count as nonimmunophilins lacking immunosuppressive properties [140,141].

1.4.1. FK506-binding proteins

FKBPs are small, predominantly soluble and ubiquitously expressed proteins which were discovered as the intracellular binding partner of tacrolimus and rapamycin

[139,142]. The tacrolimus/FKBP complex competitively binds to the Ca^{2+}- and calmodulin-dependent phosphatase calcineurin thereby inhibiting its activity which results in attenuated T-cell activation and the consequent immunosuppression [143]. The characterization of immunophilins has largely focused on cells from the immune system, however, FKBPs were also found to be abundantly expressed in brain tissue even more than 10 times higher compared to peripheral immune tissue [144]. Not only immunosuppressive features were linked to FKBPs but also protective effects in neuronal cell death pathways. The complex formation of tacrolimus/FKBPs in the brain enhances phosphorylation of several proteins, such as nitric oxide synthase (NOS), which is due to the inhibitory effect on calcineurin. This increased phosphorylation of NOS mediates protective effects against glutamate-induced excitotoxicity in cortical neurons [145]. Moreover, *in vivo* studies in models of global and transient focal ischemia revealed a crucial role for FKBPs as the treatment with tacrolimus exhibits neuroprotective effects. Furthermore, FKBPs are linked to neurological disorders such as PD [146–148].

1.4.2. Parvulins

Protein interacting with NIMA (never in mitosis A)-1 (Pin1) is the main representative of the parvulin subfamily of PPIases. Pin1 was discovered as the first nonimmunophilin catalyzing the isomerization of proline bonds. However, in contrast to the other family members of the PPIases, Pin1 exerts its isomerase activity only when a serine or threonine preceding the target proline is phosphorylated [149]. This phosphorylation-dependent isomerase activity places Pin1 in a central role of signaling pathways in cell proliferation and tumorgenesis [150], in neuronal differentiation and survival as well as in the pathology of AD [151,152]. The two proteins tau and amyloid precursor protein (APP) which are associated with AD pathology become phosphorylated by protein kinases as part of their physiological function, exhibiting a trans-conformation. A loss of Pin1 function results in elevated cis-ptau and cis-pAPP motifs representing the pathological conformations in AD [152]. Pin1 is sensitive to oxidative stress and the loss of Pin1 function in AD is reported to be due to the oxidation of Pin1 which results in decreased isomerase activity and accordingly in increased cis-ptau and cis-pAPP levels [153]. Thus, Pin1 exhibits a pro-survival role in the pathology of AD. However, Pin1 is also linked to neuronal apoptosis by activating the mitochondrial apoptotic machinery due to the interaction with the Bcl2

family member Bcl-2 interacting mediator of cell death (Bim_{EL}). Bim_{EL} is located at the mitochondria and promotes neuronal cell death after growth factor deprivation or activation of the p75 death receptor. JNK-induced phosphorylation of Bim_{EL} at Ser65 induces mitochondrial dysfunction and neuronal cell death [154,155]. In neurons Pin1 is enriched at the mitochondria and during apoptosis it interacts with pSer65 Bim_{EL} leading to the stabilization by attenuating the proteasomal degradation of Bim_{EL} and thereby promotes mitochondrial demise and cell death [156]. Since Pin1 is involved in the mitochondrial apoptotic machinery in neurons, this work investigates the contribution of Pin1 in glutamate-induced cell death and the impact on mitochondrial dynamics in HT22 neurons.

1.4.3. Cyclophilins

Cyclophilins (Cyps) which represent the third class of PPIases are ubiquitous proteins and evolutionarily well conserved. Human Cyps consists of 16 family members, among them CypA is the most abundant, which makes up to ~0.1-0.6 % of all cytosolic proteins [157]. CypA and D (partly CypB) are the two main representatives which are involved in cell death pathways. CypB exhibits an amino-terminal signal sequence that targets it to the ER [158]. In contrary to the other two mentioned cyclophilins, CypB has anti-apoptotic features in endoplasmatic reticulum (ER) stress-induced cell death pathways. ER stress induces the upregulation of different ER chaperons, including CypB. CypB overexpression suppresses apoptosis in H9C2 cells associated with elevated ROS and Ca^{2+}-levels and depletion of CypB with siRNA renders cells more susceptible for ER stress [159]. Another important ER stress response factor is CCAAT/enhancer-binding protein-homologous protein (CHOP), which is upregulated upon ER stress-induced apoptosis or after hypoxia [160]. CypB interacts with CHOP after hypoxia and cooperates with p300 E4 ligase to modulate the ubiquitination of CHOP thereby preventing hypoxia-induced cell death [160]. These studies demonstrate a pro-survival role for CypB. In contrast, CypD which is part of the mitochondrial PTP together with the voltage-dependent anion channel (VDAC) and adenine nucleotide translocator (ANT) is associated with cell death [161]. It has been reported that CypD-deficient mouse embryonic fibroblast are less susceptible to H_2O_2-induced oxidative stress. Furthermore, in an ischemic injury model, where Ca^{2+}-overload and oxidative stress mediate cell death, CypD-deficient mice exhibited reduced brain infarct size after middle cerebral artery occlusion (MCAO) and

reperfusion which denotes a pivotal role for CypD in neuronal cell death induced by oxidative stress stimuli [162]. Recently, Cyps were furthermore associated with cell cycle regulation. In particular, Cyp18 was shown to be involved in p53 regulation [163]. As previously mentioned in this work, p53 is a tumor suppressor which up- or down-regulates several target genes and thereby engages a key role in executing cellular response due to different types of stress/stimuli. The most intensively studied pathways are cell cycle control, DNA repair and recombination, apoptosis and the self-regulation of intracellular levels of p53 [164]. Cyp18 was discovered as an interaction partner of p53 thereby regulating p53-dependent apoptosis. The interaction of Cyp18 and p53 reduced the sequence-specific DNA binding of p53, whereas the impairment of the Cyp18-p53 complex increased p53-reporter gene activity. Inhibition of this interaction resulted in more pronounced accumulation of cells in the G2/M cell cycle phase, demonstrating a modulating role for Cyp18 in cell cycle regulation [163].

However, in this study the main focus lies on CypA. CypA is the prototype of the cyclophilin family as it was discovered as the first intracellular binding partner of the immunosuppressive drug CsA from this family [165]. CsA exerts its immunosuppressive action via a ternary complex between CsA, CypA and calcineurin, which inhibits the phosphates activity of calcineurin and its biological function [143]. Besides the immunosuppressive properties, CypA is known to be involved in several cellular events, such as protein folding and trafficking of proteins, formation and infectivity of virions of the human immunodeficiency virus (HIV)-1, folding of neuronal receptors and cell division in living cells [157]. Most of these pathways are sensitive to the inhibitory effect of CsA on CypA. CypA expression is particularly high in brain tissue, where it is expressed mainly in the cytoplasm but can also be found in the nucleus [166]. As mentioned before CypA is involved in cell death pathways as an obligate cofactor for AIF-mediated chromatin condensation [62] and it mediates excitotoxin-induced apoptosis in rat neuronal B50 cells [167]. Cells lacking CypA are relatively resistant to AIF-induced cell death. *In vitro* recombinant AIF and CypA exhibit a higher DNase activity than each of the proteins alone [62]. Mutant CypA which lacks peptidyl-prolyl isomerase activity still cooperates with AIF, mediating chromatin condensation. Furthermore, this feature was not abrogated by CsA, indicating that isomerase activity is not involved in CypA-mediated cell death and that CsA is not a pharmacological tool to investigate this particular cell death pathway [62]. Moreover, in

in vivo models of CypA knockout mice ($CypA^{-/-}$ mice) the infarct volume after cerebral hypoxia-ischemia was reduced by 47% compared to their wild-type littermates [168]. It is further reported, that AIF translocation to the nucleus in $CypA^{-/-}$ mice was reduced and vice versa, in AIF-deficient Hq mice CypA translocation to the nucleus was diminished, which suggests that both proteins are required for each other's translocation [168]. Recent findings from Tanaka et al. revealed that CypA/AIF complex formation and co-translocation to the nucleus mediates motor neuron degeneration in a mouse model of ALS [169]. All these findings exhibit a crucial role for CypA in neuronal cell death. The aim of this study was to examine the contribution of CypA to oxidative stress-induced cell death by glutamate in HT22 cells and since the AIF release was prohibited in $CypA^{-/-}$ mice, if CypA also targets mitochondrial function and integrity.

1.5. The HT22 cell model

To investigate the role of Pin1, AIF and CypA and trypsin-like serine proteases in the paradigm of oxidative stress-induced neuronal cell death, mouse hippocampal neuronal cells (HT22 cells) were used. This cell line is immortalized using a temperature-sensitive SV40 T-antigen [170]. Since HT22 cells lack ionotropic glutamate receptors, high extracellular glutamate concentrations (in millimolar ranges) lead to cell death via the inhibition of the xCT-antiporter, which is localized at the plasma membrane. This blockage results in decreased intracellular cystine concentrations resulting in depleted GSH levels, which leads to the activation of 12/15-Lox and then to the generation of elevated ROS levels [72,171]. This is accompanied by an increase of intracellular Ca^{2+}-levels [172]. The accumulation of ROS accordingly triggers the translocation of pro-apoptotic proteins, such as Bid, Bax and Drp1 to the mitochondria where they induce mitochondrial fission and a second much more pronounced increase in ROS levels, generated by the mitochondria. Accordingly, AIF is released from the mitochondria and translocates to the nucleus where it promotes cell death (Figure 3) [70,71,173]. Even though HT22 cells lack NMDA receptors this cell line is an established model to study the mechanisms of glutamate-induced oxidative stress, because increased intracellular Ca^{2+}-levels and elevated ROS levels are common features in neurodegenerative diseases.

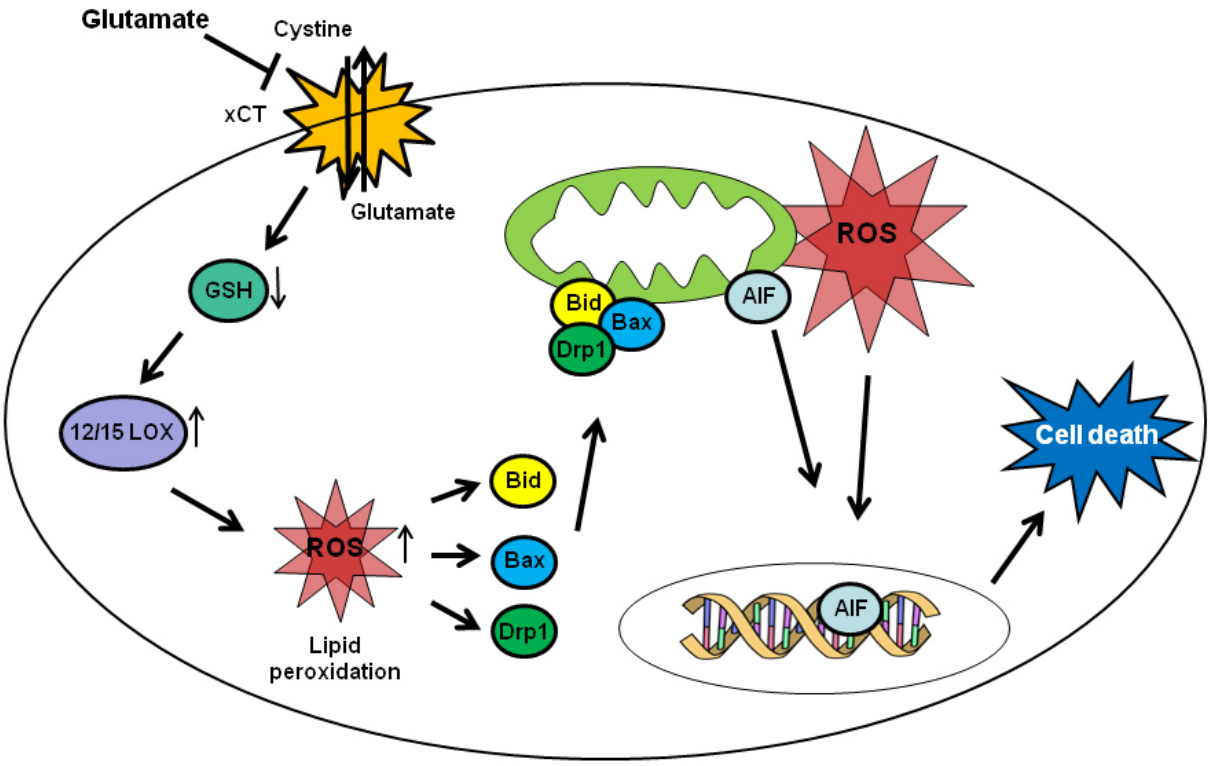

Figure 3: Schematic mechanism of glutamate-induced cell death in HT22 cells

HT22 cells express an xCT-antiporter in the cell membrane. High extracellular glutamate concentrations (mM) block the antiporter, resulting in elevated intracellular cystine levels which lead to a GSH depletion. Thus, 12/15-Lox is activated leading to enhanced ROS generation and lipid peroxide production which mediates the activation and translocation of pro-apoptotic proteins like Bid, Bax and Drp1 to the mitochondria. This triggers mitochondrial AIF release and translocation to the nucleus and subsequently cell death (modified from Tobaben).

1.6. Aims of this study

Oxidative stress and mitochondrial demise are linked to several neurological disorders, however, very little is known about the involved mediators upstream and downstream of mitochondrial damage and possible regulatory mechanisms of post-translational protein modification which may contribute to mitochondrial dysfunction. Such post-translational protein modifications may include protein-protein interactions, isomerization of proteins and protein cleavage which determine protein functions and subcellular localization, thereby regulating cellular homeostasis and resilience versus mitochondrial demise and cell death.

In particular AIF-mediated PCD pathways are linked to neuronal cell death *in vitro* and *in vivo.* The lethal AIF release from the mitochondria and the subsequent translocation to the nucleus is a major feature of caspase-independent neuronal cell death after TBI, cerebral focal and global ischemia, epilepsy and after oxidative stress. The immunophilin CypA is an important cofactor of AIF to induce chromatinolysis. However, the mechanism of cell death induced by the CypA/AIF complex is largely unknown. Thus, the first part of this thesis investigated the role of CypA in conditions of oxidative stress induced by glutamate and the impact of CypA on mitochondrial function. For this purpose, siRNA approaches of CypA were used to gain more insight into the particular role of CypA in neuronal cell death. Another representative of the PPIase family to which CypA belongs is Pin1. Pin1 is associated with the mitochondrial apoptotic machinery and thus another central issue of this study was to examine the influence of Pin1 on mitochondrial parameters. For this reason, a specific inhibitor (Br57) was used to investigate the influence of Pin1 on mitochondrial demise and cell death in HT22 cells.

The second part of this thesis addressed the question if serine proteases are involved in oxidative stress-induced cell death pathways in HT22 cells. It is well-established that caspases are major contributors to extrinsic as well as intrinsic apoptotic pathways. However, recent evidence suggests that also other proteases, such as serine proteases are linked to neuronal cell death. To elucidate the influence of trypsin-like serine proteases in glutamate-induced cell death the inhibitor TLCK was used and the impact on cell viability and several mitochondrial parameters was examined. To extend the results obtained from HT22 cells, TLCK was applied to mouse embryonic cortical neurons and the impact on cell viability was analyzed.

2. Material and methods

2.1. Chemicals and reagents

All standard chemicals were obtained from Sigma-Aldrich (Taufkirchen, Germany) and Roth (Karlsruhe, Germany), if not otherwise declared. All buffers and solutions were prepared using demineralized, ultrapure water (bidest dH_2O) that was prepared with the SG Ultra Clear UV plus pure water system (VWR, Darmstadt, Germany) and autoclaved with a steam autoclave (Systec V-40, Systec GmbH, Wettenberg, Germany).

2.2. Cell culture materials

All sterile plastic materials which were used are listed in Table 1.

Table 1: Plastic materials

Plastic material	**Company**
T75 flasks	Greiner, Frickenhausen, Germany
T175 flasks	Greiner, Frickenhausen, Germany
24-well plates	Greiner, Frickenhausen, Germany
96-well plates	Greiner, Frickenhausen, Germany
96-well E-plates	Roche, Penzberg, Germany
8-well ibidi slides	Ibidi, Munich, Germany
15 ml tubes	Greiner, Frickenhausen, Germany
50 ml tubes	Greiner, Frickenhausen, Germany
0.5, 1.5, 2 ml tubes	Sarstedt, Nümbrecht, Germany
Rubber policeman	Sarstedt, Nümbrecht, Germany
0.22 µm sterile filter	Whatman, Dassel, Germany
1,5, 10 ml Injekt®	Braun, Melsungen, Germany

2.3. Cell culture

2.3.1. Cultivation of HT22 cells

HT22 cells were generated by David Schubert (Salk Institute, San Diego, USA) and obtained from Gerald Thiel (Homburg/Saar). These cells were originally selected from HT4 cells based on glutamate sensitivity and immortalized from primary hippocampal neurons using a temperature-sensitive SV-40 T antigen [170].

HT22 cells were cultured in Dulbecco's modified Eagle medium (DMEM, Invitrogen, Karlsruhe, Germany) supplemented with 10% heat inactivated fetal calf serum, 100 U/ml penicillin, 100 µg/ml streptomycin and 2 mM stable L-glutamine (all PAA Laboratories GmbH, Cölbe, Germany, Table 2) and cultured in 75 cm² flasks in an humidified incubator at 37°C and 5% CO_2. Twice a week stock cells were split in a 1:10-1:20 ratio. For splitting and seeding the cells in different plate formats, cells were washed once with phosphate buffered saline (PBS, Table 3) to remove the growth medium completely. Thereafter, cells were incubated with a Trypsin/EDTA solution (1x TE, Table 4) for a few minutes to detach the cells from the bottom of the culture dish. By adding the 3-4 fold amount of growth medium, the protease activity of trypsin was stopped. The cell suspension was centrifuged at 1,000 rpm for 5 min. and after discarding the supernatant, cells were resuspended in fresh growth medium. The cell number was determined by counting the cells with a counting chamber (Neubauer Zählkammer, Brand, Wertheim, Germany). For experiments the required cell number was added into different culture dishes (listed in Table 5) and adjusted depending on the cell growth and the passage number. After 24 h of seeding, cells were treated with the mentioned cell death inducers and inhibitors of apoptosis (2.3.2 and 2.3.3) for 4-18 h depending on the following experiments and analysis. For this purpose old growth medium was removed and new medium containing the different drugs was added.

Table 2: HT22 medium

DMEM-medium with 4.5 mg/l glucose and 110 mg/l sodium pyruvate	440 ml
Heat inactivated fetal calf serum (FCS)	50 ml
L-alanyl-L-glutamine 200 mM	5 ml
Penicillin 10.000 U/ml / streptomycin 10 mg/ml	5 ml

Table 3: Phosphate buffered saline (PBS), pH 7.4

NaCl	9 g
Na_2HPO_4	0.527 g
KH_2PO_4	0.144 g
HCl	q.s. for pH adjustment
Bidest dH_2O	ad 1,000 ml

Table 4: Trypsin/EDTA solution (1x TE)

0.05 % Trypsin (7.500 U/mg)	100 mg
0.02 % EDTA	40 mg
1x PBS	ad 200 ml

Table 5: Cell numbers and volumes in cell culture dishes

Cell culture dish	**Cell number per well**	**Total volume of medium per well**
96-well plate	~ 8,000-10,000 cells/well	100 µl
96-E-plate	~ 8,000-10,000 cells/well	100 µl
Ibidi slides	~ 16,000-20,000 cells/well	200 µl
24-well plate	~ 60,000 cells/well	900 µl
6-well plate	~ 120,000-200,000 cells/well	2 ml
75 cm^2 flask	~ 1,5 Mio cells/flask	15 ml
175 cm^2 flask	~ 3,0-3,5 Mio cells/flask	25 ml
10 cm^2 dish	~ 1,5 Mio cells/dish	10 ml
14,5 cm^2 dish	~ 3,0 Mio cells/ dish	20 ml

2.3.2. Inducers of apoptosis

A stock solution of glutamate was prepared using DL-glutamic acid monohydrate (Sigma-Aldrich, Taufkirchen, Germany) which was dissolved in Earle's balanced salt solution (1x EBSS) or Dulbeccos's modified eagle medium (DMEM; PAA Laboratories GmbH, Cölbe, Germany) to a stock concentration of 1 M. The stock solution was stored at -20°C. The working solution with final concentrations of

2-7 mM glutamate was directly put on HT22 cells to induce cell death. Depending on the experiments cells were harvested or analyzed 4-18 h after induction of cell death.

For Hydrogen peroxide-induced cell death (H_2O_2, Sigma-Aldrich, Taufkirchen, Germany), a stock solution of H_2O_2 with a concentration of 30% was diluted in HT22 medium to final concentrations of 800-900 µM prior to use.

tBid-induced apoptosis was performed by transfecting HT22 cells with the tBid vector as described in 2.4.1..

2.3.3. Inhibitors of apoptosis

Nα-Tosyl-L-lysinchlormethylketon hydrochlorid (TLCK; Sigma Aldrich, Taufkirchen, Germany; Figure 4) was dissolved in DMSO at a stock concentration of 10 mM and stored at -20°C. TLCK was used at a final concentration of 50 µM in normal growth medium, if not otherwise indicated. HT22 cells were co-treated with TLCK except in tBid-induced cell death experiments. In these experiments cells were pretreated with TLCK for 1 h prior to glutamate challenge.

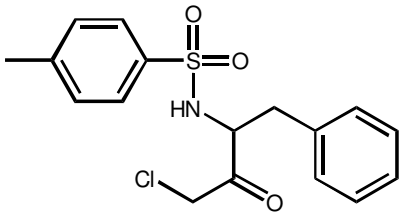

Figure 4: Chemical structure of TLCK

Np-Tosyl-L-phenylalaninechlormethylketon (TPCK; Sigma Aldrich, Taufkirchen, Germany, Figure 5) was dissolved in DMSO at a stock concentration of 10 mM and stored at -20°C. TPCK was used at indicated concentrations and cells were co-treated with this inhibitor in culture medium.

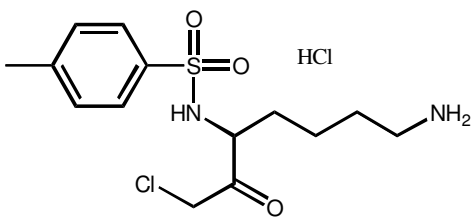

Figure 5: Chemical structure of TPCK

Compound Br57 (specific Pin1 inhibitor; kindly provided by Manfred Braun, Düsseldorf, Germany; Figure 6) was dissolved in DMSO at stock concentrations of 10 mM and stored at -20°C [174].

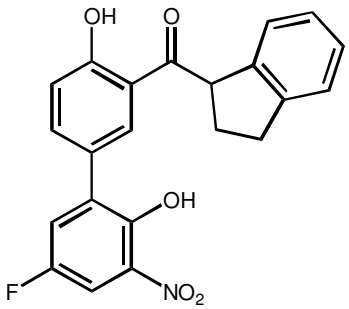

Figure 6: Chemical structure of the Pin1 inhibitor Br57

Br57 is an aryl 1-indanylketone derivate with an inhibitory efficacy for the Peptidyl-prolyl isomerase Pin1.

Bid inhibitor BI-6c9 (Sigma-Aldrich, Taufkirchen, Germany; Figure 7) was dissolved in DMSO at a stock concentration of 10 mM. It was used at a final concentration of 10 µM in HT22 growth medium as a positive control in different experiments.

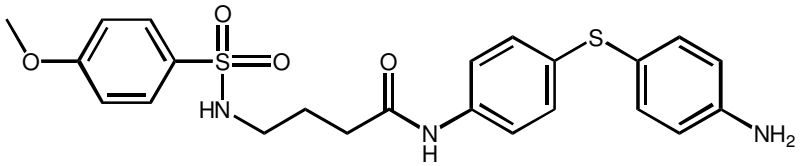

Figure 7: Chemical structure of the Bid inhibitor BI-6c9

2.4. Chemical and reagents

2.4.1. Transfection reagents

Opti-MEM I (Invitrogen, Karlsruhe, Germany) was used for DNA and siRNA transfections as basal, antibiotic- and serum-free medium.

For siRNA complexe formation the transfection reagent Lipofectamin® RNAiMAX (Invitrogen, Karlsruhe, Germany) was used.

Attractene transfection reagent (Qiagen, Hilden, Germany) was used to transfect DNA plasmids. In a 24-well format 4.5 µl of attractene were used to transfect 2 µg of DNA.

2.4.1.1. Plasmid vectors

The tBid vector was generated as described previously [175].

The plasmid pcDNA 3.1 was used as a control vector (Invitrogen, Karlsruhe, Germany).

All plasmids were amplified using the QIAGEN Plasmid Plus Midi Kit (Qiagen, Hilden, Germany) according to the manufacturer's protocol. Plasmid DNA-concentrations were defined with a NanoVue Plus Spectrophotometer (Implem, GE Healthcare Europe GmbH, Freiburg, Germany).

2.4.1.2. SiRNA sequences

CypA siRNA 1 (5'-CUG-AAU-GGC-UGG-AUG-GCA-A-3') and 2 (5'-UUG-CCA-UCC-AGC-CAU-UCA-G-3'), which were mixed in equal amounts to a final concentration of 25 nM, and the nonspecific mutant siRNA (scrambled siRNA, 5'-UAA-UGU-AUU-GGA-ACG-CAU-A-3') were obtained from Eurofins (Eurofins MWG Operon, Ebersberg, Germany). Particular siRNAs were entitled siCypA and siScr in this work.

Pin1 siRNA (MISSION® esiRNA, Sgima Aldrich, Taufkirchen, Germany) consists of an endoribonuclease-prepared siRNA pool comprised of a heterogeneous mixture of siRNAs that all target the same mRNA sequence. As control siRNA for Pin1 experiments the nonspecific mutant siRNA RLUC (MISSION® esiRNA, Sgima Aldrich, Taufkirchen, Germany) was used to equally compare Pin1 siRNA results because of the same construction. SiRNAs were entitled esiPin1 and siRLUC in this work.

The second Pin1 siRNA is an ON-TARGET plus mouse Pin1 siRNA-SMAART pool, which consists of a mixture of four target sequences (5'-CAA-GUA-UAC-UCU-AGC-AAA-G-3'; 5'-GAU-UAU-AGC-CAA-ACA-GUC-A-3', 5'-UAA-GAG-UGC-AUA-CGU-AUA-A-3' and 5'-GCA-GAA-ACC-AUU-UGA-GGA-U-3') and was obtained from Dharmacon (Thermo Scientific, Darmstadt, Germany). As control siRNA siScr was used and in this work the SMAART pool siRNA was entitled siPin1.

2.4.2. Primary antibodies

All primary antibodies used for western blot analysis are listed in Table 7. They were diluted in Tris-buffered saline (TBS, Table 6) containing 0.05 % Tween 20 (TBST) and 5 % nonfat skim milk powder or TBST containing 5 % BSA (all Sigma Aldrich, Taufkirchen, Germany).

Table 6: 10x Tris-buffered saline (TBS)

Trizma® base	24.2 g
NaCl	292 g
HCl	q.s. for pH adjustment
Bidest dH_2O	ad 1,000 ml

Table 7: Primary antibodies

Primary antibody	**Secondary antibody**	**Dilution in**	**Company**
α-Tubulin	Mouse	1:50,000 5 % milk in TBST	Sigma Aldrich
Actin Clone: C4	Mouse	1:100,000 5 % milk in TBST	MP Biomedicals
AIF (D-20)	Goat	1:1,000 5 % milk in TBST	Sante Cruz
AIF (E-1) (IP)	Mouse	7.5 µg ad 200 µl PBST	Santa Cruz
Cox-IV	Rabbit	1:1,000 5 % milk in TBST	Cell Signaling
Cyclophilin A	Rabbit	1:1,000 5 % milk in TBST	Merck Millipore
Cyclophilin A	Rabbit	1:1,000 5 % milk in TBST	Cell Signaling
DLP-1	Mouse	1:1,000 5 % milk in TBST	BD Transduction Laboratories™
DLP-1 (IP)	Mouse	7.5 µg ad 200 µl TPBS	BD Transduction Laboratories™

Lamin A/C	Rabbit	1:1,000 5 % milk TBST	Cell Signaling
MitoProfile® Total OXPHOS Rodent WB AB Cocktail	Mouse	1:500 5 % milk TBST	Abcam
TIM23	Mouse	1:1,000 5 % milk in TBST	BD Transduction Laboratories™

Cell Signaling, Danvers, Massachusetts, USA

BD Transduction Laboratories™, Heidelberg, Germany

Sigma Aldrich, Taufkirchen, Germany

Merck Millipore, Darmstadt, Germany

MP Biomedicals, Eschwege, Germany

Santa Cruz, Santa Cruz, California, USA

Abcam, Cambridge, UK

2.4.3. Secondary antibodies

Horse radish peroxidase (HRP) labeled secondary antibodies were obtained from Vector Labs (Burlingame, California, USA) and used in a dilution of 1:2,500 in TBS containing 0.05 % Tween 20 and 5 % nonfat skim milk powder.

Conjugated secondary antibodies Alexa 568 and Alexa 488 (Molecular Probes, Eugene, USA) were used for immunocytochemistry in a 1:200 dilution in 1x PBS containing 3 % horse serum in case of AIF immunostaining and 3 % goat serum for CypA immunostaining, respectively (Invitrogen, Karlsruhe, Germany).

2.4.4. Kits

All kits used in this work are listed in Table 8 and were used according to the manufacture`s protocol.

Table 8: Kits

Kit	**Company**
Annexin-V-FITC Detection Kit	Promokine, Heidelberg, Germany
Bodipy (581/591 C11)	Invitrogen, Karlsruhe, Germany
Dual-Luciferase® Assay Kit	Promega, Madison, USA
Dynabeads® Protein A for Immunoprecipitation	Invitrogen, Karlsruhe, Germany
Guave® Cell Cycle Reagent	Merck Millipore, Darmstadt, Germany
InviTrap® Spin Universal RNA Mini Kit	Stratec Molecular GmbH, Berlin, Germany
Lipofectamine® RNAiMAX	Invitrogen, Karlsruhe, Germany
MitoPT $\Delta\Psi_m$	ImmunoChemistry Technologies, Bloomington, USA
Nuclear Extract Kit	Active Motif Europe, Rixensart, Belgium
OxiSelect™ 96-well Comet Assay Kit	Biocat GmbH, Heidelberg, Germany
Pierce BCA Kit	Perbio Science, Bonn, Germany
QIAGEN Plasmid Plus Midi Kit	Qiagen, Hilden, Germany
SuperScript III One Step RT-PCR System with Platinum® Taq	Invitrogen, Karlsruhe, Germany
ViaLight™ Plus Cell Proliferation and Cytotoxicity BioAssay Kit	Lonza, Köln, Germany
XF Cell Mito Stress Test Kit	Seahorse Bioscience, Copenhagen, Denmark

2.5. Transfection protocols

2.5.1. SiRNA transfection

For siRNA transfection, siRNAs for indicated proteins and scrambled siRNA were diluted in Opti-MEM I (Invitrogen, Karlsruhe, Germany). Afterwards, 2.4 µl/ml Lipofectamin® RNAiMAX were added to the Opti-MEM I/siRNA solution, mixed by pipetting a few times and incubated at RT for 20 min. Following, 100 µl of this Opti-MEM mixture were added to each well of a 24-well plate and a final concentration of

10-25 nM was achieved. In 8-well ibidi slides the complete Opti-MEM mixture was equally reduced to a final volume of 40 µl for each well and in 6-well plates the mixture volume was extended to finally 400 µl. Control cells were treated with an Opti-MEM I/Lipofectamin® RNAiMAX mix, respectively. Subsequently, the cell suspension with a cell number of 33.000 cells/500 µl for 24-well plates; 17.000 cells/200 µl for ibidi slides and 120.000 cells/2 ml for 6-well plates was added to the transfection mixture and cells were allowed to grow for 48 h before treatment.

2.5.2. DNA transfection

HT22 cells were seeded in 24-well plates with a cell density of 40,000 cells/ well. After 24 h of seeding cells were transfected with Attractene Transfection Reagent. Therefore, 2 µg of DNA plasmid were diluted in Opti-MEM I and 9 µl/ml of attractene were added and mixed by pippeting. The mixture was incubated for 20 min. at RT and during the incubation time the medium of the 24-well plate was changed. Afterwards 60 µl of the Opti-MEM mixture were added dropwise to each well. Control cells were treated with an Opti-MEM I/attractene mix and pcDNA 3.1 plasmid was used as control vector.

2.6. Cell viability assays

2.6.1. MTT assay

The yellow monotetrazolium salt 3-(4, 5-dimethylthiazol-2-yl)-2, 5-diphenyltetrazolium bromide (MTT) belongs to a group of organic compounds which forms an insoluble, purple formazan after its reduction. Not only active mitochondria in living cells are able to reduce the MTT salt, but also intracellular vesicles like endosomes and lysosomes were identified to do so [176]. This colorimetric assay was used in this work to measure the enzymatic activity after induction of cell death and/or co-treatment with protective substances or after knockdown of particular proteins.

HT22 cells were seeded in 96-well plates and after 24 h of seeding cells were treated with glutamate and/or with different inhibitors of cell death. After 12-17 h, depending on the morphological changes of the cell, 20 µl of a 2.5 mg/ml MTT stock solution (Sigma Aldrich, Taufkirchen, Germany) prepared in 1x PBS were added to each well (final concentration per well: 0.5 mg/ml). Cells were then incubated at 37°C for 1 h and the reaction was finished by completely removing the medium containing the

MTT salt. Accordingly, cells were put for at least 1 h at -80°C. Cell viability was measured after another 1 h at 37°C on a shaker (150 rpm) dissolving the formazan crystals in 70 µl DMSO. Absorbance was quantified with a microplate reader (FluoStar OPTIMA, BMG Labtech, Offenbach, Germany) at 570 nm and background signals at 630 nm were subtracted. Control conditions were set to 100 % cell viability. All experiments were repeated at least three times.

2.6.2. xCELLigence System

The xCELLigence System (Roche, Penzberg, Germany), which contains a series of Real Time Cell Analyzer (RTCA), is a cell-based assay system monitoring biological processes of living cells due to changes in the electrical impedance. The system relies on a micro-electronic biosensor built into each well of a 96-well plate (E-plate; Roche, Penzberg, Germany). This sensor measures the electrical impedance of cells, which correlates with cell growth and cell proliferation. As a function of time, the normalized cell index (NCI) was used to depict cell growth, cell proliferation and changes in cell morphology in a curve. During cell death HT22 cells become round, detach from the bottom of the culture E-plate and decreases in the impedance measurements can be seen, which is visualized in a decrease in the NCI [177].

For background determination of the growth medium, 100 µl were added to each well of the E-plate. After measuring the background impedance, the medium was removed an HT22 cells were seeded at a density of ~8,000 cells/well. Treatment of the cells with glutamate and/or different cell death inhibitors was performed after the CI reached a value of 1. Using RTCA Software 1.2 (Roche Diagnostics, Penzberg, Germany) cell indices were recorded.

After the experiments E-plates were cleaned by first removing the medium, then washing each well with bidest dH_2O and afterwards 100 µl of 1x TE were put for 15-20 min. 1x TE was removed and wells were again washed three times with bidest dH_2O and following put under UV light for 30 min. to ensure sterility. All experiments were repeated at least three times.

2.6.3. Comet assay

The comet assay, or single cell gel electrophoresis assay (SCGE), is a common technique to measure DNA strand breaks in single cells. Damaged DNA, containing fragments and strand breaks, is separated from intact DNA by gel electrophoresis,

resulting in a typical ‘comet shape’ under the microscope. To determine DNA damage in HT22 cells after glutamate toxicity cells were seeded at a density of 60,000 cells/well in 24-well plates and after 24 h of growing cells were treated with 4 mM glutamate for indicated time points. Afterwards, samples were prepared for DNA analysis with the OxiSelect^{TM} 96-well Comet Assay Kit (Biocat GmbH, Heidelberg, Germany). Briefly, cells were trypsinzed with 1x TE, centrifuged for 5 min. at 700x g, washed once in ice cold 1x PBS (without Ca^{2+} and Mg^{2+}) and collect in 80 µl of 1x PBS. Samples were stored at -80°C for further experiments or directly used. OxiSelect^{TM} comet agarose was heated for 20 min. at 90-95°C in a water bath and was then transferred for another 20 min. to a 37°C water bath. Lysis buffer, alkaline solution and electrophoresis running solution were prepared prior to use according to the manufacturer’s protocol and were chilled to 4°C thoroughly. The OxiSelect^{TM} comet slide was warmed up in the 37°C room for 15 min. to promote agarose attachment. Following, diluted cell samples were combined with agarose gel in a 1.5 ml tube at a 1:10 ratio (v/v; ~50 µl), mixed by pipetting and immediately 20 µl/well were transferred onto the OxiSelect^{TM} 96-well slide by spreading the suspension over the well to ensure complete well coverage . This work was performed in the 37°C room to avoid gelation of the samples before they were pipetted on the slide. Afterwards, slide was transferred to 4°C in the dark for 30 min. to allow agarose attachment and gelation. Then slide was immersed for 30-60 min. at 4°C in a small basin containing pre-chilled lysis buffer (~50-100 ml/slide) and following lysis buffer was replaced with pre-chilled alkaline solution (~50-100 ml/slide) and put for 30 min. at 4°C in the dark. Subsequently, alkaline electrophoresis was performed in a horizontal electrophoresis chamber. The running time was 45 min. at 25 V and the electrophoresis volume was adjusted to produce a current setting of 300 mA. Afterwards, the slide was immersed for 2 min. in pre-chilled bidest dH_2O, repeated twice and was accordingly put for 5 min. in cold 70% ethanol. Ethanol was removed and slide was air-dried in the dark. Once the agarose and slide were completely dry 50 µl/well of diluted Vista Green DNA dye were added and incubated at RT for 15 min. Then slides were analyzed using an epiflourescence microscope (DMI6000B, Leica, Wetzlar, Germany) with a 20x objective. DNA damage was quantified by counting the displacement between the genetic material of the nucleus (‘comet head’) and the resulting ‘tail’. For each condition 200 nuclei were counted and assigned to the category ‘with tail’ or ‘w/o tail’. FITC was excited at 488 nm and

emission was detected through a 530 ± 40 nm band pass filter. Control cells were set up to 100% and all experiments were repeated three times.

2.7. ATP assay

Adensoin triphosphate (ATP) can be used to evaluate the functional integrity of living cells since each cell contains and requires ATP to stay alive. Detection of cell proliferation and cytotoxicity is mediated by an indirect ATP measurement, which is based on a bioluminescent assay. Every cell injury leads to a decrease in cytoplasmic ATP levels, which can be measured by an enzymatic response of ATP and luciferin according to the following reaction:

$$\text{ATP} + \text{Luciferin} + O_2 \xrightarrow[Mg^{2+}]{\text{Luciferase}} \text{Oxyluciferin} + \text{AMP} + PP_i + CO_2 + \text{Light}$$

To determine ATP levels in HT22 cells ~9,000 cells/well were seeded in white 96-well plates (Greiner, Frickenhausen, Germany) and after 24 h of seeding, cells were treated with glutamate and/or cell death inhibitors. After 15-16 h of glutamate challenge, ATP levels were detected by luminescence measurements with the ViaLight^{TM}Plus Kit (Lonza, Köln, Germany) according to the manufacture`s protocol. Briefly, the culture plate was removed from the incubator and was cooled down to RT for 5 min. Nucleotide releasing reagent was put on the cells for 10 min. and afterwards the ATP monitoring reagent was added for another 2 min. Then the luminescence was detected immediately (FluoStar OPTIMA, BMG Labtech, Offenbach, Germany) and the emitted light intensity of control cells was set up to 100 %. All experiments were repeated at least three times.

2.8. OCR measurements

To gain insight into cellular metabolism and to assess mitochondrial respiration, the oxygen consumption rate (OCR) was measured with the seahorse XF96 system (Bioscience, Copenhagen, Denmark). For this purpose, the XF Cell Mito Stress Test Kit was used. HT22 cells were seeded at a density of 10,000 cells/well in special XF96-well microplates and after growing over night, cell death was induced with glutamate (16 h, 4 mM) and different inhibitors were applied simultaneously. Before measurements were performed growth medium was replaced with ~180 µl of assay medium (with 4.5 g/L glucose as the sugar source, 2 mM glutamine, 1 mM pyruvate, pH 7.35) and cells were incubated for 60 min. at 37°C. Three baseline

measurements were recorded before cells were metabolically perturbed by the addition of three different compounds in sequence. First, oligomycin was added in Port A (20 µl) at a final concentration of 3 µM. Oligomycin is an ATP coupler, which inhibits ATP synthesis by blocking the proton channel of the ATP synthase (complex V). Due to this inhibition the proton gradient increases followed by a slower electron transport, which is accompanied by a decrease in oxygen consumption. The second compound FCCP (22.5 µl in Port B) was applied at a concentration of 0.4 µM. FCCP is an uncoupler of the electron transport chain resulting in a decreased proton gradient and a collapse of the MMP, leading to a rapid consumption of oxygen, exhibited in rising OCR. The third application was a combination of Rotenone and Antimycin A (25 µl in Port C), which was added at a concentration of 1 µM. Rotenone is a complex I inhibitor and Antimycin A inhibits complex III, resulting in a complete shutdown of mitochondrial respiration, illustrated in an OCR decrease. Three measurements were performed after the addition of each compound (4 min. mixing followed by 3 min. measuring). Measurements were done by Amalia Dolga. All experiments were repeated three times (n=6).

2.9. FACS-analysis

2.9.1. FITC AnnexinV/propidium iodide staining

FITC conjugated AnnexinV (AV) and propidium iodide (PI) are dyes usually used for FACS-analysis to quantitatively determine the amount of cell death. The membrane phospholipid phosphatidylserin (PS) is normally localized at the inner leaflet of the plasma membrane of living cells. During apoptosis or programmed cell death, PS is translocated to the outer leaflet while the plasma membrane stays intact. AV is a calcium-dependent phospholipid binding protein, which is not able to permeate intact cell membranes. Thus early apoptotic cells can be distinguished from late apoptotic and necrotic cells (only AV positive). Late stages of apoptosis and necrotic cell death are accompanied by the loss of plasma membrane integrity and thereby AV is able to bind also to late apoptotic and necrotic cells. To differentiate between apoptotic and necrotic cells a second dye, PI, is used. Viable cells with intact plasma membranes exclude PI, whereas damaged cells are permeable for PI. Accordingly, early apoptotic cells are AV positive and PI negative, whereas late apoptotic cells and

necrotic cells are AV and PI positive. In this work the amount of early and late apoptotic cells (AV and PI positive) was illustrated in bar graphs.

Cells were seeded in 24-well plates and treated with indicated concentrations of glutamate and inhibitors. Afterwards cells were harvested with 1x TE, washed once with 1x PBS and were then incubated in the dark with a solution containing FITC AV and PI for 5 min. at RT (AnnexinV FITC Detecion Kit, Promokine, Promocell, Heidelberg, Germany). Following, samples were put on ice and cell death was determined using FACScan (BD, Bioscience, Heidelberg, Germany) for siRNA CypA transfected cells and Guava EasyCyte™ Flow Cytometer (Merck Millipore, Darmstadt, Germany) for all other experiments, respectively. FITC AV was excited at 488 nm and emission was detected through a 530 ± 40 nm band pass filter. PI was excited at 488 nm and fluorescence emission was detected using a 680 ± 30 nm band pass filter. To exclude cell debris, cells were gated by forward versus side scatter and 10,000 events per sample were collected from 3-4 independent samples per condition. All experiments were repeated at least three times.

2.9.2. Detection of lipid peroxides

C11-BODIPY$^{581/591}$ is a fluorescent dye sensitive to lipid peroxidation and antioxidant efficacy in living cells. Its fluorescent properties are located in the red range of the visible spectrum (emission maximum 595 nm) and upon free radical-induced oxidation a shift from red to green can be detected by FACS-analysis. To measure lipid peroxidation in HT22 cells after glutamate challenge, 60,000 cells/well were seeded in 24-well plates and after at least 24 h of growing cell death was induced. After indicated time points cells were loaded with 2 µM C11-BODIPY$^{581/591}$ (Invitrogen, Karlsruhe, Germany) for 1 h in 0.5 ml growth medium. Afterwards, cells were trypsinized with 1x TE, centrifuged for 5 min. at 1,000 rpm, washed once with 1x PBS and were re-suspended in 300 µl 1x PBS for FACS-analysis on a Guava EasyCyte™ Flow Cytometer (Merck Millipore, Darmstadt, Germany) by using 488 nm UV line argon laser for excitation and lipid peroxidation emission was recorded at 530 nm (green) and at 585 nm (red). To exclude cell debris, cells were gated by forward versus side scatter and 10,000 events per sample were collected from 3-4 independent samples per condition. All experiments were repeated at least three times.

2.9.3. Assessment of mitochondrial membrane potential

To determine changes in the MMP in HT22 cells after glutamate exposure the Mito PT $\Delta\Psi_m$ Kit (Immunochemistry Technologies, Hamburg, Germany) was used. For this purpose cells were seeded in 24-well plates at a density of 60,000 cells/well and were treated after at least 24 h of growing with glutamate. SiRNA transfected cells were seeded at a density of 33,000 cells/well and were allowed to grow for at least 48 h. After indicated time points cells were harvested by trypsinization with 1x TE, centrifuged for 5 min. at 1,000 rpm and to detect the loss of MMP, the lipophilic, cationic fluorescening dye tetramethylrhodamine ethyl ester (TMRE) was added at a final concentration of 200 nM in normal growth medium. Cells were then put for 20 min. at 37°C and afterwards centrifuged for 5 min. at 1,000 rpm, washed once in 1x PBS and were re-suspended in TMRE assay buffer. The lipophilic and cationic properties of TMRE allow the dye to concentrate within the intact and negatively charged mitochondria and thereby exhibiting red fluorescence. A decrease in the MMP is accompanied by a reduction in the red fluorescence, which was detected by Guava EasyCyte™ Flow Cytometer (Merck Millipore, Darmstadt, Germany) using excitation at 550 nm and detecting emission at 570 nm. To exclude cell debris, cells were gated by forward versus side scatter and 10,000 events per sample were collected from 3-4 independent samples per condition. All experiments were repeated at least three times.

2.9.4. Cell cycle determination

The DNA content of cells varies in the different stages of the cell cycle. By labeling cellular DNA with propidium iodide (PI) cell cycles can be discriminated, as resting cells (G0/G1 phase) contain less DNA, cells in S phase have increased DNA amount and after replication of all chromosomes (G2/M phase) cells exhibit the double amount of DNA, resulting in increased PI intercalation and thus fluorescence intensity is enhanced. To evaluate the stages of cell cycles HT22 cells were transfected with 25 nM of siCypA in 24-well plates (33,000 cells/well) and were allowed to grow for 48 h. Accordingly, cells were washed once with cold 1x PBS, collected by trypsinization with 1x TE, centrifuged at RT for 5 min. at 450x g, were again washed in 1x PBS and afterwards fixed in ice-cold 70% ethanol, which was added dropwise to cell samples. Cells were refrigerated in 70% ethanol for at least 1 h (up to 12 h) at 4°C and subsequently centrifuged (RT, 5 min., 450x g) and washed once with

1x PBS. Following cells were stained with the Guava cell cycle reagent (200 µl for each sample) for 30 min. at RT and analyzed by FACS measurements. PI was excited at 488 nm and fluorescence emission was detected using a 680 ± 30 nm band pass filter with the Guava EasyCyte^{TM} Flow Cytometer (Merck Millipore, Darmstadt, Germany). To exclude cell debris, cells were gated by forward versus side scatter and 10,000 events per sample were collected from 3-4 independent samples per condition. Experiments were repeated at least three times.

2.10. Immunocytochemistry

2.10.1. Staining of mitochondria

Visualization of mitochondrial morphology was performed using the dye MitoTracker DeepRed (MitoTracker® DeepRed FM, Invitrogen, Karlsruhe, Germany), a red fluorescent dye which stains mitochondria in living cells and can be used for mitochondrial localization. A stock of 50 µM was prepared in DMSO and a final concentration of 200 nM was used in all experiments. Cells were seeded in 8-well ibidi slides and were, prior to glutamate challenge, incubated for 20 min. at 37°C with growth medium containing MitoTracker DeepRed. Additionally, a counterstaining of the nuclei was accomplished using 4′, 6-Diamidin-2-phenylindol (DAPI, 1 µg/ml), a blue fluorescent dye which accumulates in AT-riche regions of the DNA. After staining of mitochondria, the medium was removed and cells were treated or not with glutamate. Accordingly, cells were washed carefully with 1x PBS, fixed with 4 % PFA for 20 min. at RT in the dark and washed again three times with 1x PBS. Cells were stored in 1x PBS at 4°C until use. Images were obtained with an epiflourescence (DMI6000B, Leica, Wetzlar, Germany) or concfocal laser scanning microscope (Axiovert 200, LSM Image Software, Carl Zeiss, Jena, Germany) with a 63 x 1.4 NA oil immersion objective. MitoTracker DeepRed fluorescence was excited at a wavelength of 633 nm (band pass filter) and emission was detected at 670 nm (long pass filter).

2.10.2. Evaluation of mitochondrial morphology

To investigate mitochondrial morphology alterations in HT22 cells after glutamate-induced cell death, mitochondria were divided in 3 categories as described before [71]. Category I represents elongated mitochondria as seen in control samples, category II depicts intermediate mitochondria spread all over the cytosol and

category III exhibits fragmented mitochondria surrounding the nucleus. HT22 cells were seeded in 8-well ibidi slides at a density of 20,000 cells/well. After one day of growing (siRNA CypA transfected cells two days), cells were stained with MitoTracker DeepRed prior to glutamate exposure and were fixed after indicated time points of glutamate treatment. At least 500 cells per condition were counted blind for quantification analysis and all experiments were repeated at least three times. For counting experiments the epiflourescence microscope equipped with a DCF360FX-camera (DMI6000B, Leica, Wetzlar, Germany) was used.

2.10.3. Immunocytochemistry

To detect the localization of CypA and AIF during apoptosis, HT22 cells were seeded in 8-well ibid slides at a density of 17,000 cells/well. After 24 h of growing glutamate was applied and after indicated time points cells were fixed with 4 % PFA and permeabilized with a solution of 0.4 % Triton-X-100 in 1x PBS (Sigma-Aldrich, Taufkirchen, Germany) for 5 min. Afterwards, blocking solution was applied (in case of AIF analysis 3 % horse serum in 1x PBS and in case of CypA analysis 3 % goat serum in 1x PBS (both Invitrogen, Karlsruhe, Germany)) for 30 min. at RT. Cells were then exposed to according first antibodies at a dilution of 1:200 in blocking buffer over night at 4°C and the next day for another 2 h at RT. Subsequent, corresponding secondary antibodies were applied for 1.5 h at RT in the dark followed by a washing step with 1x PBS, which was repeated twice. For AIF examination anti-goat Alex 568 and for CypA detection anti-rabbit Alexa 488 secondary antibodies (Molecular Probes, Eugene, USA) were used. DAPI was applied for counterstaining of the nuclei. Images were acquired using a confocal laser-scanning microscope (Axiovert 200, Carl Zeiss, Jena, Germany) and light was collected through a 63x 1.4-NA oil immersion objective. DAPI fluorescence was excited at 364 nm and emission was achieved by a 385 nm long pass filter. For digital imaging the LSM Image Browser 4.2.0 software (Carl Zeiss, Jena, Germany) was used. Confocal images for AIF and CypA immunocytochemistry were taken from Amalia Dolga and Nunnziana Doti.

2.11. Protein analysis

2.11.1. Western blot sample preparation

2.11.1.1. Total protein lysates

For western blot analysis total cell protein lysates were used to investigate protein regulation during cell death. Cells were seeded in 6-well plates at a density of 150,000-180,000 cells/well, in case of transfection 120,000 cells/well, and were allowed to grow for at least one day, transfected cells for two days. Following, cells were treated with different glutamate concentrations and/or cell death inhibitors. After indicated time points cells were harvested by trypsinization with 1x TE, washed once with 1x PBS and lysed in 50-100 µl protein lysis buffer (Table 9). All steps were performed on ice. Cells were kept for another 15 min. on ice and subsequently stored at –80°C. Prior to further use, cell lysates were thawn up, centrifuged at 10,000 g for 10 min. at 4°C to remove cell debris and membrane fragments. The supernatant was used for western blot analysis.

Table 9: Protein lysis buffer pH 7.8

0.25 M D-Mannitol	4.56 g
0.05 M Trizma® base	0.788 g
1 mM EDTA	0.038 g
1 mM EGTA	0.038 g
HCl	q.s. for pH adjustment
Bidest dH_2O	ad 100 ml

This stock solution was stored at -20°C in 10 ml aliquots. Prior to use the solution was completed with:

DTT (100 mM)	0.1 ml
Triton-X 100	0.1 ml
1 tablet per 10 ml of Complete mini protease inhibitor cocktail	
1 tablet per 10 ml of phosphatase inhibitor	

Protease and phosphates inhibitor tablets were obtained from Roche (Mannheim, Germany). All other substances listed in Table 9 were obtained from Sigma Aldrich (Taufkirchen, Germany).

2.11.1.2. Mitochondrial fractionation

HT22 cells were fractionated to enrich mitochondrial proteins for western blot analysis. Briefly, ~10 million cells (equates to three 175 cm^2 flasks) per condition were plated and after 24 h treated with glutamate. All following steps were performed at 4°C. After indicated time points cells were harvested by scrapping with a rubber policeman, washed twice in cold 1x PBS and re-suspended in 0.5 ml Buffer 1. Cells were disrupted using a glass douncer (25 passes) followed by 15 passes with a 20G needle. Afterwards cells were centrifuged at 4°C for 10 min. at 900x g and supernatant 1 (S1) was retained. Cell pellet was again homogenized in 0.5 ml Buffer 1 with the glass douncer and the 20G needle, centrifuged and supernatant 2 (S2) was combined with S1 and following centrifuged at 4°C for 10 min. at 16,800x g. Supernatant was discarded and cell pellet was washed twice with 500 µl Buffer 1 and finally re-suspended in 80 µl Buffer 1 for protein analysis.

Table 10: Buffer 1 for mitochondrial fractionation pH 7.5

250 mM Sucrose	4.279 g
20 mM HEPES	0.2383 g
3 mM EDTA	0.0558 g
HCl	q.s. for pH adjustment
Bidest dH_2O	ad 50 ml

Buffer 1 was always fresh prepared and supplemented with 1 tablet per 10 ml of Complete mini protease inhibitor cocktail prior to use.

2.11.1.3. Nuclear fractionation

The nuclear extraction was performed with the Nuclear Extract Kit (Actif Motif Europe, Rixensart, Belgium) to investigate the translocation of particular proteins during glutamate-induced cell death from the mitochondria/cytosol to the nucleus. For each condition three 75 cm^2 flasks were used with a cell density of 1 million cells per flask. After growing and indicated time points of cell death induction, the medium of

each flask was collected, centrifuged for 5 min. at 1,000 rpm and the cell pellets were combined with the cell lysates resulting from the cell collection. For cell collection, the remaining monolayer in the flask was washed with 5 ml ice-cold PBS/phosphatase inhibitors (provided in the kit) and afterwards 3 ml were added and cells were collected by gently scrapping with a rubber policeman. Following, cells were centrifuged at 500 rpm for 5 min. at 4°C and the supernatant was discarded. To get the cytoplasmic fraction, the cell pellet was re-suspended in 400 µl 1x Hypotonic Buffer by pipetting up and down several times and was incubated for 15 min. on ice. Accordingly, 20 µl Detergent was added, cell suspension was vortexed at highest speed and centrifuged for 30 seconds at 14,000x g at 4°C. The resulting supernatant included the cytoplasmic fraction and was stored at -80°C until further use. The cell pellet was washed with 1x Hypotonic Buffer and afterwards re-suspended in 80 µl Complete Lysis Buffer and vortexed 10 seconds. The suspension was incubated for 30 min. on ice on a rocking platform at 150 rpm, vortexed again for 30 seconds and centrifuged for 10 min. at 14,000x g at 4°C. The nuclear fraction (supernatant) was stored at -80°C until further use.

2.11.2. Quantification of protein amount

To determine the protein amount in different samples the bicinchoninic acid assay (BCA assay) was used. This assay relies on 2 reactions: First, Cu^{2+} ions are reduced to Cu^{+} ions by peptide bonds in proteins under alkaline conditions in a temperature depending step. This step is proportional to the protein amount and was performed at 60°C. Secondly, 2 molecules of bicinchoninic acid build a complex with 1 Cu^{+} ion, forming a purple-colored product [178].

The Pierce BCA Kit (Perbio Science, Bonn, Germany) was used for the protein amount determination. One hundred µl of a 1:50 mixture of reagent B: reagent A were prepared and 2.5 µl of protein samples were added and mixed by vortexing. Afterwards, samples were incubated at 60°C for 30 min. on a platform shaker (650 rpm). Each sample was pipetted into a 96-well plate (Nunc, Wiesbaden, Germany) and absorption was measured at 590 nm using a microplate reader (Fluostar OPTIMA, BMG Labtech, Offenburg, Germany). A standard curve containing 0-200 µg/100 µl bovine serum albumin (Perbio Science, Bonn, Germany) was used to calculate the protein amount in each sample.

2.11.3. Immunoprecipitation

For IP experiments 2.5 mg of total protein lysates were used. According to the manufacture`s protocol (Invitrogen, Karlsruhe, Germany) magnetic Dynabeads A were tagged with 7.5 µg primary antibody diluted in 200 µl 1x PBS containing 0.02 % Tween 20 (PBST) and incubated for 15 min. on a rotator at RT. Afterwards, the beads-antibody complex was washed with PBST and fresh prepared BS^3 crosslinker (2.5 mM) was added at a final volume of 1 ml PBST and incubated for 30 min. at RT on the rotator. Again, a washing step was performed and quenching buffer was put at a final concentration of 50 mM (Tris-HCl pH 7.4) for another 15 min. at RT on the rotator. After a further washing step protein samples (2.5 mg) were added to the dynabeads-antibody complex in a total volume of 800 µl. The incubation time accounted 2 h and was performed for 1 h at 4°C and the second hour at RT on a rotator. Following, the dynabeads-antibody-antigen complex was washed three times with PBST and then boiled with 70 µl 2.5x SDS for 10 min. at 95°C. The protein lysate was removed and stored at -80°C until further use for western blot analysis. As a flow through control 25-50 µg protein amount were loaded on the gel.

2.11.4. Gel electrophoresis and western blot analysis

Sodium dodecyl sulfate polyacrylamide gel electrophoresis (SDS-PAGE) is a model system to separate proteins due to their molecular weight in an electrical field. This method is used to fractionate proteins by their size.

The solutions listed in the following tables were used for SDS-PAGE:

Table 11: 0.5 M Tris pH 6.8

Tris-HCl	7.88 g
HCl	q.s. for pH adjustment
Bidest dH_2O	ad 100 ml

Table 11: 1.5 M Tris pH 8.8

Tris-HCl	23.6 g
HCl	q.s. for pH adjustment
Bidest dH_2O	ad 100 ml

Table 12: 10 % Ammoniumpersulfat (APS)

Ammoniumpersulfat	1 g
Bidest dH_2O	ad 10 ml

Table 13: 10 % Sodium dodecyl sulfate (SDS)

SDS	1 g
Bidest dH_2O	10 ml

Table 14: 12.5 % Separation gel

1.5 M Tris pH 8.8	2.5 ml
10 % SDS	0.1 ml
10 % APS	0.05 ml
30 % Acrylamid/Bis solution 37, 5:1	4 ml
TEMED	0.01 ml
Bidest dH_2O	ad 10 ml

Table 15: 3.5 % Stacking gel

0.5 M Tris pH 6.8	2.5 ml
10 % SDS	0.1 ml
10 % APS	0.05 ml
30 % Acrylamid/Bis solution 37, 5:1	1.2 ml
TEMED	0.01 ml
Bidest dH_2O	ad 10 ml

Table 16: 10x Electrophoresis buffer

Trizma® base	30 g
Glycine	144 g
SDS	10 g
Bidest dH_2O	ad 10 ml

The 10x electrophoresis buffer was diluted 1:10 with bidest dH_2O before use.

Table 17: 5x SDS sample buffer

1.5 M Trizma® HCl pH 6.8	4 ml
Glycerol	10 ml
β-Mercaptoethanol	5 ml
SDS	2 g
1 % Bromophenol blue	1 ml

The solutions listed in the following tables were used for western blot analysis:

Table 18: 10x Transfer buffer

Trizma® base	30 g
Glycine	144 g
HCl	q.s. for pH adjustment
Bidest dH_2O	ad 1,000 ml

The 10x transfer buffer was diluted 1:10 with bidest dH_2O before use. 20 % methanol was added to 1x transfer buffer for wet blotting.

Table 19: 1x TBS/Tween 20 (TBST)

10x TBS	100 ml
Tween 20	0.5 ml
Bidest dH_2O	ad 1,000 ml

Table 20: 5 % Blocking buffer

Skim milk powder	25 g
TBST	ad 500 ml

Table 22: Stripping buffer

Glycine	15 g
SDS	1 g
Tween 20	10 ml
HCl	q.s. for pH adjustment
Bidest dH_2O	ad 1,000 ml

Depending on the incidence of the protein to be analyzed, 25-70 µg total protein amount were loaded on the gel. Gels were prepared using BIO-RAD (München, Germany) gel casting stand and casting frames with a 12.5 % polyacrylamide separation gel and a 3.5 % polyacrylamide stacking gel (Table 14 and 15). Protein samples were loaded with 5x SDS sample buffer(Table 17), filled up with bidest dH_2O to equal total volumes and were heated for 5-8 min. at 95°C on a shaking platform (650 rpm). To identify the molecular weight of the particular proteins, 5 µl of PageRuler^{TM} Plus Prestained Ladder (Fermentas, St. Leon-Rot, Germany) were added on the gel next to the protein samples. Gel electrophoresis was performed first at 60 V for 20-30 min. to get samples through the stacking gel and was then increased to 120-130 V until the required separation of the proteins was reached. Subsequently, proteins were blotted on a polyvinylidenfluorid membrane (PVDF, Bio-Rad, München, Germany). For this purpose, the PVDF membrane was incubated for 1-2 min. in methanol and afterwards for another 10 min. in 1x transfer buffer containing 20 % methanol. During this time, the gel and filter papers were also incubated in 1x transfer buffer. Blotting was performed in a Mini Trans-Blot® Electrophoretic Transfer Cell (Bio-Rad, München, Germany) for 20-22 h at 20 mA per gel at 4°C. The next day, membrane was washed for 5 min. with 1x TBS and afterwards blocked with 5 % milk blocking buffer for 1 h at RT. Following, the first antibody (Table 7) was added to the membrane and incubated over night at 4°C. The next day, the antibody was incubated for another hour at RT and after a 5 min. washing step with 1x TBST, the membrane was probed with the corresponding HRP-conjugated secondary antibody (Vector Laboratories, Burlingame, USA) for 1 h at RT and washed again 3 times for 15 min. with 1x TBST. Thereafter, the membrane was put in a chemiluminescent substrate solution HRP-Juice (PJK GmbH, Kleinblittersdorf, Germany) and after 1-2 min. chemiluminescent signals were

detected by the semi-automated Chemidoc-XRS Imaging System (Bio-Rad, München, Germany) and quantified with the Quantity One software (Bio-Rad, München, Germany). For equal protein loading and quantification of protein amounts actin was used in total lysates. For mitochondrial fractions Tim 23 and for nuclear fractions Lamin A/C was used as loading control.

2.12. RNA analysis

2.12.1. RNA sample preparation

For RNA extraction and analysis cells were seeded in 6-well plates at a density of 200,000 cells/well and afterwards RNA extracts were prepared using the InviTrap® Spin Universal RNA Mini Kit (Stratec Molecular GmbH, Berlin, Germany). Briefly, medium was discarded, cells were washed once with 1x PBS and Lysis Solution TR containing 1 % β-mercaptoethanol was added. Cells were collected with a rubber policeman and lysates were pipetted directly onto a DNA-Binding Spin Filter, incubated for 1 minute and centrifuged for 2 min. at 11,000x g to remove cell debris. The Spin Filter was discarded and ethanol was added to the RNA containing lysate to extract nucleic acids. Then the whole sample was put onto a RNA-RTA Spin Filter, incubated for 1 minute and centrifuged for 1 minute at 11,000x g. The flow-through was discarded and Wash Buffer R1 was applied on the Spin Filter, centrifuged for 1 minute at 11,000x g and the flow-though again discarded. The same procedure was performed tiwce with Wash Buffer R2 to remove immoderate electrolytes. To eliminate any traces of ethanol a centrifugation step for 4 min. at maximum speed was followed. To elute the total RNA from the RNA-RTA Spin Filter, Elution Buffer R was pipetted onto the membrane, incubated for 2 min. and centrifuged for 1 minute at 11,000x g. RNA samples were stored at -80°C until further use. All buffers used for this procedure were applied in the kit.

2.12.2. RNA amount determination

The NanoVue Plus Spectrophotometer (Implem, GE Healthcare Europe GmbH, Freiburg, Germany) was used to quantify the total RNA amount of the RNA samples. A wavelength of 260 nm was used to detect RNA levels and the quality of the purified RNA was determined at the reference wavelength of 280 nm.

2.12.3. Reverse transcriptase polymerase chain reaction (RT-PCR)

RT-PCR is the combination of two methods to detect RNA expression levels. First, RNA is transcribed into complementary DNA (cDNA) using the enzyme reverse transcriptase and secondly the resulting cDNA is amplified by the enzyme DNA-polymerase in a PCR. This one-step PCR was performed using SuperScript III One Step RT-PCR System with Platinum® Taq (Invitrogen, Karlsruhe, Germany). Primers used for the RT-PCR were obtained from Eurofins (Eurofins MWG Operon, Ebersberg, Germany) and are listed in Table 23.

Table 23: Primer sequences used for RT-PCR

Primer	**Sequence**
CypA forward	5`-CCACCGTGTTCTTCGACATCACG -3`
CypA reverse	5`-GCTGGTCTTGCCATTCCTGACCC-3`
GAPDH forward	5`-CGTCTTCACCACCATGGAGAAGGC-3`
GAPDH reverse	5`-AAGGCCATGCCAGTGAGCTTCCC-3`
PIN1 forward	5`-CTGGGAGAAGCGTATGAGTC-3`
PIN1 reverse	5`-GTGAGGCCAGAGATTCAAAG-3`
CypB forward	5`-GACTTCATGATCCAGGGTGG-3`
CypB reverse	5`-CCAGGAGGTCTTGACTGTGG-3`
CypD forward	5`-AGGAGGGAGGTCCATCTACG-3`
CypD reverse	5`-ACATCCATGCCCTCTTTGAC-3`

The samples used for RT-PCR were prepared as listed in Table 24 and 25.

Table 24: Sample preparation for GAPDH

2x Reaction buffer	12.5 µl
Sample	100-500 ng
Forward primer (5 µM)	1 µl
Reverse primer (5 µM)	1 µl
Taq polymerase	0.5 µl
RNase free water	ad 25 µl

Table 25: Sample preparation for CypA, CypB, CypD and PIN1

2x Reaction buffer	12.5 µl
Sample	100-500 ng
Forward primer (5 µM)	1 µl
Reverse primer (5 µM)	1 µl
Taq polymerase	1 µl
RNase free water	ad 25 µl

The RT-PCR steps for the amplification were set as listed in Table 26-29.

Table 26: RT-PCR cycler program for murine GAPDH

60°C	30 min.	
95°C	2 min.	
95°C	30 sec.	} x 26
57°C	1 min.	
70°C	2 min.	
70°C	10 min.	
4°C	∞	

Table 27: RT-PCR cycler program for murine CypA

60°C	30 min.	
95°C	2 min.	
95°C	30 sec.	} x 25
67°C	30 sec.	
70°C	1 min.	
70°C	10 min.	
4°C	∞	

Table 28: RT-PCR cycler program for murine CypB and CypD

60°C	30 min.	
95°C	2 min.	
95°C	30 sec.	x 27
55°C	30 sec.	
70°C	1 min.	
70°C	10 min.	
4°C	∞	

Table 29: RT-PCR cycler program for murine PIN1

60°C	30 min.	
95°C	2 min.	
95°C	30 sec.	x 24
54°C	1 min.	
70°C	1 min.	
70°C	10 min.	
4°C	∞	

2.12.4. Agarose gel electrophoresis

The PCR amplification products were visualized by an ethidiumbromid (EtBr) staining, which is a fluorescent agent that intercalates in DNA and can be then detected under UV-light. For this purpose the PCR samples were supplemented with 5 µl 10x loading dye and separated by agarose gel electrophoresis using 1.5 % agarose (Sigma Aldrich, Taufkirchen, Germany) suspended in 1x Trsi-Acetat-EDTA buffer (50x TAE stock, view Table 30). The agarose was dissolved in 1x TAE by heating in a microwave and after applying the suspension into a gel frame, 2 µl of a 10 mg/ml EtBr stock were added to 50 ml suspension and were stirred. After the gel became solid samples were added into the pockets of the gel and were allowed to run for 30-60 min. at 80 V. As a reference marker for size identification GeneRuler 100 bp Plus DNA Ladder (Thermo Scientific, Dreieich, Germany) was loaded on the gel. Separated PCR products were detected under UV-light (excitation 260 nm) with the Chemidoc Imaging System (Bio-Rad, München, Germany) and pictures were analyzed with the Quantity One software (Bio-Rad, München, Germany).

Table 30: 50x TAE buffer

Trizma® base	242 g
Glacial acetic acid	57.1 ml
0.5 M EDTA pH 8.0	10 ml
Bidest dH_2O	ad 1,000 ml

2.13. Statistical analysis

All data are given as means + standard deviation (SD). Statistical comparisons between multiple groups was performed by analysis of variance (ANOVA) followed by Scheffé's post hoc test or Bonferroni test. Calculations were achieved with the WinSTAT Standard Statistical Software (R. Fitch Software, Bad Krozingen, Germany).

3. Results

3.1. Glutamate sensitivity of HT22 cells

HT22 cells are immortalized mouse hippocampal neurons growing in an adherent monolayer with spindle shaped morphology. Despite lacking NMDA receptor expression, HT22 cells exhibit a high sensitivity to glutamate. The sensitivity of HT22 cells to glutamate varies depending on the cell density and the passage number of cells. Therefore, glutamate concentrations were used in a range from 2-7 mM and depending on the performed experiments time points were adjusted. After induction of apoptosis with glutamate HT22 cells round up and detach from the culture plate (Figure 8). Cell death occurred in a time- and dose-dependent manner, as cell viability analysis revealed determined by MTT assay (Figure 8A). Cell proliferation was detected by real-time impedance measurement using the xCELLigence system. A decrease of the Normalized Cell Index (NCI) due to a loss in impedance is associated with cell death induced by glutamate (Figure 8B).

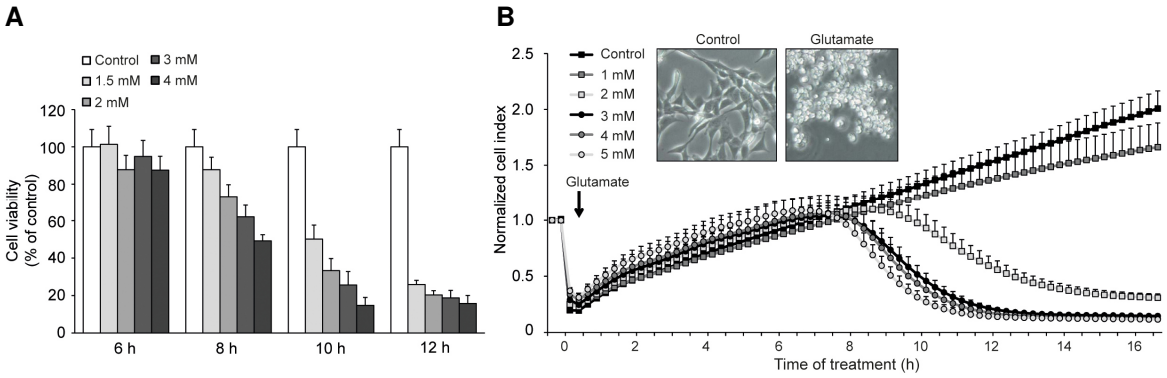

Figure 8: Glutamate-induced oxidative stress leads to decreased cell viability in HT22 cells

A: Glutamate treatment led to a decrease in cell viability in a concentration- and time-dependent manner as determined by the MTT assay (n=8). **B:** Photomicrographs (100x magnification) revealed alterations in the cell morphology after glutamate toxicity. HT22 cells were treated with different concentrations of glutamate and cell impedance was measured over time with the xCELLigence system and a loss in impedance which occurred after 7-9 h of treatment implicated cell death (n=6). Experiments were repeated at least three times and results are given as mean + SD.

DNA damage and fragmentation have been considered a hallmark of apoptosis, which occurs at a late and irreversible stage of cell injury after ischemia. However, DNA strand brakes induced by ROS represent an early event after neuronal injury [179]. The evaluation of DNA strand breaks after glutamate exposure in HT22 cells revealed a time-dependent increase in DNA fragmentation (Figure 9). The COMET assay was used to investigate DNA damage induced by glutamate. For this purpose, two categories were defined to quantify the displacement between the genetic material of the nucleus ('comet head') and the resulting 'tail', which occurred after DNA strand breaks ('with tail' or 'w/o tail', Figure 9A). HT22 cells were seeded in 24-well plates and after indicated time points the COMET assay was performed. After staining the DNA with Vista Green DNA dye, nuclei were visualized under an epifluorescence microscope (20x objective) and 200 nuclei were counted per condition. Glutamate exposure resulted in moderate DNA damage at early time points and was increased after 8-10 h, and after 14 h of treatment more than 55 % of cells exhibited DNA fragmentation (Figure 9B). The DNA damage inducing agent etoposide was used as positive control (21 h, 50 µM).

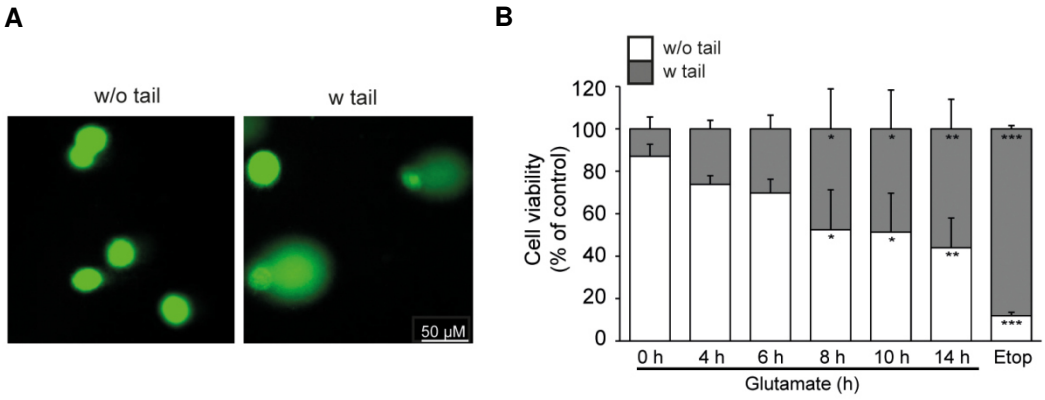

Figure 9: Time course of DNA damage after glutamate toxicity

A: Two categories ('with tail' and 'w/o tail') were defined to analyze DNA fragmentation induced by glutamate. Control cells exhibited no tail formation, while glutamate exposure led to a tail formation, which indicated DNA strand breaks. After indicated time points the COMET assay was performed and visualized DNA was assigned to the category 'with tail' (right panel) or 'w/o tail' (left panel). **B:** Quantification of 200 nuclei per condition revealed a moderate increase in DNA damage at early time points, which rose in a time-dependent manner (n=3). Etoposide was used as positive control. Experiments were repeated three times and results are given as mean +SD (***p< 0.001; **p< 0.01; *p< 0.05; ANOVA, Bonferroni test).

3.2. Mitochondrial dysfunction induced by glutamate

Glutamate exposure leads to a detrimental increase in ROS and due to this to high levels of lipid peroxides in HT22 cells (Figures 17 and 32; [72]). This feature of oxidative stress was accompanied by changes in the mitochondrial morphology and by enhanced mitochondrial fission. To quantify these changes, mitochondria were divided in three categories (Figure 10A). In healthy HT22 cells mainly category 1 mitochondria can be observed. They appear elongated and are spread all over the cytosol, forming a tubular network. Intermediate category 2 mitochondria are rounded up, but are still distributed in the cell body, while cells show normal morphological features and are still attached on the bottom of the culture plate. In contrary to living cells, apoptotic and damaged cells exhibit primarily category 3 mitochondria, which are fragmented and surround the nucleus. To evaluate the changes in mitochondrial morphology, cells were seeded in 8-well ibidi slides and prior to treatment they were stained for 30 minutes with the mitochondrial dye MitoTracker DeepRed. Following, glutamate was applied and after indicated time points cells were fixed with 4 % PFA. For quantification analysis 500 cells were counted blind per condition. The number of category 1 mitochondria was decreased, while the number of category 3 mitochondria was significantly increased after glutamate exposure, which is in line with decreased cell viability (Figure 10B).

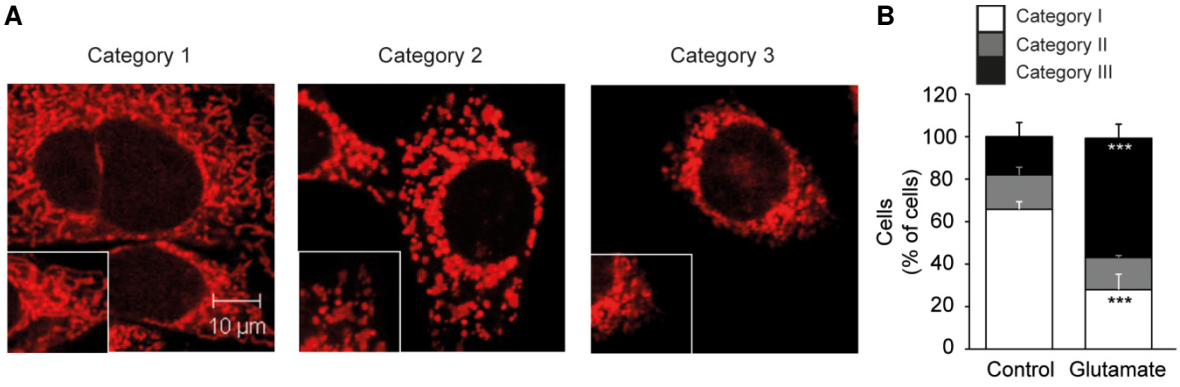

Figure 10: Categorization and quantification of mitochondrial morphology

A: Confocal images (63x objectives) represented MitoTracker DeepRed stained mitochondria which exhibited different mitochondrial morphology structures. Category 1: elongated, category 2: intermediate and category 3: fragmented mitochondria. **B:** Quantification of mitochondrial categories after glutamate toxicity (2 mM, 14 h) revealed elevated mitochondrial fragmentation which was represented in an increase of category 3 mitochondria. For each condition 500 cells were counted blind. Experiments were repeated three times and results are given as mean +SD. (***p< 0.001; ANOVA, Scheffé's test).

Another hallmark associated with cell death in HT22 cells is the loss of MMP. To analyze the impact of glutamate on MMP, cells were seeded in 24-well plates and after 24 h cells were treated with 3 mM glutamate. After 15 h of treatment the medium of the culture plate was collected for each sample and cells were trypsinized and combined. Afterwards all samples were stained with TMRE for 20 minutes and washed once in 1x PBS. Since TMRE stains only healthy mitochondria, a decrease in red fluorescence could be detected in damaged cells by FACS-analysis (Figure 11). This decrease implicated a loss of MMP in HT22 cells due to oxidative stress, which is in accordance with elevated mitochondrial fission.

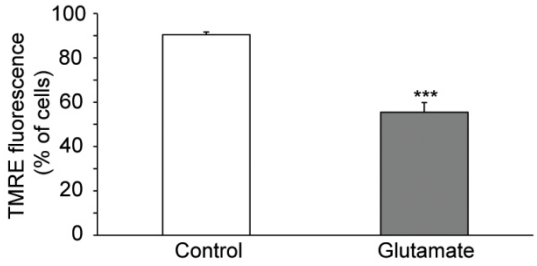

Figure 11: Glutamate toxicity results in impaired MMP

HT22 cells were treated with glutamate (15 h, 3 mM) and afterwards stained for 20 min. with TMRE and subsequently analyzed by FACS-analysis, which illustrated a loss in MMP after glutamate toxicity (n=4). Experiments were repeated three times and results are given as mean +SD. (***p< 0.001; ANOVA, Scheffé's test).

3.3. AIF and CypA are mediators of glutamate-induced cell death in HT22 cells

3.3.1. Translocation of AIF and CypA to the nucleus after glutamate toxicity

One of the pivotal occasions of apoptotic processes is the opening of the mitochondrial permeability transition pore, which is under control of Bcl-2 family members, inducing the release of pro-apoptotic proteins from the mitochondrial intermembrane space, such as Cytc or AIF [180–182]. Under physiological conditions, AIF is anchored in the inner mitochondrial membrane and upon induction of apoptosis it is released from the mitochondria and translocates to the nucleus where it induces, in a caspase-independent manner, DNA degradation and chromatin

condensation [54,58,59]. In HT22 cells this phenomenon was first described by Landshamer et al. and later on by others, that high extracellular glutamate concentrations induce the release and the translocation of AIF from the mitochondria to the nucleus resulting in cell death [70,72,183]. To illustrate the localization and after glutamate exposure the translocation of AIF in this study, cells were placed in 8-well ibidi slides and after glutamate treatment and fixation with 4% PFA, cells were incubated with an AIF primary antibody, afterwards with the corresponding conjugated secondary antibody and following images were acquired using a confocal microscope. DAPI was used for counterstaining of the nuclei. Under control conditions AIF is localized in the mitochondria. However, after glutamate toxicity AIF was released from the mitochondria and translocated within 12 h to the nucleus (Figure 12A). These findings were confirmed by western blot analysis of nuclear extracts. In control conditions AIF was not detected in the nucleus, while after 10-12 h of glutamate exposure AIF protein levels increased in nuclei (Figure 12B).

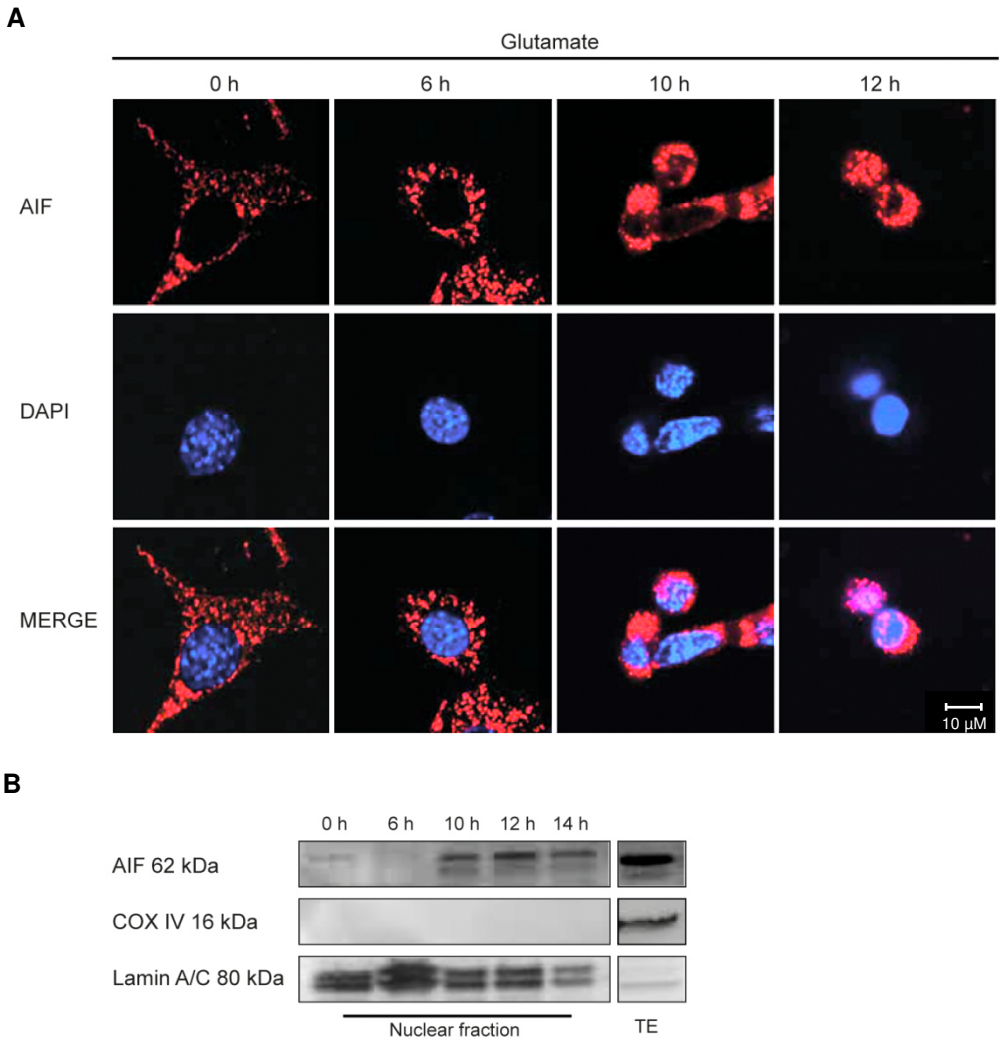

Figure 12: Glutamate-induced translocation of AIF to the nucleus

A: Confocal images (63x objective) exhibited the translocation of AIF (red) from the mitochondria to the nucleus (DAPI, blue) after glutamate exposure (2 mM) in a time-dependent manner. **B:** Western blot analysis of nuclear extracts illustrated an increase in nuclear AIF after 10-12 h of glutamate treatment (2 mM). Lamin A/C was used as nuclear marker and CoxIV was used as mitochondrial marker to exclude mitochondrial cross-contamination; TE: total extract

Recent evidence suggests that AIF alone is not able to induce chromatinolysis and that therefore CypA is needed [62]. In HT22 cells, CypA is mainly localized in the cytosol, however, it can be also found in the nucleus under control conditions. Within 6-8 h after the onset of glutamate CypA translocates to the nucleus (Figure 13). Interestingly, CypA translocation occurred before AIF translocation, indicating that CypA and AIF translocated independent of each other to the nucleus.

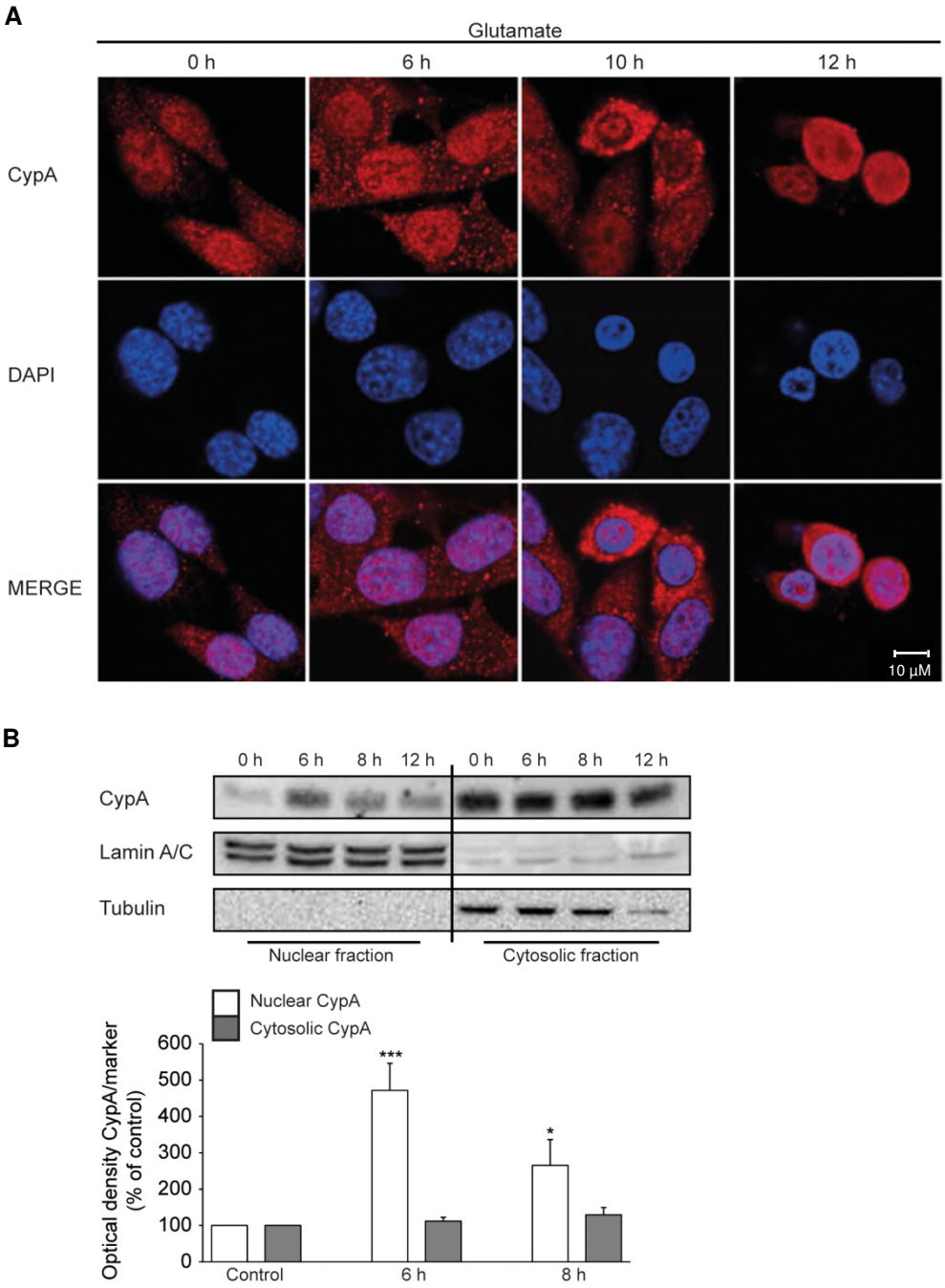

Figure 13: CypA translocation to the nucleus is induced by glutamate

A: Confocal images (63x objective) revealed the translocation of CypA (red) from the cytosol to the nucleus (DAPI, blue) after glutamate exposure (2 mM) in a time-dependent manner. **B:** CypA translocation to the nucleus was confirmed by western blot analysis of nuclear extracts after glutamate treatment (2 mM). Lamin A/C was used as nuclear marker and tubulin was used as a cytosolic marker to exclude cross-contamination. Bar graphs depict protein amounts of CypA in the nucleus and in the cytosol (n=3). Results are given as mean +SD. (***p< 0.001; *p< 0.05; ANOVA, Scheffé's test).

3.3.2. CypA and AIF build a pro-apoptotic complex after glutamate toxicity

The physical and functional interaction of AIF and CypA was discovered by Candé and colleagues. Since both proteins alone are not able to mediate chromatinolysis, the formation of a pro-apoptotic complex of AIF and CypA is required to induce chromatin condensation [62].

Under physiological conditions, CypA and AIF do not co-localize in HT22 cells as it was visualized by confocal images and determined by immunoprecipitation (IP) experiments (Figure 14). However, upon glutamate toxicity AIF and CypA do not only translocate to the nucleus but also co-localize in the nucleus as confocal pictures revealed (Figure 14A). IP experiments confirmed the interaction of CypA and AIF after glutamate exposure. CypA was not detected as interaction partner of AIF in control conditions, while after glutamate challenge the interaction could be observed (Figure 14B). The IP experiment was also performed vice versa. Immunoprecipitation of CypA and the following western blot analysis of co-immunoprecipitated AIF revealed that in control conditions AIF was not bound to CypA, while after glutamate toxicity AIF could be detected as interaction partner of CypA (Figure 14C).

Taken together, these findings revealed that AIF and CypA translocate to the nucleus and interact after glutamate toxicity in HT22 cells.

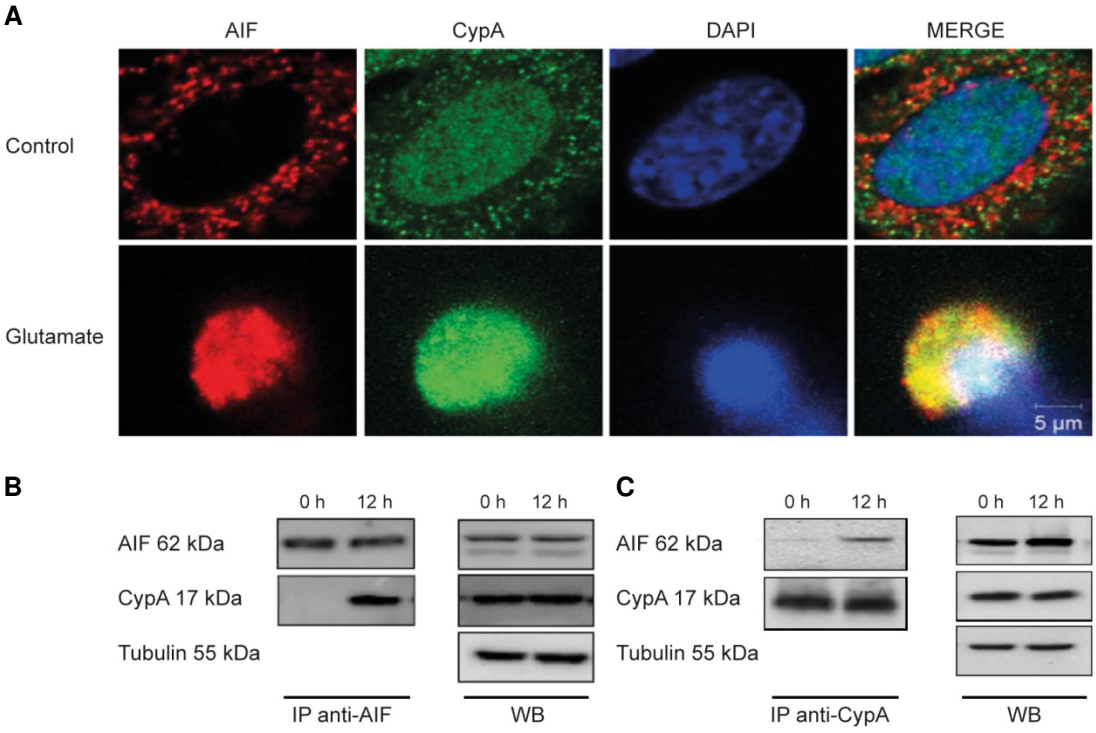

Figure 14: AIF and CypA build a pro-apoptotic complex after glutamate challenge

A: Glutamate (12 h, 2 mM) induced the translocation of AIF (red) and CypA (green) to the nucleus (DAPI, blue), which was illustrated by confocal images (63x objective). Upper panels show control conditions while lower panels exhibit glutamate-induced translocation of both proteins to the nucleus and the pro-apoptotic complex formation (yellow). **B:** Immunoprecipitation analysis of AIF protein (2.5 mg of total protein lysates) confirmed the interaction of AIF and CypA after glutamate exposure (12 h, 2 mM). The left panel illustrates western blot analysis of the AIF pulldown. The interaction of AIF and CypA was detected only after glutamate exposure. The right panel shows western blot analysis of total protein lysates with tubulin as loading control. **C:** Reversed experimental set up of IP experiments shown in figure B. Pull down of CypA and following western blot analysis of AIF after glutamate challenge.

3.4. The particular role of CypA in glutamate-induced cell death

Since AIF has no DNase activity and the interaction of AIF and CypA is necessary to induce cell death, the next issue was to investigate the role of CypA in glutamate-induced cell death in HT22 cells. For this purpose the knockdown of CypA was achieved by small interfering RNA (siRNA) transfection of HT22 and the impact on cell viability and mitochondrial function was verified.

3.4.1. CypA siRNA prevents cell death in HT22 cells

The cyclophilin family consists of different isozymes among them CypA, B and D are the main representatives which are known to be involved in different cell death

mechanisms. ER-localized CypB exhibits pro-survival features and is associated with ER stress-induced apoptosis [159]. CypD, a major regulator of the mitochondrial permeability transition pore, is involved in pore opening which is triggered by elevated Ca^{2+}-levels or oxidative stress and thereby mediates the release of pro-apoptotic factors leading to cell death [184].

To prove the specificity of the CypA siRNA (siCypA), mRNA levels of all three cyclophilins were analyzed by RT-PCR. Only CypA mRNA levels were depleted compared to CypB and CypD, which demonstrated the specificity of the siCypA (Figure 15A and B). The knockdown of CypA at the protein level was analyzed by western blot analysis (Figure 15C). SiCypA was used at a concentration of 25 nM and scrambled siRNA (siScr), a nonsense sequence of the siRNA target sequence, was used as negative control in all experiments.

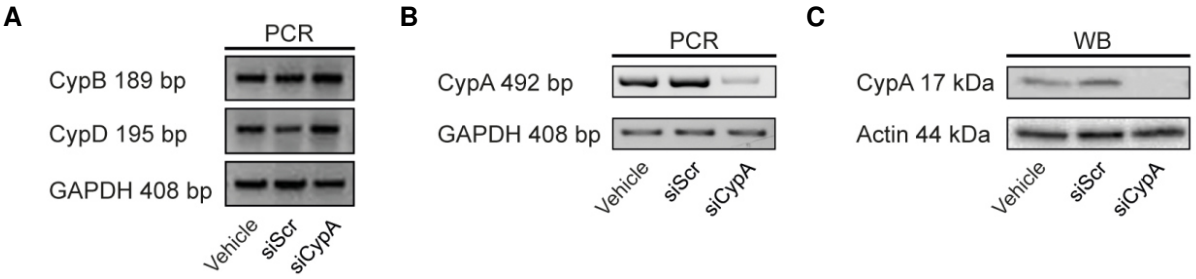

Figure 15: CypA knockdown on mRNA and protein levels

A: RT-PCR analysis of cyclophilin mRNA revealed a specific knockdown of CypA compared to CypB and CypD. The transfection was performed with 25 nM siCypA for 48 h. GAPDH was used as loading control. **B:** Western blot analysis showed the knockdown of CypA at the protein level. 25 µg were loaded on the gel and actin was used as loading control.

To evaluate the impact of CypA silencing after glutamate challenge in HT22 cells, cell viability was measured by MTT assay. While glutamate treatment resulted in depleted cell viability below 25%, CypA silencing could prevent this decrease and restored cell viability up to 80% of control levels (Figure 15A). Furthermore, morphological alterations due to glutamate treatment were prevented (Figure 16B). This protective effect was confirmed by AnnexinV/propidium iodide (AVPI) staining and subsequent FACS-analysis. After 12 h of glutamate treatment nearly 40% of cell death was detected in controls and cells transfected with scrambled siRNA. CypA silencing reduced cell death almost to control levels (Figure 16C). In this experiment

the Bid inhibitor BI-6c9 was used as positive control. In addition the protective effect of CypA depletion was confirmed by real-time impedance measurements with the xCELLigence system (Figure 16D). After glutamate exposure measured cell impedance started to decrease within 6-7 h of treatment which resulted in cell death. After another 3-5 h the cell index was completely decreased in glutamate-treated cells. In contrast, glutamate-induced loss in NCI could completely be prevented by silencing of CypA (12 h, 2 mM; Figure 16D).

Overall, these data indicate a crucial role for CypA in glutamate-induced cell death, as silencing of CypA results in increased cell viability and depicts a protective effect of morphological alterations in HT22 cells.

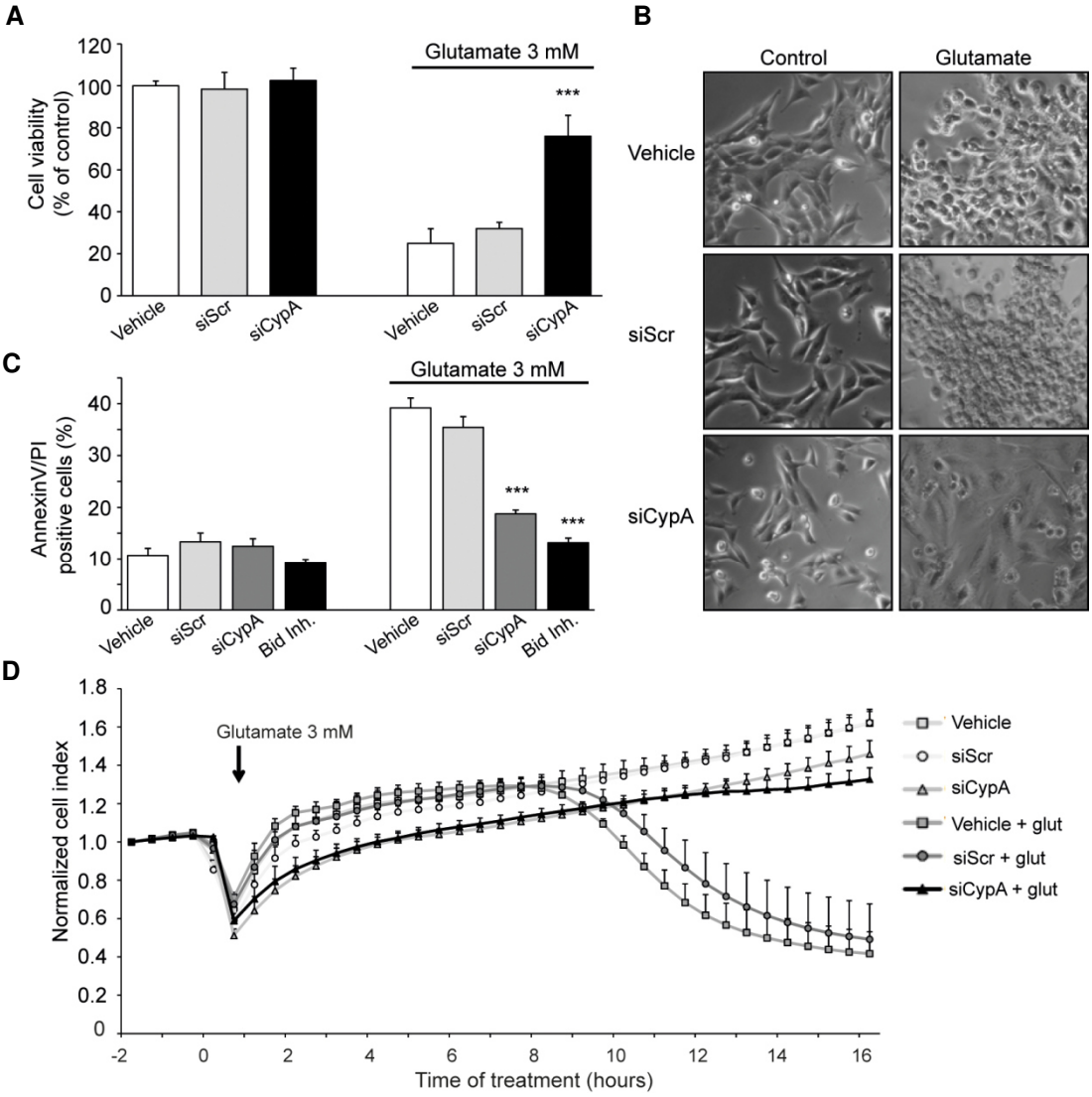

Figure 16: Silencing of CypA increases cell viability after glutamate toxicity in HT22 cells

A: After 48 h of siCypA transfection cells were treated with 2 mM glutamate for 12 h and cell viability was determined by MTT assay. Vehicle- and siScr-treated control cells exhibited a decrease in cell viability, which could be prevented by CypA depletion (n=8). **B:** Microphotographs exhibit control-like cell morphology of CypA knockdown cells after glutamate exposure. **C:** FACS-analysis of transfected HT22 cells after AVPI staining revealed an increase in cell death of glutamate-treated controls, which was prevented by CypA silencing. **D:** Cells were seeded and transfected in 96-well E-plates (4.000 cells/well) and after 48 h cell death was induced by glutamate. Cell impedance was detected by real-time measurements with the xCELLigence system, which depicted decreased cell viability in vehicle- and siSc- treated control cells compared to siCypA-treated cells (n=6). Experiments were repeated three times and results are given as mean +SD (***p< 0.001; ANOVA, Scheffé's test).

3.4.2. Lipid peroxidation is decreased after glutamate toxicity and CypA silencing

In HT22 cells glutamate toxicity leads to enhanced formation of ROS and increased lipid peroxidation, causing neuronal cell death. As described by Tobaben et al. a two-step increase in ROS occurs after glutamate toxicity. The first slight increase in lipid peroxidation was detected within the first 6 h, while the much more pronounced second increase occurred at later time points (~8-17 h) [72]. To analyze the impact of CypA on lipid peroxidation, cells were stained with BODIPY after indicated hours of glutamate challenge and following analyzed by FACS-analysis. Silencing of CypA decreased lipid peroxidation after 10 h of glutamate exposure. However, levels of lipid peroxides could not be decreased to control levels (Figure 17A and B).

This indicates that CypA depletion abolishes the second (mitochondrial) increase in ROS without affecting the first ROS increase.

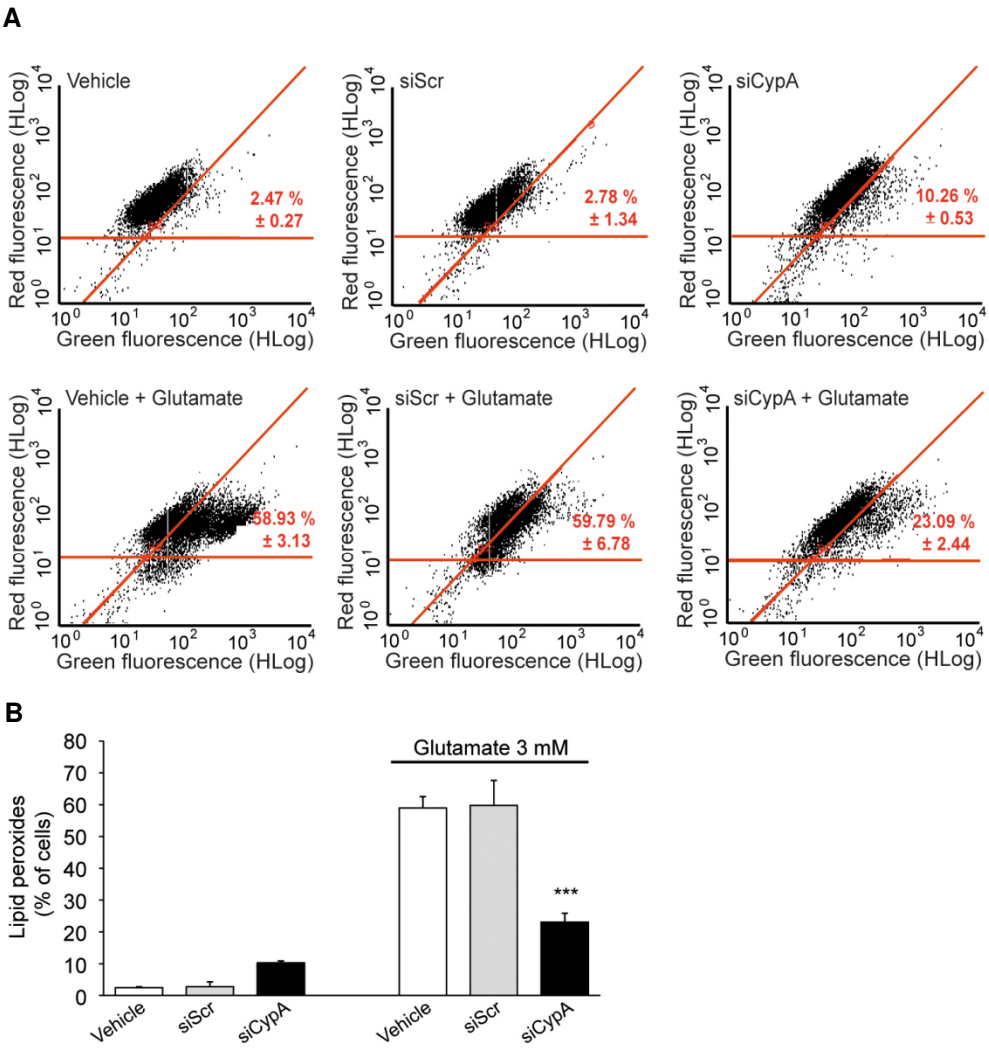

Figure 17: Glutamate-induced lipid peroxidation was decreased after CypA silencing

A: HT22 cells were transfected with 25 nM siCypA in 24-well plates and after 48 h treated with 3 mM glutamate for 14 h. Glutamate induced the production of lipid peroxides, which was reduced in conditions of siCypA treatment (n=3). **B:** Quantification of cells with lipid peroxides. Experiments were repeated three times and results are given as mean +SD (***p< 0.01; ANOVA, Scheffé's test).

3.4.3. CypA silencing prevents mitochondrial AIF release, the impairment of the MMP and reduces mitochondrial fission

As previous results depicted, the interaction of CypA and AIF is necessary to induce cell death in HT22 cells. The next issue of interest was to analyze the translocation of AIF from the mitochondria to the nucleus after CypA depletion and glutamate exposure. For this purpose, cells were seeded in 8-well ibidi slides and were treated after 48 h with 2 mM glutamate for 12 h. Accordingly, immunocytochemistry was

performed to visualize AIF and nuclei, which were counterstained with DAPI. Images were taken with a confocal microscope (63x objective). Upon glutamate treatment AIF translocated to the nucleus in siScr-treated cells. However, after CypA silencing AIF was not released from the mitochondria (Figure 18)

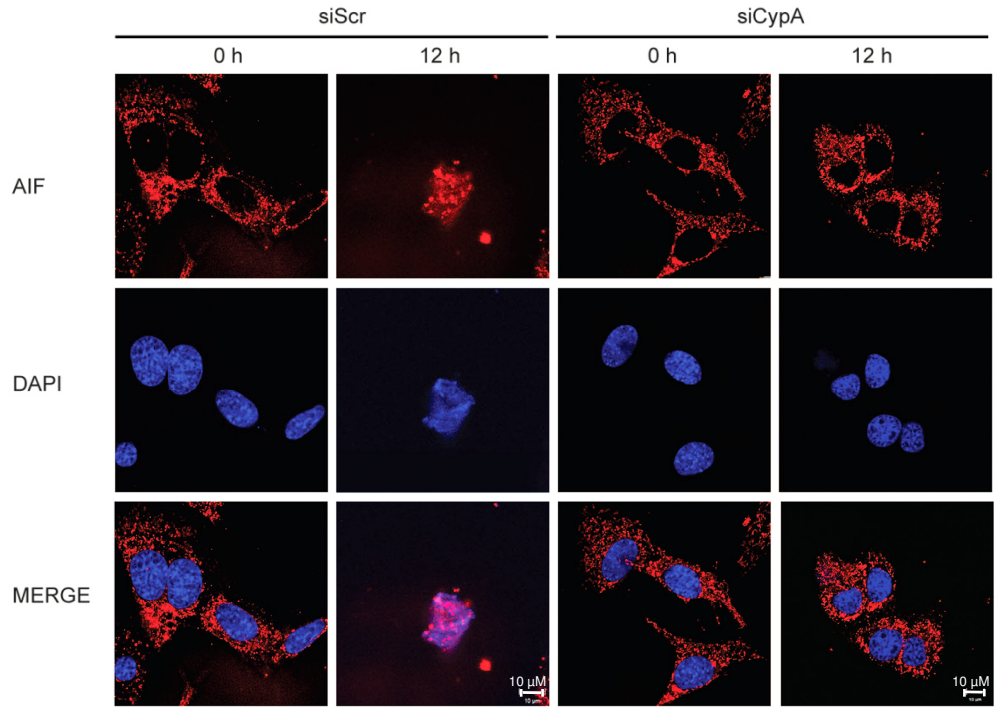

Figure 18: CypA silencing prevents AIF release from the mitochondria after glutamate toxicity

Confocal images (63x objective) demonstrated the release of AIF (red) from the mitochondria to the nucleus (DAPI, blue) after glutamate toxicity (2 mM, left panels). This release of AIF was prevented in CypA knockdown cells (right panels).

Recent studies suggest that intrinsic death pathways are linked to extensive mitochondrial fragmentation [4,185–187,188]. To gain more insight into the role of CypA acting upstream of mitochondrial levels, as the lethal AIF release was prohibited by CypA silencing, the present study examined, whether CypA has even regulatory effects on mitochondrial dynamics after glutamate challenge in HT22 cells. The depletion of CypA levels with siRNA prevented mitochondrial fission induced by glutamate and prohibited the characteristic shift from elongated mitochondria (category 1) to small, highly fragmented organelles (category 2 and 3, Figure 19).

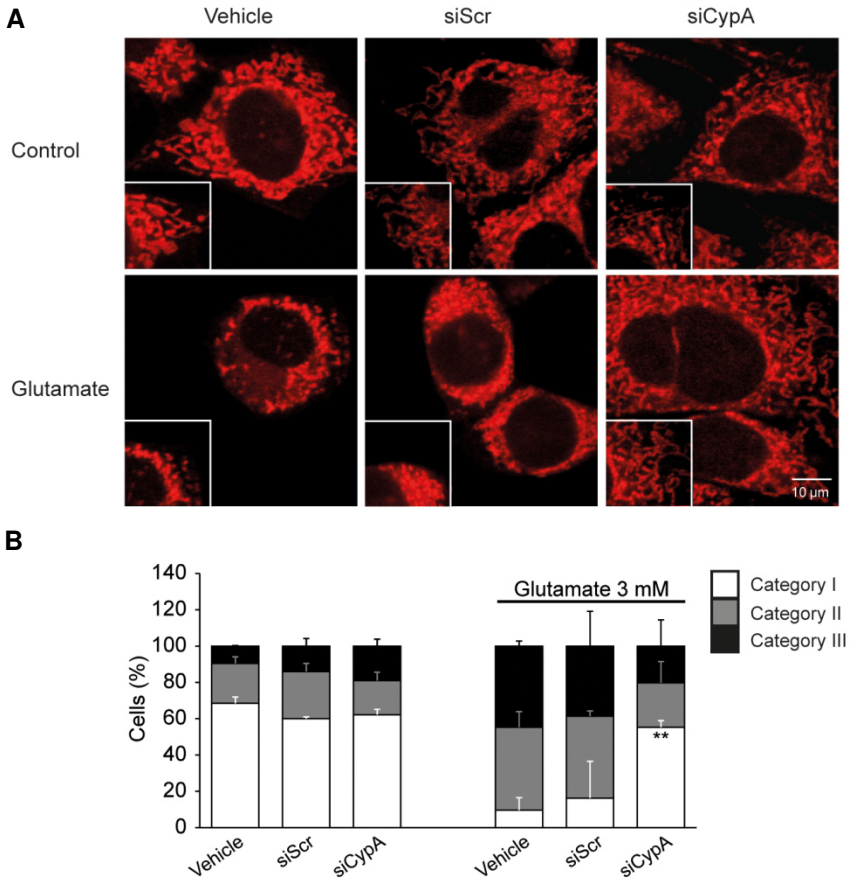

Figure 19: Silencing of CypA prevents glutamate-induced mitochondrial fragmentation

A: HT22 cells were transfected with 25 nM siCypA in 8-well ibid slides and after 48 h cells were stained with MitoTracker DeepRed for 30 min. and subsequently treated with 2 mM glutamate for 12 h. Confocal images (63x objective) showed glutamate-induced mitochondrial fragmentation, which was prevented by siCypA. **B:** Quantification of mitochondrial categories revealed a decrease in category 3 and an increase in category 1 mitochondria in CypA knockdown cells compared to vehicle- or siScr-treated control cells. For each condition 500 cells were counted blind. Experiments were repeated three times and results are given as mean +SD (**p< 0.01; ANOVA, Scheffé's test).

The loss of MMP is a major feature of glutamate-induced cell death in HT22 cells that is associated with mitochondrial fragmentation and precedes the lethal release of AIF and execution of caspase-independent cell death [70,71,173]. Since CypA is assumed to work upstream of mitochondrial demise after glutamate challenge, the impact of CypA on MMP was analyzed by TMRE staining and subsequent FACS-analysis. The impairment of the MMP was detected by a loss in red TMRE-fluorescence, which occurred after 17 h of glutamate treatment (Figure 20). This apoptotic feature was abolished after CypA silencing (Figure 20). Carbonylcyanide-3-

chlorophenylhydrazone (CCCP) was used as positive control to illustrate the loss of MMP.

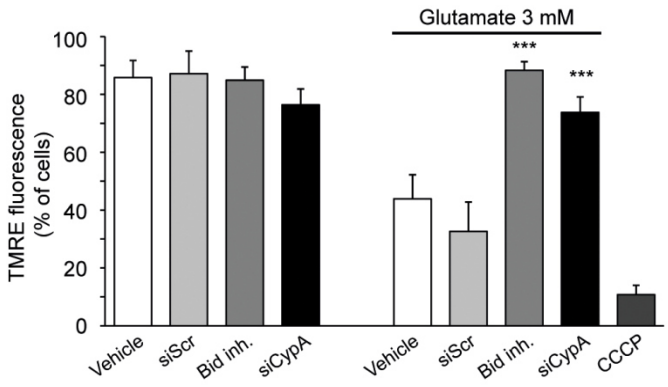

Figure 20: CypA knockdown restores MMP

After 48 h of siCypA transfection HT22 cells were treated with 3 mM glutamate for 17 h and were afterwards stained with TMRE for 20 min. SiCypA treatment prevented the impairment of the MMP induced by glutamate. Experiments were repeated three times and results are given as mean +SD (***p< 0.001; ANOVA, Scheffé's test).

These findings implicate, that CypA is not only acting as a downstream mediator of mitochondrial demise, but also acts upstream of mitochondrial levels, as CypA siRNA prevented glutamate-induced AIF release, preserved mitochondrial morphology alterations and prevented the impairment of the MMP.

3.4.4. Influence of CypA silencing on cell cycle phases

The protective effect of CypA silencing in HT22 cells in conditions of oxidative stress and the impact on mitochondrial morphology and function have been discovered in this study. However, the mechanism is still elusive. Cyclophilins were linked in the last years as molecular targets to affect cell cycle phases [163,189]. Hence, the impact of CypA silencing on the different cell cycle phases was investigated using the Guava® Cell Cycle Assay. After transfection of HT22 cells in 24-well plates with CypA siRNA for 48 h, cells were stained and subsequently analyzed by FACS-analysis. This experiment revealed that CypA silencing had no impact on cell cycle phases (Figure 21). Nocodazol induced a G2/M cell cycle arrest and was used as a positive control.

These results imply that in HT22 cells CypA has no influence on the cell cycle and that depletion of CypA and the resulting protective effect after glutamate challenge is not due to changes in cell cycle phases.

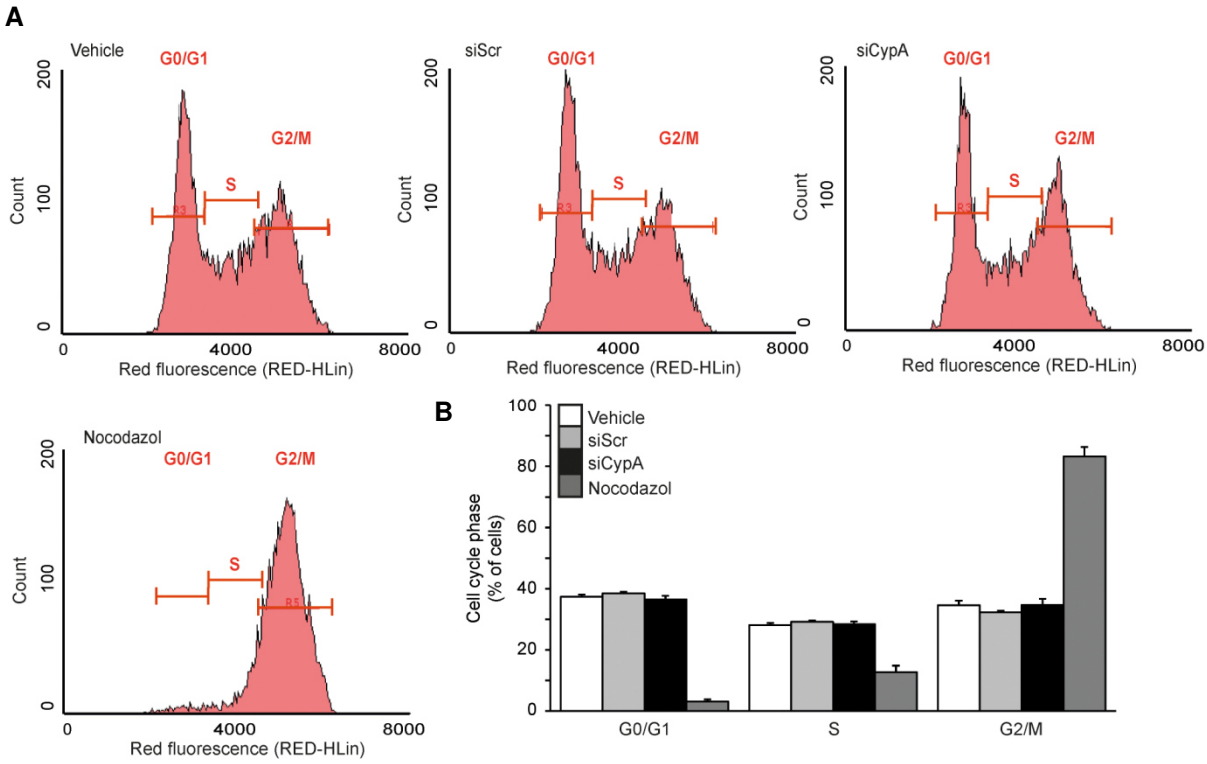

Figure 21: CypA siRNA does not alter cell cycle phases in HT22 cells

A: HT22 cells were transfected with 25 nM siCypA and after 48 h cell cycle phases were determined by PI staining and FACS-analysis. Silencing of CypA did not alter stages of cell cycle phases in HT22 cells. **B:** Assessment of cell numbers in each cell cycle phase (n=3). Nocodazol treated cells arrested with a G2/M phase DNA content and were used as a positive control. Experiments were repeated three times and results are given as mean +SD.

3.4.5. The role of H2AX in glutamate toxicity in HT22 neurons

Recently, besides CypA another important binding partner of AIF has been discovered, namely the histone H2AX. Baritaud and colleagues revealed H2AX as '*the missing link'* in AIF-mediated caspase-independent cell death. H2AX is necessary for the interaction of AIF and CypA in cell death pathways induced by extensive DNA-damage, which is provoked by alkylating substances, such as 1-methyl-2-nitro-1-nitrosoguanidine (MNNG) [63]. To evaluate the role of H2AX in glutamate toxicity in HT22 cells, the histone was depleted by siRNA transfection (Figure 22A) and afterwards cells were treated with 7 mM glutamate. As the MTT assay revealed the depletion of H2AX had no impact on cell viability after glutamate exposure. The same decrease in cell viability was measured in H2AX knockdown cells as in vehicle-treated control cells (Figure 22B). This finding was confirmed by real-time impedance measurements with the xCELLigence system, demonstrating that silencing of H2AX exhibited no protective effect against oxidative stress-induced cell death in HT22 cells (Figure 22C).

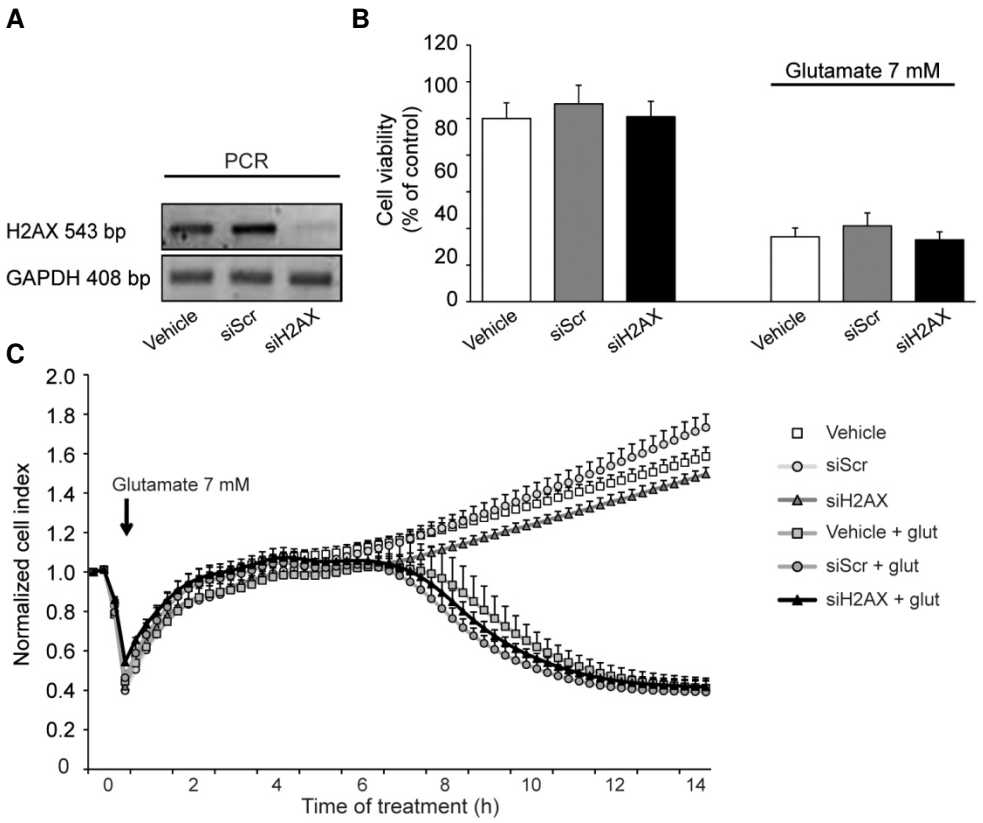

Figure 22: H2AX siRNA does not prevent glutamate-induced cell death in HT22 cells

A: H2AX mRNA levels were depleted by siRNA transfection and analyzed by RT-PCR. The transfection was performed with 20 nM siH2AX for 30 h and GAPDH was used as loading control. **B:** SiH2AX transfected HT22 cells were treated with 7 mM glutamate and cell viability was determined by MTT assay (15.5 h). Silencing of H2AX did not rescue cells from cell death (n=8). **C:** XCELLigence measurements depicted that a downregulation of H2AX did not provide protective effects upon glutamate treatment (n=6). Experiments were repeated three times and results are given as mean +SD.

3.5. The involvement of the PPIase Pin1 in neuronal cell death

The family of PPIases consists beside cyclophilins also of the parvulin Pin1, which is known to mediate the activation of the mitochondrial apoptotic pathway [156,190]. Since previous results of this work revealed an important role for the immunophilin CypA in glutamate-induced cell death, the next step was to evaluate the contribution of Pin1, as another member of the PPIase family, to cell death in HT22 cells.

3.5.1. Pin1 inhibition promotes cell survival

Pin1 was identified to be an interacting partner of the Ser65-phosphorylated BH-3 only protein Bim_{EL}, thereby stabilizing Bim_{EL}, which results in neuronal apoptosis by activating the mitochondrial machinery [156]. To evaluate the role of Pin1 in glutamate-induced cell death in HT22 cells, the Pin1 inhibitor Br57 was applied with or without glutamate and the impact on cell viability was analyzed. In the presence of glutamate, Br57 led to an increase in cell viability as determined by the MTT assay and real-time impedance measurements with the xCELLigence system (Figure 23A). Furthermore, morphological alterations due to glutamate were prevented (Figure 23). This protective effect was confirmed by AVPI staining and subsequent FACS-analysis, which revealed a decrease in cell death after Pin1 inhibition and glutamate exposure (Figure 23B).

These data indicate an important role for Pin1 in glutamate toxicity, as the Pin1 inhibitor Br57 led to sustained increased cell viability and reduced cell death.

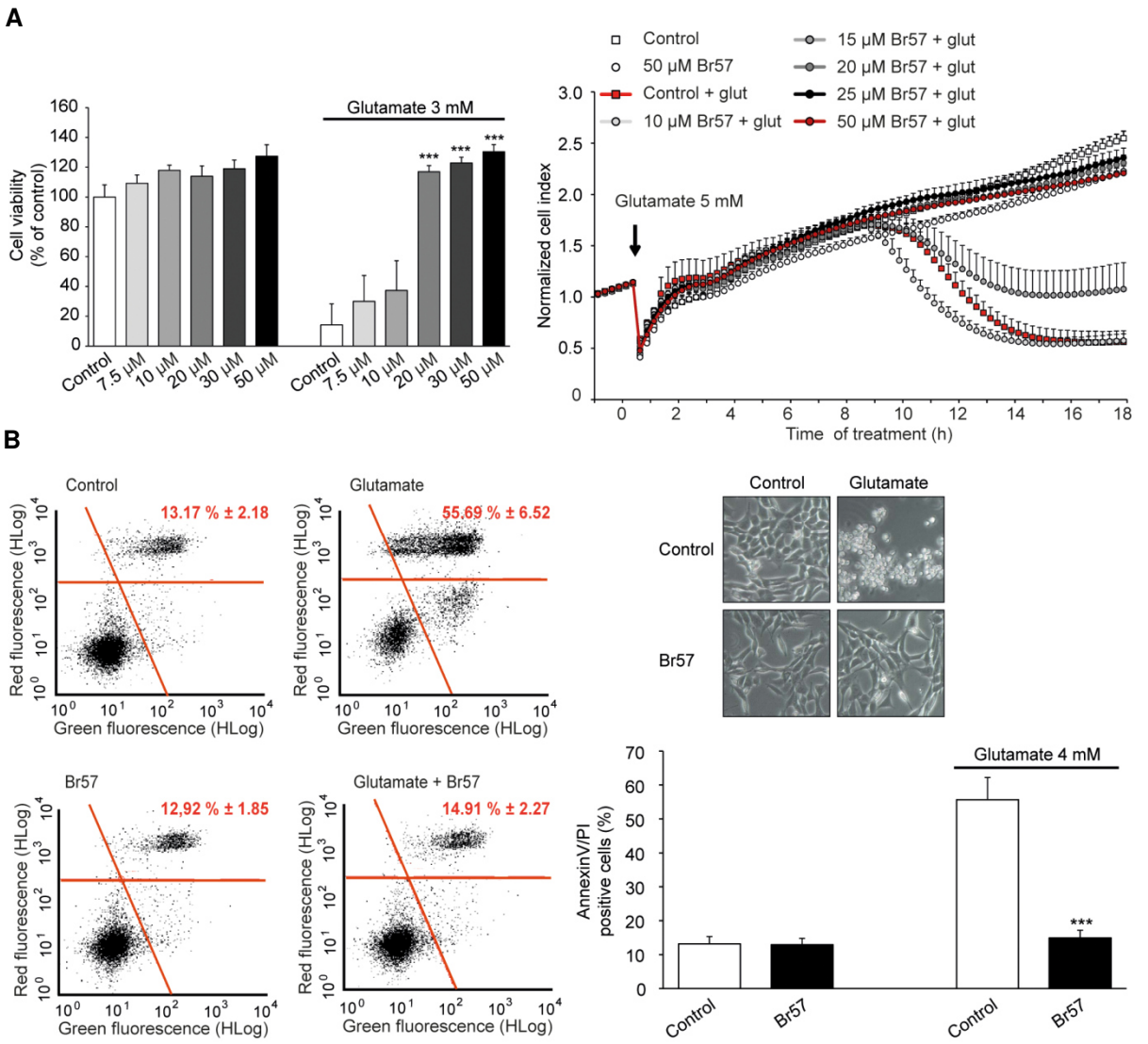

Figure 23: Pin1 inhibition with Br57 provides protective effects against glutamate toxicity

A: HT22 cells were treated with 50 µM Br57 with or without 3 mM glutamate and after 15.5 h cell viability was analyzed by MTT assay (left panel, n=8) and real-time impedance measurements with the xCELLigence system (right panel, n=6). As both methods confirm, Br57 was able to significantly increase cell viability. **B:** Cell death was determined by AVPI staining and subsequent FACS-analysis. Br57 decreased cell death after glutamate toxicity (14 h, 4 mM). Quantification of double positive stained cells (lower right panel, AV and PI positive, n=4). Experiments were repeated three times and results are given as mean +SD (***p< 0.01; ANOVA, Scheffé's test).

3.5.2. Pin1 inhibition shifts mitochondrial morphology towards intermediate category 2 mitochondria and restores the MMP

It has been observed that Pin1 is associated with mitochondrial death pathways [156]. To gain further insight into Pin1-mediated cell death and the impact on mitochondrial morphology, Br57 was applied for 17 h in the presence or absence of glutamate (5 mM) and mitochondrial morphology alterations were evaluated by counting 500 cells per condition blind. The glutamate-induced shift from category 1 to category 3 mitochondria in control cells could be prevented by Pin1 inhibition. However, the quantification of mitochondrial morphology revealed a strong shift towards intermediate category 2 mitochondria independent of glutamate treatment (Figure 24A and B). Both, in Br57 treated control cells and in conditions of glutamate treatment, Pin1 inhibition led to an increase in category 2 mitochondria to nearly 80% (Figure 24B). On the basis of the observed alterations in mitochondrial morphology induced by the Pin1 inhibitor Br57, the next step was to analyze the influence of Br57 on the MMP. As described above glutamate toxicity led to an impairment of the MMP in HT22 cells. FACS-analysis of HT22 cells revealed a protective effect of Br57 as the inhibition of Pin1 prevented the loss of MMP induced by glutamate (15.5 h, 4 mM, Figure 24C). However, as maybe expected based on previous results of changes in mitochondrial morphology, MMP-analysis did not show any differences. Br57-treated control cells showed equal MMP compared to non-treated control cells.

These findings depict a protective effect of Br57 against glutamate-induced mitochondrial fragmentation and the loss of MMP. However, Pin1 inhibition resulted in pronounced mitochondrial fission with a shift towards category 2 mitochondria, which was nevertheless accompanied by increased cell viability.

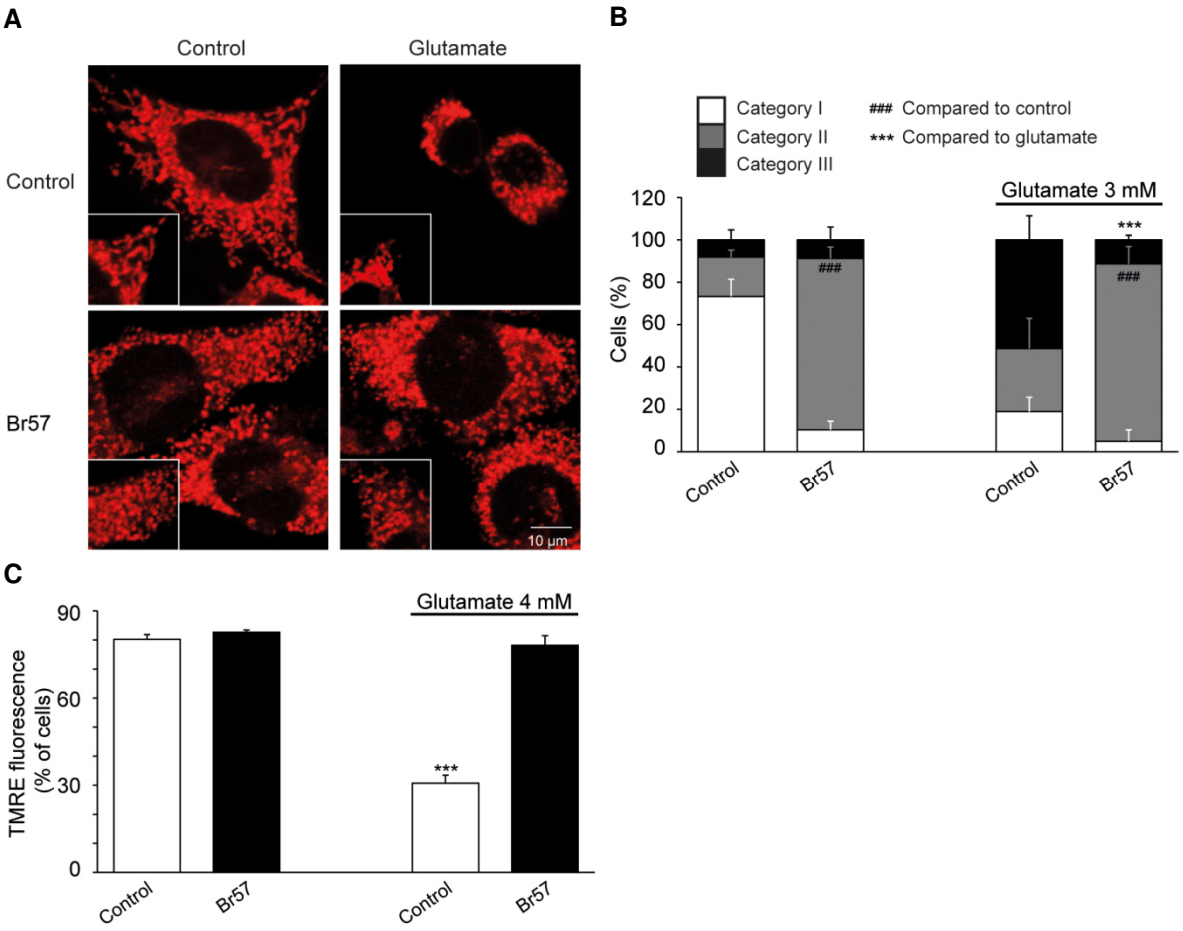

Figure 24: Br57 alters mitochondrial morphology and restores MMP after glutamate toxicity in HT22 cells

A: Confocal images (63x objective) of MitoTracker DeepRed stained mitochondria illustrated a pronounced shift towards category 2 mitochondria of Br57-reated cells (independent of glutamate treatment). **B:** Quantification of mitochondria revealed a decrease in mitochondrial fragmentation after Pin1 inhibition and glutamate exposure (15 h, 4 mM), however an increase of category 2 mitochondria was observed. For each condition 500 cells were counted blind. **C:** Br57 prevented the impairment of MMP after glutamate toxicity (15.5 h, 4 mM) determined by FACS-analysis of TMRE stained HT22 cells (n=4). Experiments were repeated three times and results are given as mean +SD ($^{###}$/***$p < 0.001$; ANOVA, Scheffé's test).

3.5.3. Pin1 inhibition prevents ATP depletion and maintains mitochondrial respiration after glutamate toxicity

The present data demonstrated the impact of Pin1 on mitochondrial morphology and on MMP. To investigate the role of Pin1 on mitochondrial metabolism, ATP levels were analyzed after Br57 and glutamate treatment. Glutamate toxicity (15.5 h, 4 mM) led to a strong decrease in ATP levels, which could be attenuated by the inhibition of Pin1 with Br57. However, the inhibition of Pin1 alone resulted in a slight decrease of about 20% in ATP levels in Br57-treated control cells (Figure 25A). Since the main ATP production and energy generation is produced by the process of Oxphos in the inner mitochondrial membrane [29], the influence of Pin1 on mitochondrial respiration was examined by measuring the oxygen consumption rate (OCR) with the XF96-Seahorese system as described before [191]. HT22 cells were seeded in XF96-well microplates and after glutamate (16 h, 3 mM) and/or Br57 treatment, growth medium was replaced with assay medium and cells were incubated for 60 min. at 37 °C. Three baseline measurements were recorded before the addition of the different compounds. Oligomycin, which is an inhibitor of ATP synthase was added in Port A (20 µl) at a final concentration of 3 µM. Inhibiting the ATP synthase results in a decreased dissipation of the proton gradient, which in turn leads to a decline in the OCR. FCCP, an uncoupler of the electron transport chain (22.5 µl in Port B) was applied at a concentration of 0.4 µM, reducing the proton gradient, which results in an enhanced OCR. Rotenone/Antimycin A, inhibitors for complex I and III (25 µl in Port C) were finally added at a concentration of 1 µM to block the whole mitochondrial respiratory chain, leading to a complete decrease in OCR [192]. Br57 alone increased the mitochondrial basal respiration and as also detected with this method, the ATP production was reduced in Br57-treated control cells (Figure 25B, area A-B). In the presence of glutamate Br57 increased maximal respiration compared to glutamate treated control cells (Figure 25B, area B-C).

These data contribute to the assumption that Pin1 inhibition directly affects mitochondrial metabolism and function.

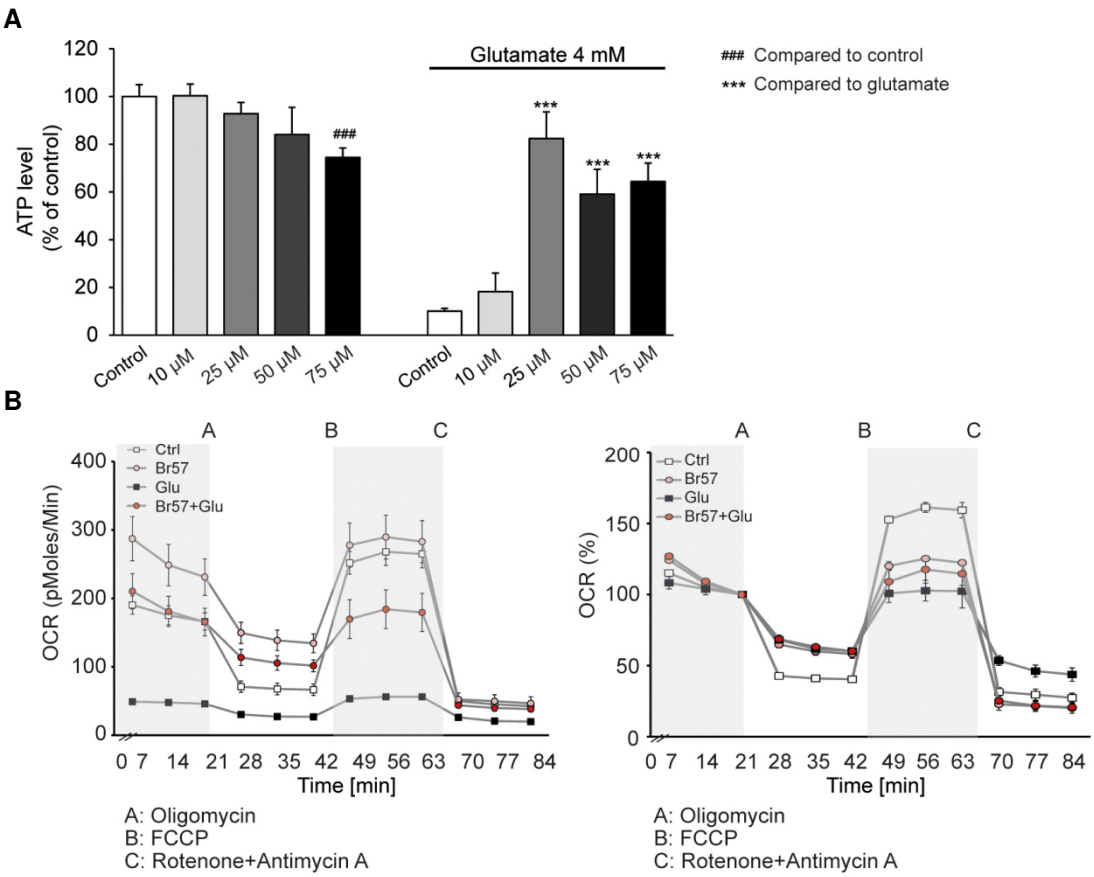

Figure 25: Br57 prevents ATP depletion and influences mitochondrial respiration after glutamate toxicity

A: HT22 cells were treated with different concentrations of Br57 with or without 4 mM glutamate and after 15.5 h ATP levels were determined by luminescence measurements. Glutamate-induced ATP depletion was prohibited with Br57 (n=8). Br57 treatment alone led to an ATP decrease of ~20 % (n=8). **B:** Br57 elicited an increase in basal respiration and reduced the ATP production in control cells. In the presence of glutamate, Br57 prevented the impairment of maximal respiration compared to glutamate-treated control cells. The right graph exhibits normalized values. Experiments were repeated three times and results are given as mean +SD ($^{###}$/***p< 0.001; ANOVA, Scheffé's test).

3.5.4. Pin1 siRNA cannot prevent glutamate-induced cell death

Previous results suggested that Pin1 is a mediator of glutamate-induced mitochondrial fission and cell death in HT22 cells. To study particular the role of Pin1, the next experiment was to analyze the impact of Pin1 silencing on cell viability. For this purpose, two different siRNAs were used to deplete Pin1 mRNA and protein levels (esiPin1 obtained from Sigma and siPin1 obtained from Dharmacon). Both siRNAs reduced Pin1 mRNA as well as protein levels in HT22 cells (Figure 26A). In contrast to the protective effect of the Pin1 inhibitor Br57, silencing of Pin1 failed to rescue HT22 cells from glutamate-induced cell death as determined by the MTT

assay (Figure 26B). However, contrarily to expectations, addition of Br57 to Pin1 depleted cells increased cell viability after glutamate toxicity (Figure 26B, black bars).

Taken together, these findings revealed that Pin1 plays an important role in mitochondrial fission and fusion processes as well as in cell death pathways as the inhibition of Pin1 with Br57 provided neuroprotection, preserved MMP and attenuated ATP depletion after glutamate toxicity. However, in contrary to these findings the specific knockdown of Pin1 with siRNA failed to rescue HT22 cells from cell death.

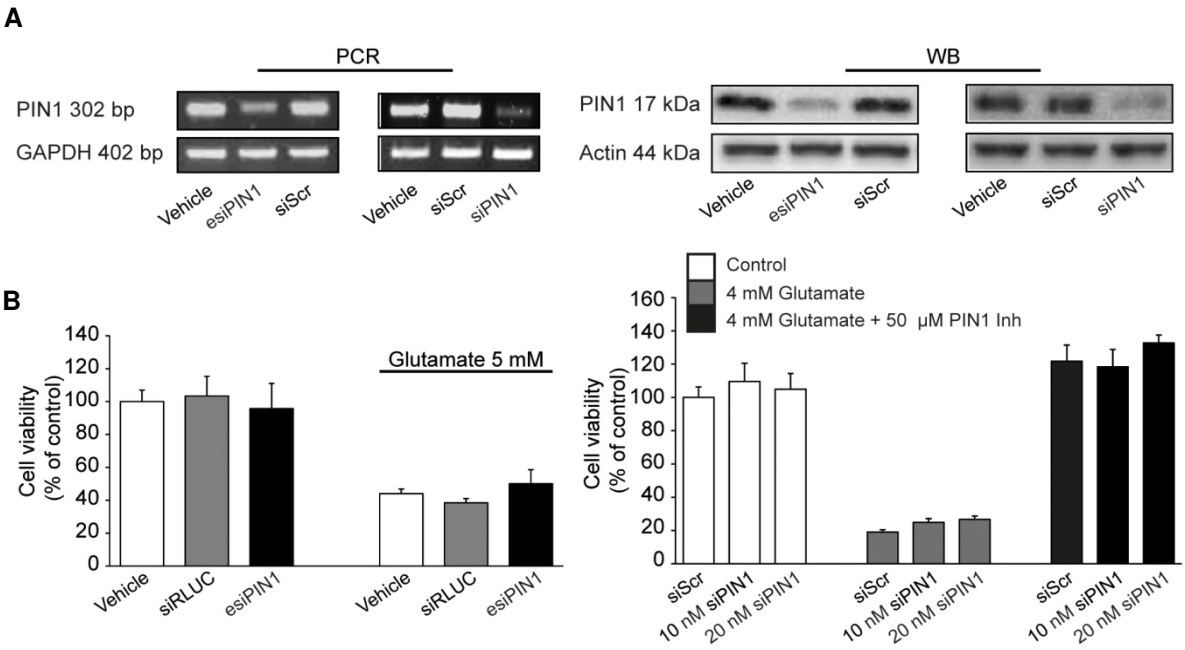

Figure 26: Pin1 siRNA does not rescue cells from glutamate-induced cell death

A: RT-PCR analysis revealed a downregulation of Pin1 mRNA levels after siRNA transfection for 48 h (two siRNAs were used) and western blot analysis confirmed the knockdown on the protein level. GAPDH and actin were used as loading control for RT-PCR and western blot experiments, respectively. **B:** Both siRNAs failed to rescue cells from cell death induced by glutamate as determined by the MTT assay (15 h, 5 mM; n=8). The addition of Br57 to Pin1 depleted cells showed complete protection against glutamate-induced cell death. Results depicted in left panels are obtained with esiPin1 (easy siRNA from Sigma Aldrich, siRLUC was used as control siRNA), while right panels are obtained with SMART pool® siPin1 (Dharmacon, Thermo Scientific). Experiments were repeated at least three times and results are given as mean +SD.

3.6. Trypsin-like serine proteases as mediators of glutamate-induced cell death in HT22 cells

The activation of proteases, such as caspases, calpains or cathepsins in signaling pathways of PCD is well-established [4,107,193–196]. However, increasing evidence suggests that also other proteases are major contributors to intrinsic pathways of PCD, namely serine proteases, such as Omi/HtrA2, granzyme B, chymotrypsin or trypsin [112,195,197]. The present study investigated the impact of activated trypsin-like serine proteases on cell survival and mitochondrial function in response to oxidative stress induced by glutamate in HT22 cells. To gain insight into the role of serine proteases in glutamate toxicity, two inhibitors were applied in the following experiments. Nα-Tosyl-L-lysine-chlormethyl ketone hydrochloride (TLCK) is an irreversible inhibitor of trypsin, but it is also reported that TLCK inhibits other proteases, such as plasmin and thrombin (10 mM TLCK to 100 units/ml of thrombin) or kinases, such as Protein Kinase C (IC_{50}= 1 mM) and the catalytic subunit of the Cyclic AMP-dependent Protein Kinase, amongst others [198–201]. Np-Tosyl-L-phenylalanyl chloromethyl ketone (TPCK) inhibits irreversibly α-chymotrypsin and chymotrypsin-like serine proteases. However, TPCK exhibits no activity for trypsin and trypsin-like serine proteases [202].

3.6.1. The trypsin-like serine protease inhibitor TLCK provides neuroprotection in HT22 cells and primary cortical neurons

In the current experiment, the protective potential of the serine protease inhibitor TLCK against glutamate toxicity was investigated. The impact of serine protease inhibition after glutamate challenge on cell viability was determined by MTT assay and real-time impedance measurements with the xCELLigence system. TLCK increased cell viability after 17 h of glutamate treatment (3 mM) and the loss of cell impedance was prevented (Figure 27A). To further confirm this neuroprotective effect, cell death was examined by AVPI staining and following FACS-analysis. Cells were treated with 3 mM glutamate for 13 h with or without 50 µM TLCK. Afterwards, cells were stained for 5 min with AVPI and subsequently analyzed by FACS. The quantification of double positive stained cells (AV and PI positive) represented the amount of cell death in each condition. Cell death was completely decreased by TLCK treatment after glutamate toxicity (Figure 27B).

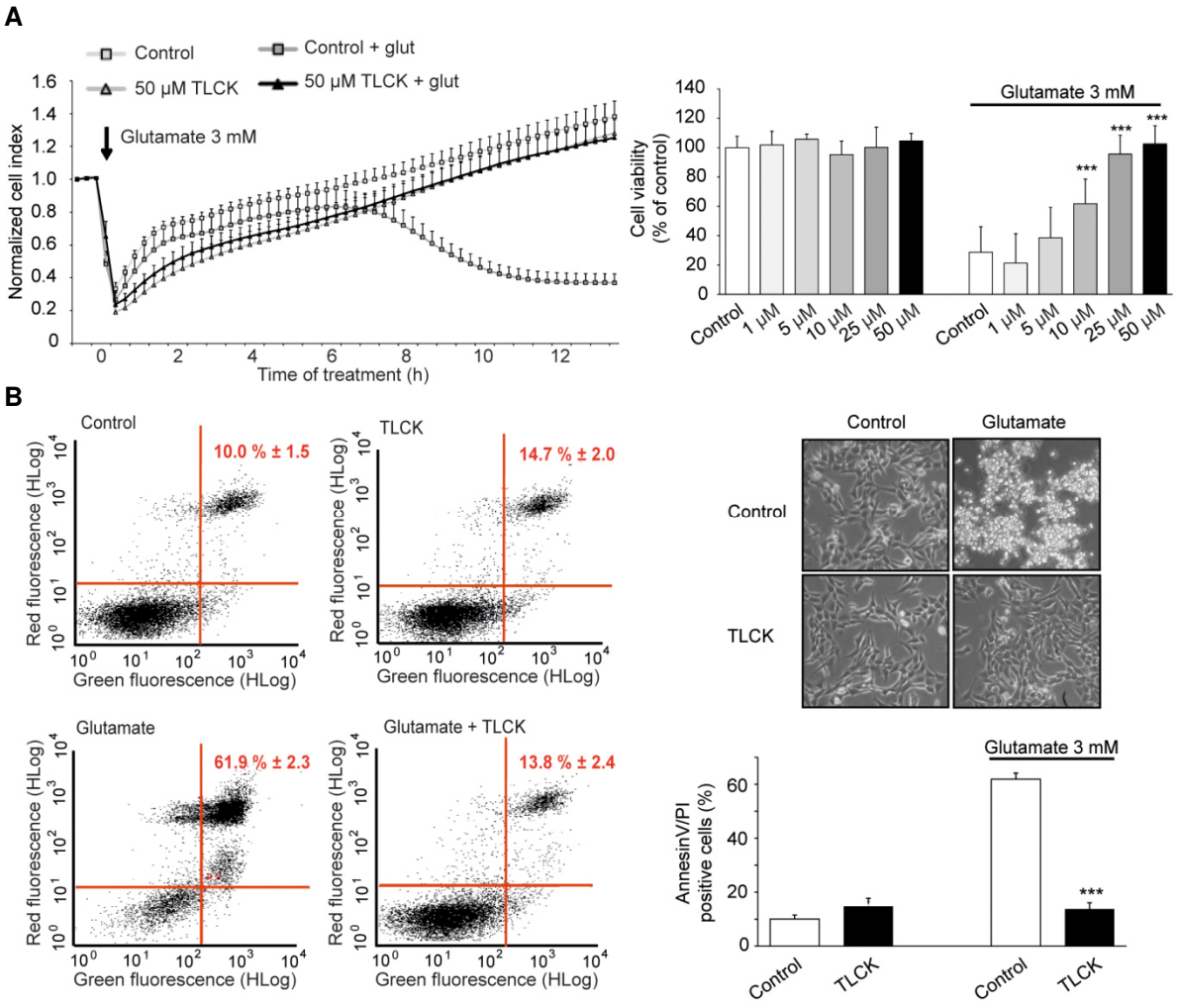

Figure 27: TLCK provides protective effects upon glutamate treatment

A: HT22 cells were treated with TLCK and after glutamate exposure (3 mM) cell viability was determined by real-time impedance measurements with the xCELLigence system (n=6, left panel) and MTT assay (17 h, n=8, right panel). TLCK increased cell viability in a concentration-dependent manner. **B:** Glutamate-induced morphological alterations were prevented by TLCK. Cell death was detected by FACS-analysis after glutamate toxicity (13 h, 3 mM) and as quantification of AVPI positive stained cells revealed, TLCK prohibited oxidative stress-induced cell death (n=4). Experiments were repeated three times and results are given as mean +SD (***p< 0.001; ANOVA, Scheffé's test).

To examine whether serine protease activation occurs early or late in response to oxidative stress, TLCK was applied 2, 4 and 6 h after the onset of glutamate and cell viability was analyzed by the xCELLigence system over time. A post-treatment with TLCK up to 2 h prevented cell death, while 4 and 6 h of post-treatment did not increase cell viability, which indicated an initial activation of serine proteases in conditions of glutamate treatment (Figure 28).

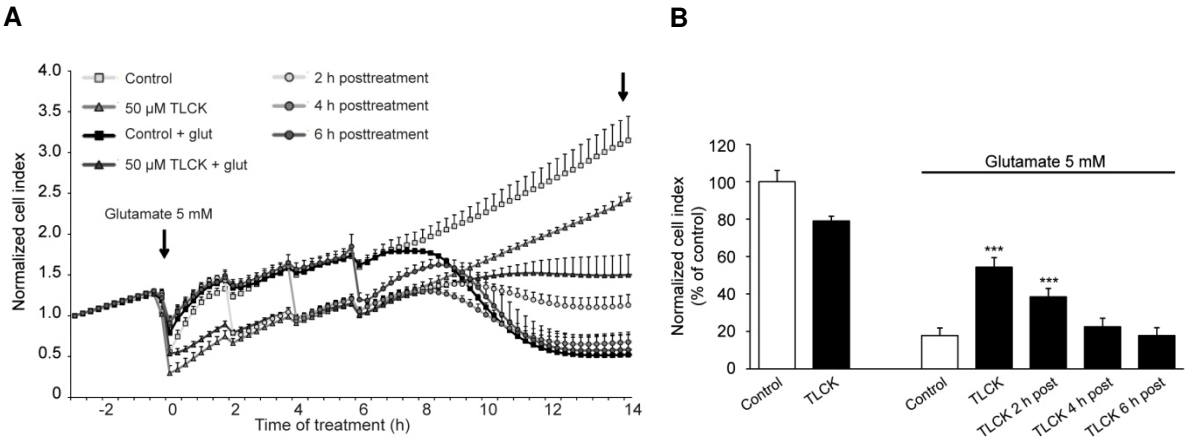

Figure 28: TLCK increases cell viability after glutamate toxicity up to 2 h of post-treatment

A: Real-time detection of cell impedance exhibited a protective effect of TLCK after glutamate toxicity in post-treatment conditions up to 2 h (n=6). **B:** Bar graph evaluation after 12 h of the xCELLigence recordings (right black arrow) from figure 28A. TLCK significantly increased cell viability in conditions of co-treatment and up to 2 h of post-treatment contrary to cells exposed to glutamate and post-treatment after 4 and 6 h. Experiments were repeated three times and results are given as mean +SD (***p< 0.001; ANOVA, Scheffé's test).

To translate this protective effect of serine protease inhibition into more physiological conditions, primary cortical mouse neurons were used to test the protective potential of TLCK. Since HT22 cells lack NMDA and AMPA/kainate receptors, this model of oxidative stress imitates only partial the mechanism of neuronal cell death occurring in neurodegenerative diseases. The activation of ionotropic glutamate receptors by glutamate leads to elevated intracellular Ca^{2+}-levels and following mitochondrial damage that triggers the extensive production of detrimental ROS levels. To analyze the effect of TLCK, primary cortical neurons were cultured for 8-10 days and following cells were treated with 25 µM glutamate for 17 h. Cell viability was afterwards determined by the MTT assay. TLCK led to increased cell viability in primary cortical neurons in a concentration-dependent manner (Figure 29).

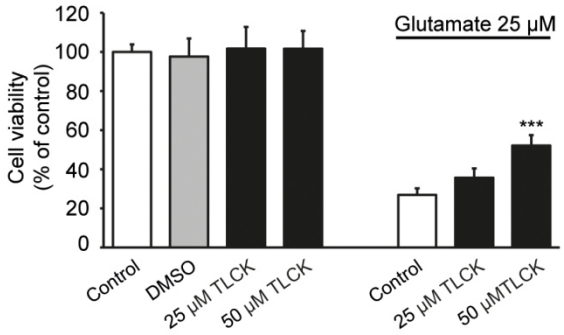

Figure 29: TLCK increases cell viability in primary cortical neurons after glutamate-induced exitotoxicity

A: Primary mouse cortical neurons were treated on day 10 for 17 h with 25 µM glutamate and two different concentrations of TLCK (25, 50 µM). As determined by the MTT assay, TLCK provided neuroprotective effects. Experiments were repeated three times and results are given as mean +SD (***p< 0.001; ANOVA, Scheffé's test).

In contrary to the protective potential of TLCK, TPCK had no protective effects against glutamate toxicity in HT22 cells. Interestingly, TPCK decreased cell viability in a concentration-dependent manner (Figure 30). These results suggest that trypsin-like serine proteases but not chymotrypsin-like serine proteases are involved in glutamate-induced cell death in HT22 cells. Therefore, TLCK was used in all further experiments.

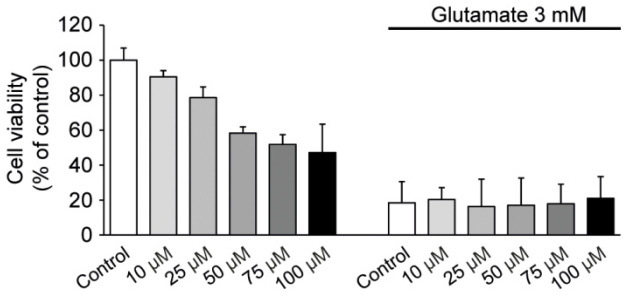

Figure 30: TPCK cannot prevent glutamate-induced cell death in HT22 cells

HT22 cells were treated for 17 h with 3 mM glutamate and the impact of TPCK on cell viability was determined by MTT assay. TPCK failed to rescue HT22 cells from glutamate-induced cell death, even exhibited toxic effects at higher concentrations (n=8). Experiments were repeated three times and results are given as mean +SD.

3.6.2. Serine proteases act upstream of Bid

The pro-apoptotic protein Bid is an important mediator of caspase-independent pathways of neuronal cell death in HT22 cells and an important regulator of mitochondrial demise [70,71]. Since serine proteases were linked to Bid activation and thereby inducing cell death [127,203], the next issue of interest was to investigate if TLCK-sensitive serine proteases act upstream or downstream of Bid activation in HT22 cells. For this purpose, cells were pre-treated with 50 µM TLCK for 1 h and following transfected with the tBid plasmid (2 µg/well, 18 h) to induce apoptosis as described previously in the work of Grohm et al. [71]. After 17 h of tBid treatment cell death was examined by AVPI staining and subsequently FACS-analysis. TLCK was not able to prevent cell death induced by tBid, indicating that activation of trypsin-like serine proteases occurred upstream of Bid activation (Figure 31).

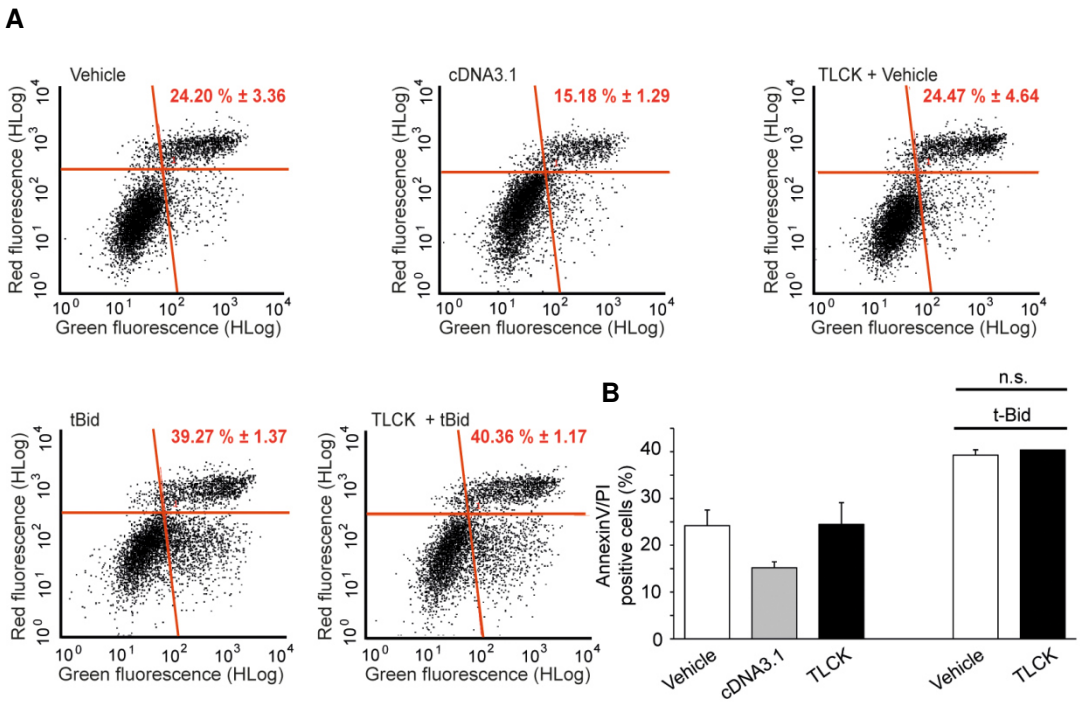

Figure 31: TLCK cannot prevent tBid-induced cell death

A: HT22 cells were pre-treated with 50 µM TLCK for 1 h prior to tBid transfection. After 18 h cells were stained with AVPI and cell death was detected by FACS-analysis. TLCK did not provide protective effects against tBid-induced cell death (n=4). CDNA 3.1 was used as control plasmid. **B:** Quantification of FACS received dot plots of double positive stained cells. Experiments were repeated three times and results are given as mean +SD.

3.6.3. TLCK abolishes glutamate-induced lipid peroxidation

In HT22 cells glutamate exposure results in depleted GSH levels leading to cell death. Since GSH is one of the major endogenous radical scavengers in cells, its depletion is associated with increased detrimental ROS accumulation and lipid peroxide production. As the work of Tobaben showed, a first increase in lipid peroxidation within the first hours after glutamate exposure was followed by a second much more pronounced increase that was associated with irreversible mitochondrial damage and cell death[72]. To investigate the influence of serine protease activation on lipid peroxide production in conditions of oxidative stress, HT22 cells were treated in the presence or absence of TLCK with 3 mM glutamate for 10 h. Lipid peroxidation was examined by FACS-analysis of Bodipy stained cells. TLCK blocked lipid peroxide production completely, even to control levels (Figure 32). This strong decrease of lipid peroxidation after glutamate toxicity indicates that TLCK acts even before the first wave of ROS increase.

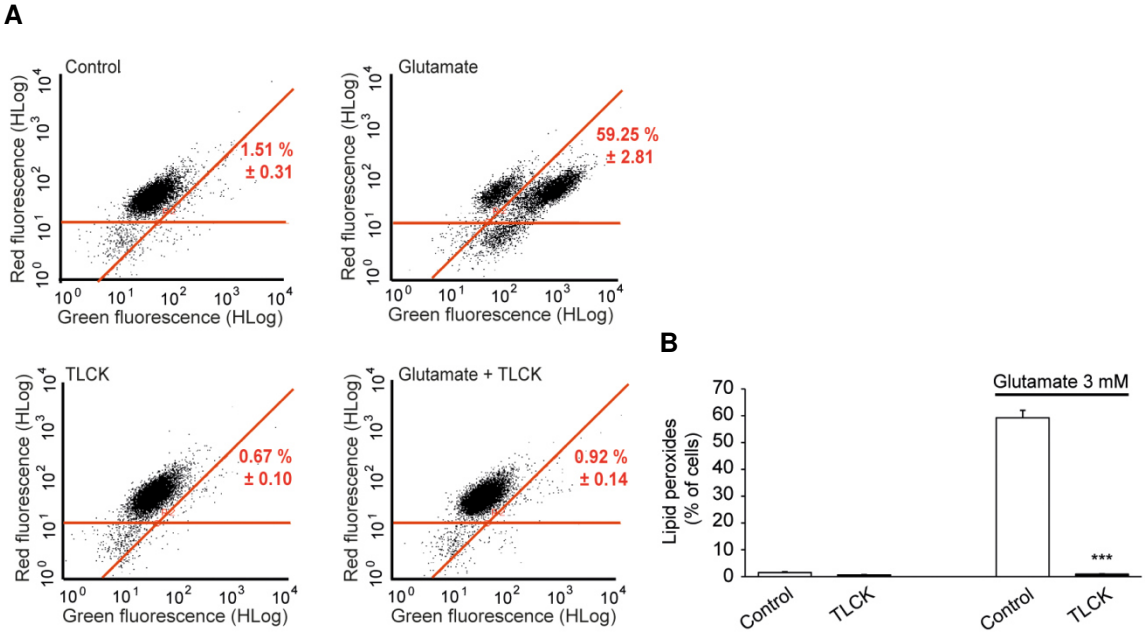

Figure 32: Glutamate-induced lipid peroxidation was completely blocked by TLCK

A: HT22 cells were treated for 10 h with glutamate (3 mM) with or without TLCK and were afterwards stained with 2 µM BODIPY reagent for 1 h. Determination of lipid peroxide production was achieved by FACS-analysis. TLCK inhibited glutamate-induced lipid peroxidation. **B:** Quantification of FACS dot plots (n=4). Experiments were repeated three times and results are given as mean +SD (***p< 0.001; ANOVA, Scheffé's test).

Recently it was reported by Takahashi et al., that TLCK exhibits antioxidative properties and due to this feature TLCK rescued H9C2 cells from H_2O_2-induced cell death [204]. Since glutamate-induced lipid peroxidation was completely abolished by TLCK (Figure 32), the hypothesis that TLCK may act as an antioxidant in glutamate toxicity and thereby rescues HT22 cells from cell death was assumed. To examine the protective potential of TLCK in H_2O_2-induced cell death, cell viability was determined by MTT assay after 15.5 h of treatment. H_2O_2 decreased cell viability in a concentration-dependent manner and TLCK was not able to prevent it, leading to the conclusion that TLCK is not acting as an antioxidant in this cell death model system (Figure 33).

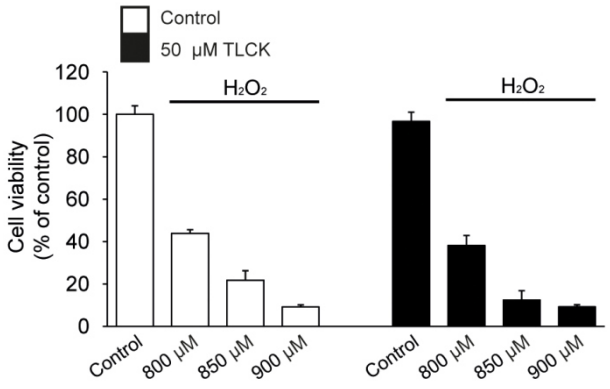

Figure 33: TLCK cannot prevent H_2O_2-indcued cell death in HT22 cells

HT22 cells were treated with different concentrations of H_2O_2 and 50 µM TLCK. Cell viability was determined by MTT assay after 15.5 h of treatment. The serine protease inhibitor TLCK did not prevent the decrease of cell viability induced by H_2O_2 (n=8). Experiments were repeated three times and results are given as mean +SD.

3.6.4. TLCK prevents glutamate-induced mitochondrial fragmentation, loss of MMP and preserves mitochondrial respiration

Mitochondrial fragmentation, the loss of MMP and depleted ATP levels are associated with glutamate-induced cell death in HT22 cells. As previous results demonstrated, TLCK seems to act in an initial phase of oxidative stress-induced cell death. To evaluate the influence of serine protease inhibition on mitochondrial parameters, mitochondrial morphology alterations were first analyzed. After TLCK and glutamate exposure (13.5 h, 2 mM) quantification of mitochondrial categories was performed as described before in this study (see 1.2). Trypsin-like serine protease inhibition with TLCK prohibited mitochondrial fragmentation induced by

glutamate, which was exhibited by a significant decrease of category 3 mitochondria (Figure 34A). Another important feature of oxidative stress-induced cell death in HT22 cells is the impairment of the MMP. Since mitochondrial alterations due to oxidative stress could be inhibited by TLCK, the next step was to examine the impact of activated serine proteases on MMP. FACS-analysis of TMRE stained cells revealed that TLCK was able to prevent the loss of MMP induced by glutamate (13 h, 3 mM, Figure 34B). The uncoupler of the MMP, carbonylcyanide-3-chlorophenylhydrazone (CCCP), was used as positive control.

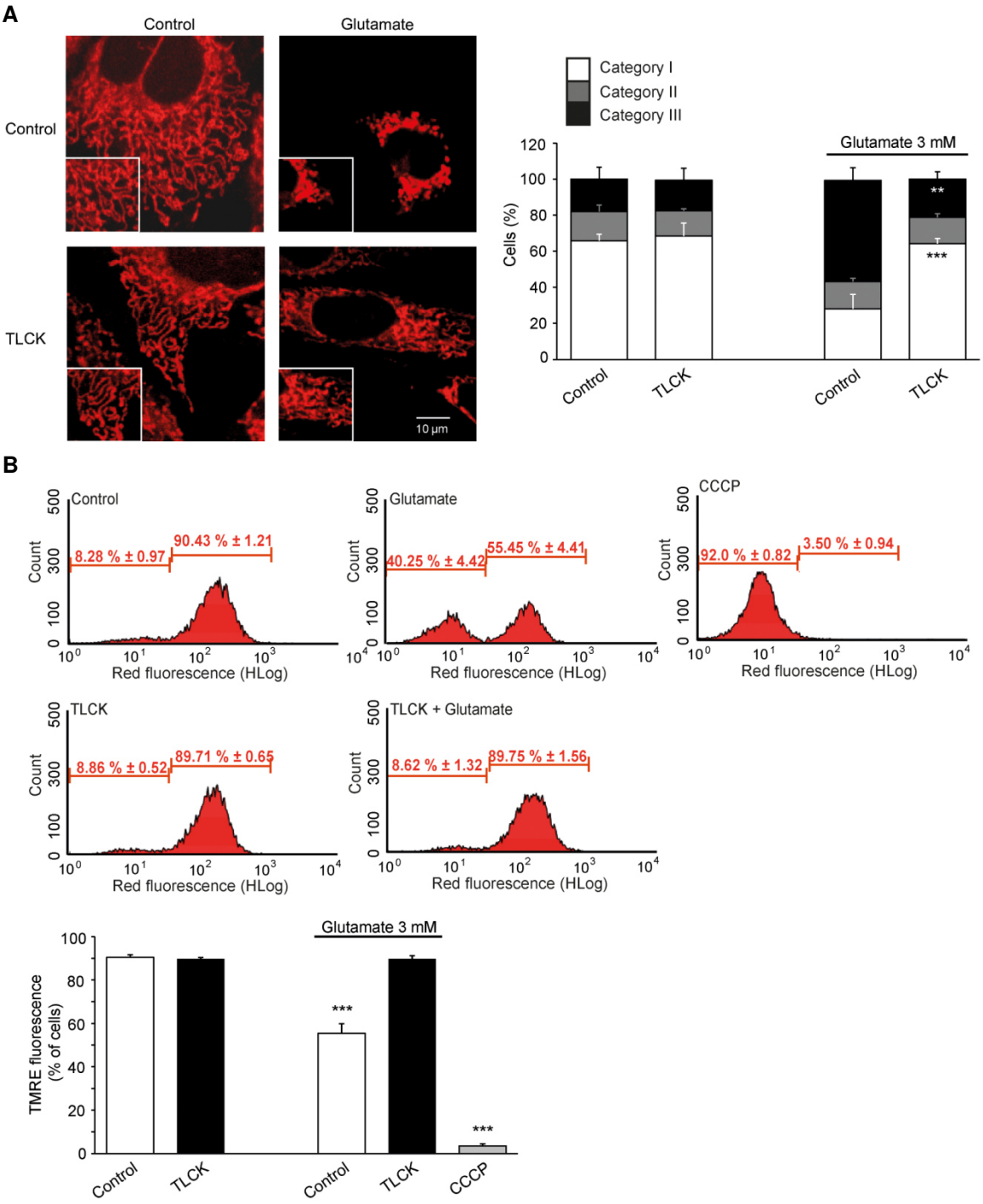

Figure 34: TLCK prohibited glutamate-induced mitochondrial morphology alterations and the loss of MMP

A: Glutamate-induced mitochondrial morphology alterations were illustrated by confocal images (63x objective) of MitoTracker DeepRed stained mitochondria. Quantification of mitochondrial categories after glutamate toxicity (15 h, 2 mM) revealed an increase of category 1 mitochondria and a decrease of category 3 mitochondria in the presence of TLCK. For each condition at least 500 cells were counted blind. **B:** MMP was analyzed by TMRE staining and following FACS measurements. Glutamate treatment (12.5 h, 3 mM) led to an impairment of the MMP, which was illustrated by a loss in red fluorescence (peak shift to the left). TLCK was able to preserve MMP impairment compared to glutamate treated controls (n=4). CCCP was used as positive control. Quantification of TMRE stained cells is illustrated in the bar graph below. Experiments were repeated three times and results are given as mean +SD (***p< 0.001; ANOVA, Scheffé's test).

As demonstrated by previous results, TLCK was able to prevent the impairment of MMP. To have a closer look directly on the energy metabolism and respiratory capacity of HT22 cells after glutamate toxicity and the impact of serine proteases, the next issue was to evaluate ATP levels and mitochondrial respiration in response to oxidative stress. HT22 cells were treated for 15 h with 3 mM glutamate and different concentrations of TLCK. Accordingly, ATP levels were determined by luminescence measurements. TLCK impeded ATP depletion completely (Figure 35A). To gain further insight into mitochondrial function related to the respiratory capacity, the XF96-Seahorse system was used to measure the OCR over time as described in 1.5.3. Glutamate induced a reduction in the basal respiration and decreased ATP production, which was prevented by TLCK. Further, maximal respiration was increased after TLCK treatment compared to glutamate treated control cells (Figure 35B).

In consequence of these results, trypsin-like serine proteases are supposed to act upstream of mitochondrial demise and preserve mitochondrial respiratory capacity.

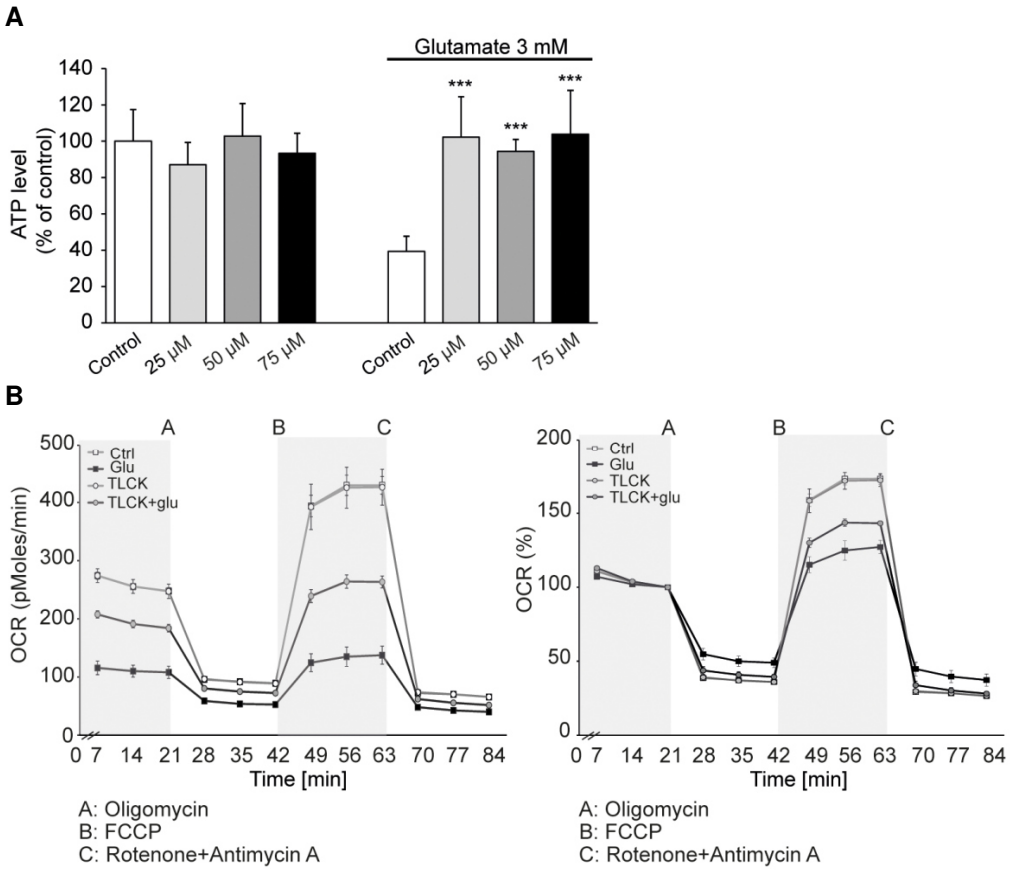

Figure 35: TLCK prevents ATP depletion and preserves mitochondrial respiratory capacity

A: ATP levels were detected by luminescence measurements after glutamate toxicity in HT22 cells. Glutamate-induced (16 h, 3 mM) ATP depletion was abolished by TLCK (n=8). **B:** Seahorse measurements revealed reduced basal respiration, reduced ATP production and decreased maximal respiration after glutamate exposure (16 h, 4 mM), which were preserved by serine protease inhibition with TLCK (n=8). The right panel exhibits the normalized curve. Experiments were repeated three times and results are given as mean +SD (***p< 0.001; ANOVA, Scheffé's test).

3.6.5. The impact of TLCK on actin/Drp1 interaction and the redistribution of Drp1 to the mitochondria after glutamate toxicity

There is some evidence suggesting that the actin cytoskeleton is involved in the movement and positioning of mitochondria and in mitochondrial fission [47–49,205]. One major regulatory protein which is associated with mitochondrial fission is Drp1 [206]. Recent data implies that Drp1-dependent mitochondrial fission is regulated by actin dynamics, as disruption of F-actin (filamentous) attenuates the recruitment of Drp1 to the mitochondria and mitochondrial fission [49]. The work of Barbier et al. shows that the F-actin network disruption and the subsequent redistribution from Drp1 to the mitochondria, which results in cell death, is caused by the activation of

chymotrypsin-like serine proteases [138]. To examine the influence of trypsin-like serine proteases on F-actin disruption and on Drp1 redistribution to the mitochondria, HT22 cells were treated for 16.5 h with 5 mM glutamate and 50 µM TLCK and subsequently IP experiments were performed. Drp1 was immunoprecipitated and co-immunoprecipitated actin protein levels were analyzed by western blot analysis. Glutamate induced a disruption of actin/Drp1 interaction, which was not prevented by serine protease inhibition with TLCK (Figure 36A and B). To evaluate if TLCK has nevertheless an influence on the translocation of Drp1 to the mitochondria after glutamate exposure, western blot analysis of mitochondrial extracts were performed. Serine protease inhibition with TLCK could not abolish glutamate-induced translocation of Drp1 to the mitochondria (Figure 36C and D).

Taken together, these results demonstrate that trypsin-like serine proteases have no impact on the interaction of actin and Drp1 and that the redistribution from Drp1 to the mitochondria after glutamate toxicity is not prohibited by TLCK.

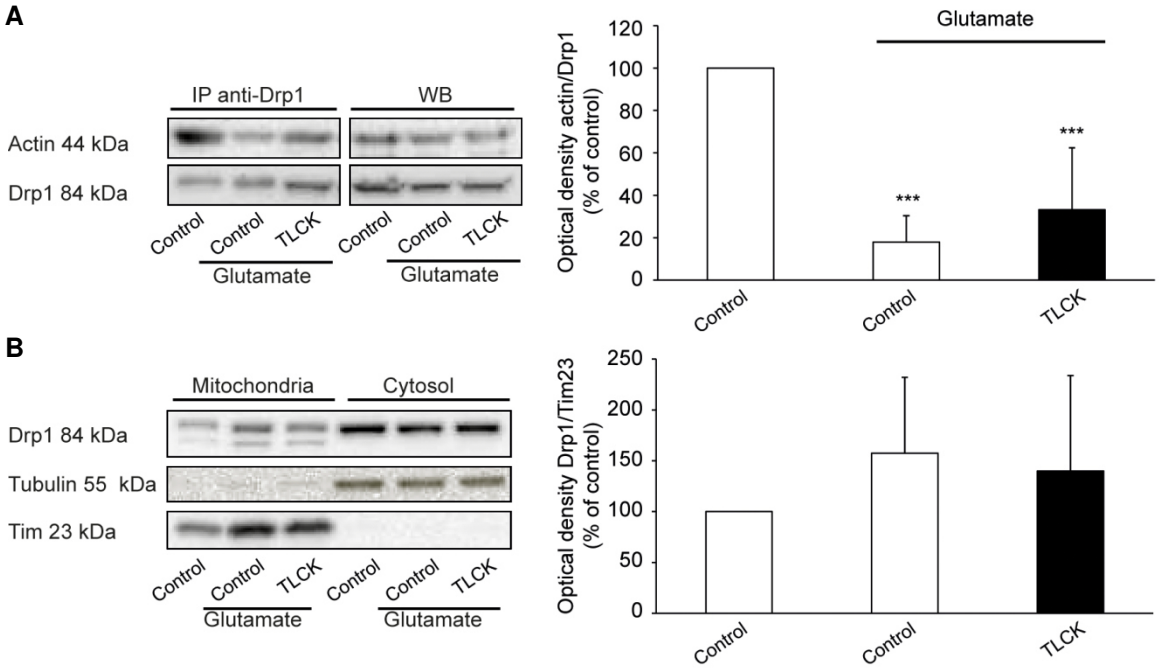

Figure 36: TLCK cannot impede Drp1/actin disruption and Drp1 translocation to the mitochondria

A: Glutamate-induced (17 h, 4 mM) release of Drp1 from the actin cytoskeleton was not prevented by TLCK as IP experiments depicted. Drp1 was immunoprecipitated and co-immunoprecipitated actin levels were analyzed. The left panel exhibits IP experiments and the right panel western blot analysis of total protein amounts. Bar graphs depict the quantification of the optical density from actin/Drp1 protein levels obtained from western blots (n=5). **B:** Drp1 translocation to the mitochondria after glutamate exposure was not attenuated by TLCK as western blot analysis of mitochondrial extracts illustrated. Quantification of optical density obtained from western blots (n=5). Tim23 was used as loading control for mitochondrial proteins.

3.6.6. The influence of serine proteases on Drp1/CypA interaction

Previous results of this work demonstrated that CypA plays a crucial role in glutamate-induced cell death in HT22 cells. As Drp1-dependent mitochondrial fission is associated with glutamate toxicity and the interaction of CypA and Drp1 was reported by Cereghetti et al., the next issue was to investigate the interaction of CypA and Drp1 in HT22 cells [51,173]. For this purpose, IP experiments were performed where Drp1 was immunoprecipitated and co-immuonprecipitated CypA protein levels were detected by western blot analysis. In control conditions Drp1 interacted with CypA. However, this interaction was diminished after glutamate toxicity (Figure 37). Interestingly, serine protease inhibition with TLCK increased the interaction of Drp1 and CypA (Figure 37).

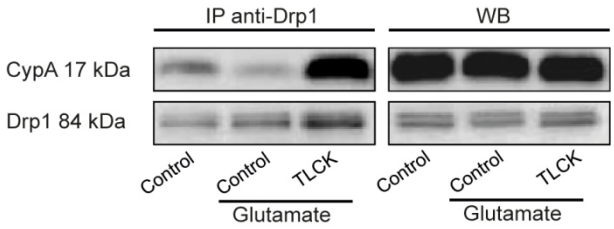

Figure 37: Glutamate-induced disruption of Drp1/CypA interaction is prevented and even increased after TLCK treatment

A: IP experiments revealed a decreased Drp1/CypA interaction after glutamate toxicity (17 h, 3 mM), which was abolished in the presence of TLCK. TLCK exhibited an even more pronounced interaction of both proteins. The left panel shows IP experiments with immunoprecipitated Drp1 and co-immunoprecipitated CypA levels analyzed by western blot analysis. The right panel shows western blot analysis of total protein amounts.

It was reported that another binding partner of Drp1 is the phosphatase calcineurin, which regulates Drp1-mediated mitochondrial fission by dephosphorylating Drp1 on serine residue 637 [51,52]. Calcineurin activity is linked to neuronal cell death [207] and since chymotrypsin regulates calcineurin activity, the speculation was that TLCK promotes its protective effect due to calcineurin inhibition. To first analyze, if calcineurin contributes at all to cell death in HT22 cells the calcineurin inhibitor tacrolimus was used to investigate the impact of calcineurin inhibition on cell viability. However, tacrolimus did not provide any protective effects after glutamate toxicity as determined by MTT assay (Figure 38).

Taken together, these results imply that trypsin-like serine proteases have an influence on the interaction between Drp1 and CypA. Though, this effect seems not to be due to modulatory effects on calcineurin activity.

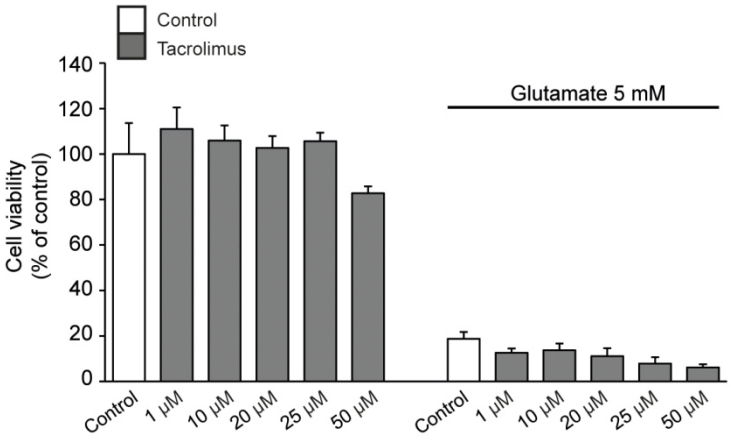

Figure 38: Tacrolimus cannot prohibit glutamate-induced cell death in HT22 cells

A: The calcineurin inhibitor tracolimus failed to prevent the glutamate-induced (16 h, 4 mM) decrease of cell viability as determined by MTT assay (n=8). Experiments were repeated three times and results are given as mean +SD.

4. Discussion

The principal aim of this study was to investigate the role of post-translational protein modifications in intrinsic pathways of neuronal cell death with particular focus on mitochondrial integrity and function. Such post-translational modifications may involve isomerization, cleavage or phosphorylation of proteins which determine protein-protein interactions or their subcellular localization and function. This modification regulates their role at key decision points in PCD pathways, e.g. at the mitochondria and in the nucleus. In particular, this study revealed a major role for CypA as a regulator of mitochondrial AIF release and further, the influence of Pin1 on the mitochondrial fission and fusion balance and on mitochondrial integrety. Moreover, this work depicts an important role for trypsin-like serine proteases in paradigms of PCD, their influence on protein-protein interactions and their implication in the subcellular redistribution of other proteins.

The first part of this study investigated the contribution of two members of the PPIase family to glutamate-induced cell death in HT22 cells, namely CypA and Pin1. The involvement of CypA was analyzed by siRNA experiments and the results of this thesis suggest that CypA plays a crucial role in oxidative stress-induced cell death upstream of mitochondrial AIF release. Silencing of CypA prevented glutamate-induced cell death and attenuated mitochondrial morphology alterations. Moreover, the critical AIF release from the mitochondria and the subsequent translocation to the nucleus was prohibited by CypA depletion, which resulted in increased cell viability. Further, lipid peroxidation was significantly reduced by siCypA. This is the first time it has been demonstrated, that CypA is not only a downstream mediator of mitochondrial demise which then leads to cell death, but that it also acts upstream of mitochondrial damage and that CypA silencing rescues mitochondrial integrity. The role of the second family member, Pin1, which is associated with the mitochondrial cell death machinery, was investigated by applying a specific inhibitor of Pin1 (Br57) to the HT22 cell model. The specific inhibition of Pin1 revealed a protective effect as cell viability was increased after glutamate toxicity. Additionally, this study demonstrated that Br57 changed mitochondrial morphology towards pronounced mitochondrial fission, however, mitochondrial fragmentation was abolished. This feature was accompanied by a slight decrease in ATP production.

The data of the second part provide evidence that trypsin-like serine proteases are major contributors to oxidative stress-induced cell death in HT22 cells and primary cortical neurons. TLCK, an inhibitor of trypsin-like serine proteases, increased cell viability in HT22 cells and primary neurons after glutamate toxicity. Furthermore, TLCK prevented glutamate-induced lipid peroxidation and attenuated the loss of ATP in HT22 cells. Moreover, serine protease inhibition preserved the MMP and abolished mitochondrial morphology alterations due to glutamate treatment. However, TLCK failed to prevent tBid-induced cell death in HT22 cells indicating that serine protease activation occurs upstream of Bid activation. Additionally, as IP data of this work demonstrated, serine proteases have no influence on the interaction of Drp1 at the cytoskeleton. The release of Drp1 and the subsequent redistribution to the mitochondria occurred after glutamate toxicity, however, this was not prevented by TLCK treatment. But serine proteases have an impact on the interaction of Drp1 and CypA.

Taken together, the first part of this work shows that CypA and Pin1 contribute to cell death pathways induced by glutamate in HT22 cells and that both proteins act upstream or at the level of mitochondria. The second part implies an important role for trypsin-like serine proteases as mediators of glutamate-induced cell death in HT22 cells and primary cortical neurons and that protease activation occurs upstream of Bid activation in HT22 cells.

4.1. Mitochondrial fragmentation induced by glutamate in HT22 cells

Mitochondria exert life-and-death decisions in cells because mitochondrial function is relevant for normal bioenergetics, maintenance of Ca^{2+} homeostasis, free radical generation and energy production. Mitochondrial dynamics are regulated by the mitochondrial fission and fusion rate, which is under control of numerous GTPases. Mitochondrial fission is essential for growing and dividing cells to generate new organelles, while fusion is stimulated by energy demand and rescues stress by complementing functional and dysfunctional mitochondria. Particularly in neurons, mitochondria engage a central role because the high energy demand of these cells to maintain neuronal function, such as neurotransmitter synthesis, is provided mainly through Oxphos in the IMM. In the present study, cell death induced by glutamate

resulted in strong mitochondrial fragmentation, which was associated with elevated mitochondrial fission and accompanied by the impairment of the MMP.

HT22 cells lack ionotropic glutamate receptors such as NMDA or AMPA/kainate receptors. However, they are sensitive to high extracellular glutamate concentrations, which induced the generation of elevated ROS levels associated with mitochondrial fragmentation and ensuing DNA damage. It was reported that the mitochondrial AIF release and the subsequent translocation to the nucleus is a critical step in this caspase-independent neuronal cell death pathway. Moreover, as demonstrated in this work, the translocation of CypA from the cytosol to the nucleus and the pro-apoptotic complex formation of AIF and CypA is required to induce cell death in HT22 cells (Figure 12-14). Thus, the maintenance of mitochondrial function and the prohibition of mitochondrial AIF release were shown in this thesis to be important targets to prevent neuronal cell death.

4.2. CypA in the paradigm of glutamate-induced cell death in HT22 cells

4.2.1. CypA – a regulator of mitochondrial AIF release

One major aspect of this study addressed the mitochondrial AIF release and the translocation to the nucleus where it induced chromatin condensation, which was shown by video recordings after glutamate toxicity in HT22 cells [70]. Silencing of AIF provided protective effects in HT22 cells and primary neurons, which make the AIF release a promising target for neuroprotection [70,77]. Since AIF requires CypA to induce chromatinolysis, this thesis provided evidence that inhibition of the CypA-AIF axis led to decreased cell death. This was supported by several findings. First, downregulation of CypA extremely reduced the susceptibility of HT22 cells to oxidative stress. Second, the typical hallmark of increased lipid peroxidation in response to glutamate was abolished. Third, mitochondrial fragmentation and the impairment of the MMP were significantly attenuated and fourth the key event in caspase-independent cell death, the mitochondrial AIF release, was prohibited. One of the most puzzling issues of AIF-mediated cell death involves the question if AIF translocation to the nucleus is dependent or not on its interaction with CypA in the cytosol. To date, two different mechanistic pathways have been proposed to explain the relocation of AIF to the nucleus. The first model suggests that AIF and CypA

translocate independent of each other to the nucleus where they induce chromatinolysis by generating a DNA-degrading complex with H2AX. In MNNG-treated MEFs AIF simultaneously interacts with CypA and H2AX. Strikingly, the association of AIF and H2AX in the nucleus occurred even in the absence of CypA but in this case DNA damage was reduced. In contrast, AIF required H2AX to cooperate with CypA [208]. A second model proposes that AIF translocation to the nucleus depends on its interaction with CypA in the cytosol. This hypothesis is based on the observation that nuclear AIF translocation was reduced in CypA$^{-/-}$ mice after HI and conversely, in Hq mice lacking AIF, nuclear translocation of CypA was diminished [168]. These controversially discussed mechanisms indicate that the caspase-independent apoptotic pathway is dependent on the cell type and the apoptotic inducing stimulus.

The present study confirmed the previously described nuclear translocation of AIF induced by glutamate in HT22 cells (Figure 12; [70]). In addition, the translocation of CypA to the nucleus and the interaction of AIF and CypA due to oxidative stress was demonstrated (Figure 13 and 14). However, in this model system the histone H2AX is not required to induce cell death as silencing of H2AX did not provide any protective effects (Figure 22). Another important finding of this work is the unequal time-dependent translocation of CypA and AIF to the nucleus in HT22 cells. Interestingly, CypA relocation to the nucleus was observed at earlier time points than AIF release from the mitochondria appeared. After 6-8 h upon glutamate challenge CypA levels were increased in the nucleus, while AIF translocation occurred 10-12 h after the onset of glutamate. Moreover, silencing of CypA abrogated mitochondrial AIF release completely, indicating a pivotal role for CypA in the nuclear translocation of AIF in glutamate-induced cell death in HT22 cells. These findings were substantiated by the work of Doti et al. that even targeting CypA in the cytosol by an AIF-peptide, which prohibits the interaction of AIF and CypA, prevented the translocation of AIF to the nucleus [209]. These results suggest that on the one hand CypA serves as a carrier for AIF and on the other hand that nuclear CypA may exhibit a platform for a feedback loop to the mitochondrial AIF release.

4.2.2. The role of CypA upstream of mitochondrial demise

High extracellular glutamate concentrations lead to increased ROS accumulation and to elevated lipid peroxide production, which is accompanied by mitochondrial

fragmentation and the loss of MMP in HT22 cells as demonstrated in this study and previously shown by others (Figure 10 and 11; [71,72]). Lipid peroxidation occurred in a biphasic manner after glutamate toxicity. An initial moderate increase appeared after 6-8 h of glutamate challenge followed by a second much more pronounced boost after 8-18 h arising from the mitochondria [72]. This work demonstrated that delivering of siCypA in HT22 cells before glutamate exposure abrogated the second boost of lipid peroxidation, while the initial increase was not affected (Figure 17). The inhibition of lipid peroxidation by siCypA was accompanied by decreased mitochondrial fragmentation and preserved MMP, which is in accordance with previous results showing that AIF release from the mitochondria was prohibited (Summary of results are depicted in Figure 39). However, the mechanism through which CypA silencing provides protective effects is still unknown. One possible mechanism could be through regulating cell cycle arrest and cell cycle transition. PPIases are known to be involved in the modulation of cellular pathways such as cell cycle regulation. In particular Pin1 regulates the stability of p53 and thereby gives rise to cell cycle arrest [210]. Cyp18, another member of the PPIase family, was identified as another interaction partner of p53. The impairment of the Cyp18-p53 interaction results in an accumulation of cells in the G2/M cell cycle phase. Moreover, Cyp18 knockout cells underwent increased p53-dependent apoptosis, suggesting an anti-apoptotic potential of Cyp18-p53 interaction [163]. In tumor lung cancer cells, CypA was identified to induce the up-regulation of cyclin D1 and cyclin-dependent kinase 4 (cdk4), whose activity is required for cell cycle G1/S transition, which resulted in cell cycle progression [189]. In fact, these findings revealed a pro-survival role for PPIases by modulating cell cycle phases, however, in the case of glutamate-induced cell death in HT22 cells there is no evidence that CypA has an influence at all on cell cycle arrest/progression/transition (Figure 21).

These findings demonstrated that CypA acts upstream of mitochondrial demise but downstream of the first moderate lipid peroxide increase. On the basis of these data, the hypothesized mechanism of glutamate-induced cell death in HT22 cells includes as a first step the translocation of CypA to the nucleus thereby creating a platform for the second step which involves the mitochondrial AIF release and the subsequent translocation to the nucleus. This assumption was substantiated by the fact that silencing of CypA prevented mitochondrial fragmentation and mitochondrial AIF release. However, it should be mentioned that other possible mechanisms cannot be

eliminated, because the exact mechanism is still elusive. Indeed, this model of glutamate-induced cell death does not clarify why CypA silencing administrated mitoprotection and prevented the lethal AIF release from the mitochondria, rather than acting downstream at the level of AIF translocation to the nucleus. However, these new findings heightened the important role of CypA in neuronal cell death as targeting CypA prevented mitochondrial demise and impeded the crucial step in caspase-independent cell death pathways, the mitochondrial release of AIF. Since mitochondrial damage marks 'a point of no return' in paradigms of PCD, mitoprotection is a more attractive target for neuroprotection than inhibiting cell death downstream of mitochondrial demise.

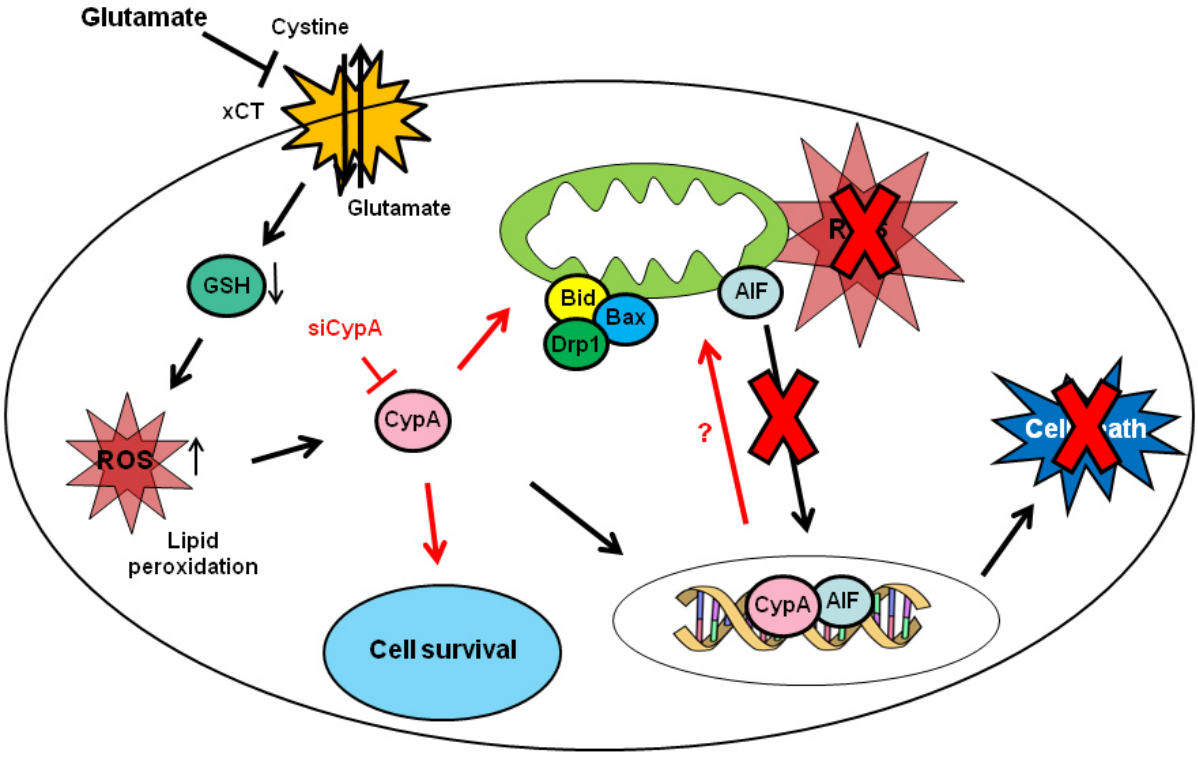

Figure 39: The role of CypA in glutamate-induced cell death in HT22 cells

High extracellular glutamate concentrations led to depleted GSH levels which induced the generation of ROS and lipid peroxide production. Following glutamate exposure CypA and AIF translocated to the nucleus where they induced chromatinolysis (black arrows illustrate the action of glutamate). CypA silencing prevented the lethal AIF release from the mitochondria, preserved the impairment of the MMP and abolished the second boost of lipid peroxidation resulting in cell survival (red arrows depict consequences of CypA depletion).

4.3. The impact of Pin1 on mitochondrial dynamics and cell death

Regarding the family of peptidyl-prolyl cis-trans isomerases, the next issue of this work dealt with the impact of another family member, Pin1, on mitochondrial dynamics and cell death induced by glutamate in HT22 cells. Barone and colleagues reported that Pin1 promotes neuronal cell death via a c-Jun dependent mechanism [211]. Moreover, Pin1 was associated with the mitochondrial apoptotic machinery especially in neurons. Since these findings exhibit an important role for Pin1 in neuronal cell death, this work strengthens the evidence that Pin1 is linked to cell death pathways in neurons. This was supported by the finding that Pin1 inhibition reduced cell death and that this protective effect was accompanied by changes in mitochondrial function and alterations of mitochondrial morphology. This was verified by the proof that Pin1 inhibition with a specific inhibitor, Br57, rescued cells from cell death and increased cell viability (Figure 23). Moreover, Pin1 inhibition led to decreased ATP production in control conditions and increased small sphere-shaped category 2 mitochondria were observed (Figure 24 and 25). Pin1 is highly expressed in proliferating cells as well as in neurons. It has been reported that in non-neural cells Pin1 is mainly localized in the nucleus [212]. However, in neuronal cells a significant amount of Pin1 is staked to the mitochondria [190]. The pro-apoptotic protein Bim_{EL} which is localized at the mitochondria triggers, after its JNK-induced phosphorylation at ser65, apoptosis particularly in neurons. Pin1 interacts with pSer65 Bim_{EL} thereby stabilizing it by inhibiting the proteasomal degradation of Bim_{EL}. A neuronal specific JNK signaling scaffold protein JIP3, which is localized at the mitochondria, is known to be an interaction partner of Pin1. This is the cause why Pin1 is also tethered to the mitochondrial membrane in neurons. Under this aspect, Pin1 is in close proximity to its substrate Bim_{EL} and due to different apoptotic stimuli Pin1 dissociates from JIP3 and concomitantly interacts with pSer65 Bim_{EL} at the mitochondria thereby promoting cell death [156]. Since Pin1 activates the mitochondrial apoptotic machinery and thus promotes cell death, the findings of this study, that Pin1 inhibition prevented cell death and more important that this was accompanied by mitochondrial alterations, were not completely unexpected. The observation that Pin1 inhibition with Br57 resulted in enhanced mitochondrial fission, illustrated in elevated category 2 mitochondria, is in line with the decrease in ATP production. To maximize the capacity of Oxphos under stressful conditions mitochondria become more fused and ATP production is increased [213]. Consequently, enhanced

mitochondrial fission is associated with depleted ATP levels. The results of this work are therefore in agreement with these facts and underline the pivotal role of Pin1 on mitochondrial metabolism. Interestingly, measurements of the MMP after Pin1 inhibition revealed no changes compared to control conditions. It was reported that a loss in mitochondrial fusion is associated with reduced respiratory capacity and reduced maximal respiration [214]. The findings of this study are in accordance with these facts. After Pin1 inhibition with Br57, not only decreased ATP levels and elevated mitochondrial fission were monitored, but also decreased mitochondrial respiratory capacity and diminished maximal respiration in control conditions (Figure 25). However, a full decrease like it occurred in glutamate treated cells was prevented by Pin1 inhibition. The certainty that Pin1 affects mitochondrial morphology and mitochondrial function was demonstrated in this thesis. However, the mechanism why elevated mitochondrial fission, depleted ATP levels and decreased respiratory capacity were outcomes of Pin1 inhibition is still elusive. Till now insufficient studies provide evidence for the impact of Pin1 on mitochondrial dynamics and to investigate the exact mechanism of how Pin1 regulates alterations in mitochondrial morphology and metabolism, more investigations have to be done.

One of the most enigmatic findings of this study was the observation that in contrast to Pin1 inhibition with Br57, Pin1 silencing with siRNA did not provide protective effects against glutamate-induced cell death. Two different siRNAs were used to examine the particular role of Pin1 on cell viability. However, as both experiments revealed Pin1 silencing did not rescue HT22 cells from cell death (Figure 26). Beyond that, the combination of siPin1 with Br57 resulted in increased cell viability even up to control levels, which is contradictory (Figure 26). There are several possibilities to explain this phenomenon. The first and easiest would be that the inhibitor Br57 is not specific for Pin1. However, as shown in the publication from Daum et al. Br57 exhibited a strong inhibitory effect of hPin1 with K_i values in the sub-micromolar range. The inhibition of hPin1 by Br57 was determined in a protease-free PPIase assay and Br57 was one of the most potent inhibitors of this work [174]. Different compounds of this work which also exhibited hPin1 inhibitory effects were tested in a luciferase reporter gene assay with a p53 response element in MCF7 cells. After DNA damage due to chemotherapeutic drugs or other stimuli the phosphorylated form of p53 interacts with Pin1. In this pathway, increased activity and higher proteolytic stability of p53 was observed due to conformational changes induced by

Pin1. The compounds tested in this model were able to reduce p53 stability and activity of the p53 reporter gene. Similarly, co-transfected Pin1-negative mutant MEFs with an expression construct for an inactive Pin1 variant failed to stabilize and activate p53, which underlines the specificity for these inhibitors. Moreover, it has to be mentioned that the compounds tested in MCF7 cells have a ten times less inhibitory potency than Br57 [174]. The second possibility could be due to the fact that the biological activity of PPIases does not directly correlate with their concentration. For instance, the yeast homolog of Pin1, Ess1, exhibits in lowest concentrations a pro-survival function, whereas the complete knockdown of Pin1 is lethal. Thus, the achieved knockdown of Pin1 in this study may not be sufficient to decrease Pin1 levels to an extent that protective effects can be determined. Another issue could be that although Pin1 levels were depleted, remaining Pin1 was enough to execute lethal effects which were inhibited by Br57. This inhibitory effect of Br57 on the biological activity of depleted Pin1 levels resulted in increased cell viability.

Taken together, this part exhibits a crucial role for Pin1 in cell death pathways induced by oxidative stress in HT22 cells. Moreover, Pin1 has a direct influence on mitochondrial dynamics as Pin1 inhibition induced an increase in mitochondrial fission which was accompanied by a slight decrease in ATP production. Furthermore, decreased respiratory capacity was observed and nevertheless, all these effects led to increased cell viability. To identify the exact mechanism of Pin1's mitochondrial activity more investigations have to be done, however, the impact at the level of mitochondria and the resulting decrease of cell death with Br57 are promising targets for mitoprotection and thereby neuroprotection.

4.4. The role of trypsin-like serine proteases in glutamate-induced cell death in HT22 cells

4.4.1. Serine protease inhibition provides protective effects in HT22 cells

The second part of the present study demonstrated a significant protective effect by inhibition of trypsin-like serine proteases, suggesting that the activation of such proteases contributes to delayed neuronal cell death. This evidence was supported by several findings showing that an irreversible inhibitor of trypsin-like serine proteases, TLCK, abolished mitochondrial dysfunction and increased cell viability. In particular, lipid peroxidation was completely reduced and mitochondrial morphology alterations due to glutamate toxicity were prevented. Moreover, the impairment of the MMP was preserved and HT22 cells and primary cortical neurons were less susceptible to glutamate. In general, many proteases are linked to neurological disorders and are associated with apoptosis, aging and several other diseases [85]. Among all proteases, caspases are the best-studied contributors to PCD pathways, while little is known about the involvement of non-caspase death regulators, such as calpains, lysosomal cathepsins and serine proteases. However, in the last years they have been associated with different paradigms of PCD and moved into the focus of apoptotic research [13,215–217]. In this work, from all proteases serine proteases engage a central role as mediators of oxidative stress-induced cell death in HT22 cells.

So far, serine proteases have been implicated in different model systems of apoptotic cell death pathways. The serine protease chymotrypsin B was shown to be involved in TNFα-induced cell death in rat liver cells. The translocation of lysosomal chymotrypsin B into the cytosol and the subsequent cleavage/activation of Bid were triggered by TNFα. Bid cleavage resulted in a rapid release of mitochondrial Cytc which was followed by cell death. In this work, the knockdown of chymotrypsin B by RNA interference and the irreversible chymotrypsin inhibitor TPCK provided protective effects [218]. In another model of cell death it was shown that neuronal cells underwent apoptosis upon treatment with the microtubule-disrupting agent colchicine. TLCK prevented nuclear fragmentation and provided protective effects, whereas TPCK failed to rescue cells from cell death [130]. In this mode of cell death caspases were also identified as mediators of apoptosis, however, TLCK exhibited a much

more pronounced protective effect than the general caspase inhibitor z-VAD-fmk. Also in paradigms of oxidative stress-induced cell death serine proteases play a crucial role. In retinal cells H_2O_2 induced enhanced expression of the mitochondrial serine protease Omi/HtrA2 which subsequently translocated to the cytosol where it promoted apoptosis in a caspase-mediated pathway. The specific Omi/HtrA2 inhibitor Ucf-101 as well as RNA interference reduced the cytosolic translocation of Omi/HtrA2, attenuated caspase-3 activation and prevented cell death. These findings suggest that the serine protease Omi/HtrA2 is involved in oxidative stress-induced cell death in a caspase-dependent manner [219]. However, Omi/HtrA2 can also mediate cell death through caspase-independent mechanisms via its serine protease activity [220]. Moreover, in the model system of glutamate-induced cell death in HT22 cells Ucf-101 exhibited protective effects as shown by the work of Landshamer [125]. Furthermore, in a model of focal cerebral ischemia the inhibitor Ucf-101 provided protective effects, indicating a pro-apoptotic function for Omi/HtrA2 in ischemic neuronal cell death [124]. Additionally, Ucf-101 protected neurons against cerebral oxidative injury [221]. Contrarily to these pro-apoptotic properties, mice lacking the Omi/HtrA2 gene die within 30 days after birth, suggesting a neuroprotective role of Omi/HtrA2 in neurons [222]. All these investigations place serine proteases in an emerging role as mediators of PCD, although the contribution and execution of cell death pathways are dependent on cell types and apoptotic inducing stimuli. This study confirmed the contribution of trypsin-like serine proteases to neuronal PCD pathways. In HT22 cells TLCK exhibited a strong protective effect against glutamate-induced cell death (Figure 27). The activation of serine proteases in this model seemed to be in a very initial phase, as TLCK prevented cell death only in post-treatment conditions up to 2 h. Future application of TLCK after 4 and 6 h after the onset of glutamate failed to rescue HT22 cells from cell death (Figure 28). This implicates that trypsin-like serine proteases are mediators of oxidative stress-induced cell death in HT22 cells and are activated in the beginning of this pathway. So far, the proposed deleterious role of serine proteases is based on results obtained in HT22 cells. To extend these findings to more physiological conditions the impact of TLCK was examined in primary cortical neurons. TLCK exhibited protective effects on cell viability in primary neurons, where glutamate-induced excitotoxicity led to apoptosis (Figure 29). This insight underlines the rising importance of serine proteases as relevant executioners of neuronal cell death in conditions of oxidative stress.

Chymotrypsin-like serine proteases (CSPs) the second subfamily of serine proteases, closely related to trypsin-like serine proteases, was associated with neuronal damage induced by ischemia. The work of Hara et al. showed that transient forebrain ischemia led to increased neuronal cell death in the CA1 region of the hippocampus in mice. The administration of the irreversible CSP inhibitor, TPCK, produced a distinct neuroprotective effect when given 1 h before or after the ischemic insult. Even when applied up to 24 h after ischemia TPCK prevented neuronal damage [129]. In contrary to these observations, the work of Movsesyan et al. clearly demonstrated that chymotrypsin-like serine proteases are not involved in neuronal cell death after TBI. TBI was associated with a progressive, time-dependent increase of CSPs activity in injured rat cortices, however, elevated trypsin-like serine protease activity was not detected. This implicates that cell death induced by TBI is mediated through activated CSPs. The administration of TPCK to rats after TBI did not affect cognitive recovery and even exacerbated motor dysfunction. Moreover, higher doses of TPCK exhibited cytotoxic effects in rat cortical neurons and other cell lines [223]. The results obtained from this work are in accordance with the findings from Movsesyan. In the HT22 model system TPCK did not prevent cell death induced by glutamate. Interestingly, TPCK even decreased cell viability in higher concentrations (Figure 30). Taken together, these findings demonstrated that trypsin-like serine protease activation contributes to glutamate-induced cell death in HT22 cells, whereas CSPs do not play a major role in this paradigm of PCD.

4.4.2. Serine protease activation – a target upstream of the pro-apoptotic protein Bid

Previous results of this work demonstrated that serine proteases were activated at an early time point after glutamate exposure. Initial events of glutamate-induced cell death in HT22 cells involve the first boost in ROS, resulting in elevated lipid peroxidation and the subsequent activation and translocation of Bid to the mitochondria [72]. Recently, the lysosomal serine protease chymotrypsin B was linked to oxidative stress-induced cell death pathways mediating its apoptogenic function via the cleavage of Bid. H_2O_2-induced lysosomal membrane permeabilization resulted in the redistribution of chymotrypsin B to the cytoplasm where it activated/cleaved Bid [127]. These findings led to the question, do trypsin-like serine proteases mediate their pro-apoptotic function upstream or downstream of Bid

activation? As the results of this study revealed, tBid-induced cell death was not prevented by TLCK (Figure 31). This finding fits to the observation that also in other model systems serine proteases led to the activation of Bid thereby potentiating apoptosis. The afore-mentioned early occurring feature of glutamate-induced cell death in HT22 cells is the initial increase in lipid peroxidation. It has to be mentioned that the specific Bid inhibitor BI6c9 provided strong protective effects in HT22 cells accompanied by the restoration of mitochondrial function. However, the primary ROS increase was not prevented by BI6c9 application in the presence of glutamate, which indicates that Bid activation occurs downstream of this feature [72]. TLCK was shown to precede its anti-apoptotic properties upstream of Bid activation and furthermore, even upstream of the first increase in ROS as TLCK completely abolished lipid peroxidation. In the presence of glutamate TLCK reduced lipid peroxide production even to control levels (Figure 32). These findings led to the assumption that TLCK may provide its protective effects by antioxidative properties. The work of Takahashi et al. revealed an antioxidative action of TLCK. H_2O_2-induced cell death in GSH-depleted cardiomyocytes and the production of ROS were significantly prevented by TLCK treatment, however, other serine protease inhibitors failed to do so [204]. The current study provided evidence that TLCK did not protect HT22 cells against H_2O_2-induced cell death (Figure 33). Based on these results, if TLCK exhibits antioxidative features, at least in this model system these properties seem not to contribute to the protective potential of TLCK as the same decrease of cell viability was observed in TLCK co-treated cells as in H_2O_2-treated control cells.

All these findings depict a pivotal role for trypsin-like serine proteases in conditions of oxidative stress-induced cell death in HT22 cells. Moreover, the activation of serine proteases occurs at a very initial phase upstream of Bid activation in this paradigm of PCD.

4.4.3. Serine proteases contribute to mitochondrial dysfunction

The present data demonstrated a crucial role for trypsin-like serine proteases in cell death pathways induced by oxidative stress. As mentioned above, mitochondrial fission and the loss of MMP are associated with caspase-independent pathways of neuronal cell death in HT22 cells. Mitochondrial dysfunction is mediated by the translocation of Bid to the mitochondria and the subsequent crucial AIF release, resulting in decreased cell viability [70,72]. The present study provided evidence that in

oxidative stress-induced cell death activation of trypsin-like serine proteases occurred upstream of the mitochondrial checkpoint. This was supported by the findings that TLCK prevented mitochondrial morphology alterations and preserved MMP (Figure 34). Glutamate induced a strong fragmentation of mitochondria which resulted in elevated levels of category 3 mitochondria. This increase was attenuated by TLCK, indicating an important role for trypsin-like serine proteases on mitochondrial dynamics. These findings are in accordance with those from Rideout et al. who revealed an involvement of trypsin-like serine proteases in DNA damage-induced cell death in neuronal cells upstream of mitochondrial Cytc release. Camptothecin-induced cell death resulted in impaired MMP following Cytc release and subsequently cell death. TLCK could prevent these events and rescued embryonic cortical neurons from cell death [137]. Another finding which strengthens the observation that trypsin-like serine proteases are activated upstream of the mitochondrial demise in HT22 cells is the fact that TLCK prevented ATP depletion which is a common feature in glutamate-induced cell death. ATP production was completely restored by serine protease inhibition with TLCK and furthermore, the impairment of the mitochondrial respiratory capacity and the decrease in mitochondrial respiration were significantly prevented (Figure 35). Indeed, the entire data on serine proteases which are demonstrated in this study revealed a pivotal role for trypsin-like serine proteases in PCD pathways induced by oxidative stress. Moreover, the mitoprotective effect places these proteases in a prominent position as new therapeutical targets for neurological disorders, where mitochondrial dysfunction causes neuronal cell death. However, why and how the inhibition of serine proteases prevents mitochondrial damage and increases cell death is largely unknown. The most pronounced effect of TLCK is indeed the inhibition of trypsin-like serine proteases, but TLCK has also shown a variety of actions beside the inhibitory effect on activated trypsin-like serine proteases, i.e. inactivation of protein kinase C [201] or blockage of cyclic AMP-dependent protein kinase [199]. Furthermore, it is reported that another property of TLCK is the inhibition of nuclear factor 'kappa-light-chain-enhancer' of activated B-cells (NF-κB) activation, which occurs due to different stimuli, i.e. interleukin 1β treatment and subsequently leads to cell death [224,225]. Although, TLCK interferes with NF-κB activation, the protective effect did not seem to be due to this mechanism in HT22 cells, as NF-κB activation after glutamate challenge did not appear in this model of oxidative stress and hence did not

contribute to cell death [230]. It is further mentioned that serine proteases have been implicated as functioning both upstream and downstream of caspases and that for instance serine proteases such as Omi/HtrA2 or granzyme B were identified as caspase activators [132,133,226]. Also chymotrypsin-like serine proteases where identified as caspase activators, as TPCK suppressed the activation of caspase-9 in apoptosis during hypoxia-reoxygenation in rat kidney cells [132]. However, as shown by Landshamer et al. caspase activation is not required for glutamate toxicity in HT22 cells as demonstrated by the findings that caspase-8 and caspase-2 inhibitors as well as the general caspase inhibitor z-VAD-fmk failed to rescue cells from oxidative stress-induced cell death [70,125]. Despite recent observations indicating a possible inhibitory effect of activated caspase-3, caspase-6 and caspase-7 of TLCK, these findings play a minor role in the model system of PCD in HT22 cells, as it is caspase-independent and nevertheless TLCK exhibited protective effects in conditions of glutamate toxicity [227]. Thus the protective effect seemed not to be due to the inhibition of the caspase-cascade cell death pathway in HT22 cells. Another interesting target of TLCK is the tumor suppressor protein p53. p53 depicts an essential role in cell-cycle progression and apoptosis which is influenced by several factors, such as cell type and stress stimuli [134,135]. Different studies revealed a protective effect of TLCK by preventing the accumulation of p53 and thereby attenuating cell death [131,137]. The work of Diemert demonstrated a protective effect of pifithrin-α, an inhibitor of p53, in the model of glutamate toxicity in HT22 cells, which may assume that the possible mechanism of TLCK's protective effect is due to the p53 pathway [230]. However, silencing of p53 with siRNA failed to rescue glutamate-induced cell death in HT22 (data not published), which contradicts this hypothesis.

Although, the target of action of TLCK and the exact mechanism how serine protease inhibition prevents cell death and rescues mitochondrial function is still elusive, this study depicted a prominent role for serine proteases as mediators of oxidative stress-induced cell death in HT22 cells.

4.4.4. The impact of serine proteases on protein interactions

Up to now, the data of this thesis demonstrated an important role for trypsin-like serine proteases in PCD pathways in HT22 cells. In particular, the mitochondria were the main focus of this research and in this context the influence of activated serine

proteases on mitochondrial function and fission and fusion processes was investigated. As mentioned before, mitochondrial shape in living cells can range from sphere-shaped morphology to tubular network structures. Since mitochondria produce the largest amount of energy for cellular processes, the distribution within cells can be very heterogeneous. They are often enriched at cellular sites where their metabolic function is required, like at synaptic terminals for instance. This mitochondrial movement is also under the control of the cytoskeleton. Eukaryotic cells contain three major kinds of cytoskeletal filaments: microfilaments (actin filaments), intermediate filaments and microtubules [228]. A growing body of evidence suggests that the actin cytoskeleton is involved in the positioning of mitochondria and also in mitochondrial fission processes. Recently it was reported that actin participates in mitochondrial clustering, ROS production and cell death upon death receptor activation [229]. Moreover, the work of Barbier et al. demonstrated that modulation of F-actin dynamics regulate a particular type of cell death, namely caspase-independent type III PCD. This form of PCD was investigated in B-cells from patients with chronic lymphocytic leukemia and is mediated by CD47 ligation which leads to the activation of CSPs, followed by F-actin disruption and the subsequent redistribution of Drp1 from the cytoplasm to the mitochondria. Interestingly, the application of TPCK inhibited actin disruption and the following Drp1 translocation to the mitochondria which indicate that chymotrypsin-like serine proteases mediated this pathway of PCD. Moreover, this implies a connection of actin dynamics with Drp1, which is one of the major regulators of mitochondrial fission and cell death. In contrast to these findings, De Vos et al. revealed that upon F-actin disruption Drp1 translocation to the mitochondria was attenuated in CV1 cells [49]. Although, these findings go in opposing directions, possibly due to different cell types and cell death stimuli, both investigators exhibited a pivotal role for F-actin in mitochondrial recruitment of Drp1 followed by mitochondrial fission and cell death. And furthermore, these events, at least evidenced in one case, seem to be mediated by serine proteases. This study demonstrated an interactive connectivity between Drp1 and actin which was lost after glutamate treatment, indicating a release of Drp1 from the actin cytoskeleton. Moreover, glutamate induced a redistribution of Drp1 from the cytoplasm to the mitochondria in conditions of oxidative stress in HT22 cells (Figure 36). Unfortunately, these steps could not be prevented by the application of the serine protease inhibitor TLCK. This implies that Drp1 is in fact connected with the

actin cytoskeleton and that glutamate induces a release and translocation of Drp1 to the mitochondria, however, these events are not mediated by trypsin-like serine proteases in conditions of glutamate toxicity in HT22 cells.

As demonstrated in the first part of this study, CypA is involved in the pathway of glutamate-induced cell death in HT22 cells. Interestingly, the work of Cereghetti et al. showed that Drp1 interacts with CypA in the cytosol. In addition, calcineurin was as well identified as an interaction partner of Drp1. Dephosphorylation of Ser637 of Drp1 by calcineurin regulates Drp1 translocation to the mitochondria and promotes mitochondrial fission resulting in apoptosis. Moreover, the interaction of CypA and Drp1 is lost by induction of calcineurin activity. These results demonstrate that the Drp1-CypA-calcineurin axis is involved in mitochondrial fission and disruption of this ternary complex leads to cell death [51]. The present study revealed that Drp1 interacts with CypA and that this interaction is diminished after glutamate treatment in HT22 cells. Surprisingly, the inhibition of trypsin-like serine proteases with TLCK led to a much more pronounced interaction of Drp1 and CypA than it was observed in control conditions (Figure 37). Despite the increased interaction of Drp1 and CypA, the redistribution of Drp1 from the cytoplasm to the mitochondria was not abolished by TLCK. As mentioned above, calcineurin mediates Drp1 dephosphorylation and translocation to the mitochondria and thereby induces mitochondrial fission. The work of Zhao et al. evidenced that calcineurin activity is regulated by the activation of CSPs. Active CSPs cleave the autoinhibitory subunit of calcineurin thereby activating it and accounting for the translocation of Drp1 from the cytoplasm to the mitochondria resulting in apoptosis (data not published, poster 100, ECDO 2013, Paris). In HT22 cells, however, calcineurin did not contribute to cell death induced by glutamate as tacrolimus, a calcineurin inhibitor, did not provide protective effects against glutamate toxicity (Figure 38).

Taken together, the second part of this thesis revealed a pivotal role for trypsin-like serine proteases in the paradigm of PCD in HT22 cells. Further, mitoprotection and complete restoration of mitochondrial function was achieved by serine protease inhibition with TLCK. Moreover, it was demonstrated that trypsin-like serine proteases act upstream of Bid activation and additionally, in HT22 cells the activation occurred in a very initial phase even before the first increase in ROS. However, the exact mechanism behind the protective effect of TLCK is still elusive. It could be

demonstrated though, that trypsin-like serine proteases are not involved in the release of Drp1 from the actin cytoskeleton and in the redistribution of Drp1 to the mitochondria as TLCK did not prevent these events. Moreover, it was shown that serine proteases have an influence on the interaction of Drp1 and CypA, however, the remaining questions are how and why is the interaction of these proteins increased. Further, this study demonstrated that calcineurin is not involved in glutamate-induced cell death in HT22 cells. But it has to be mentioned that trypsin-like serine proteases exhibit a potential target for therapeutical approaches in neurological diseases because the inhibition seems to abolish cell death features in an initial phase and thereby may rescue cell death before the so called 'decision points' of life and death in cells (Figure 40, scheme of serine protease-mediated cell death).

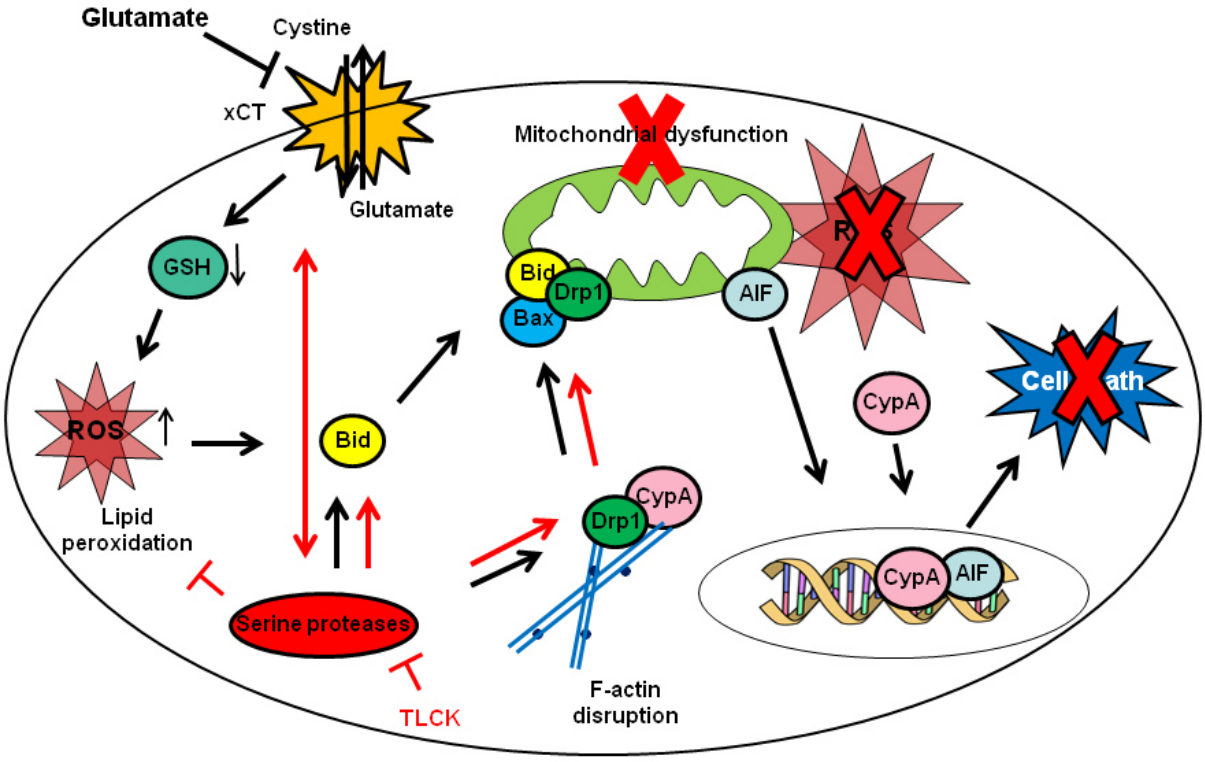

Figure 40: Serine protease-mediated cell death and the impact of TLCK

Glutamate-induced GSH depletion which resulted in increased ROS accumulation and mitochondrial dysfunction led to cell death in HT22 cells (black arrows depict the action of glutamate). Serine protease inhibition with TLCK prevented all features associated with mitochondrial dysfunction and decreased cell death. Trypsin-like serine proteases act upstream of Bid activation and TLCK did not prevent the release of Drp1 from the actin cytoskeleton and the following redistribution to the mitochondria but increased the interaction of Drp1 and CypA. Lipid peroxidation was completely abolished by TLCK treatment placing serine proteases in a more initial phase of this cell death pathway (red arrows/marks illustrate the consequence of serine protease inhibition).

5. Summary

Many neurological disorders and neurodegenerative diseases are associated with mitochondrial abnormalities. Mitochondria are essential organelles regulating the energy metabolism of the cell, thereby, determining essential cellular functions and viability. This accounts particularly for neurons which show a pronounced energy demand and where mitochondria play a pivotal role in balancing the Ca^{2+} homeostasis, controlling ROS formation and providing most of the energy for neurotransmitter metabolism and maintenance of the membrane potential. Further, mitochondria are essential organelles controlling the 'point of no return' in intrinsic pathways of programmed cell death where the decision between cellular life and death involves post-translational protein modifications determining mitochondrial dysfunction and release of detrimental proteins such as AIF. Therefore, major aims of the present thesis included the characterization of the key regulators of protein modifications that occur upstream of mitochondrial demise and AIF release. In this context, the role of two PPIases, CypA and Pin1, and the involvement of serine proteases in paradigms of PCD were investigated. Most experiments were performed in an immortalized neuronal cell line (HT22 cells) which depicts a well-established model to study caspase-independent cell death induced by glutamate. The most prominent feature in this model of cell death is the mitochondrial AIF release and the subsequent translocation to the nucleus where it induces chromatinolysis. To substantiate the importance of these results further experiments were performed in a model of glutamate-induced excitotoxicity in primary cortical neurons.

The findings of the first part of this study revealed a prominent role for CypA in glutamate-induced mitochondrial AIF release and cell death. Glutamate toxicity resulted in the translocation of CypA to the nucleus where it built a pro-apoptotic complex with AIF, thereby inducing chromatinolysis. Silencing of CypA protected HT22 cells against glutamate toxicity. Moreover, the depletion of CypA preserved mitochondrial fission and the loss of MMP and also prevented the release of AIF from the mitochondria. Furthermore, lipid peroxidation arising from the mitochondria was attenuated which supported increased cell viability.

Further experiments addressed the involvement of a second family member of PPIases, Pin1, in neuronal cell death pathways. The inhibition of Pin1 with Br57

resulted in decreased susceptibility of HT22 cells to glutamate toxicity. This increase in cell viability was attended by changes at the level of mitochondria. Pin1 inhibition led to enhanced mitochondrial fission, but further, complete mitochondrial fragmentation induced by glutamate was attenuated. This elevated mitochondrial fission rate was accompanied by a slight decrease in ATP levels in Br57-treated controls, however, the strong ATP depletion that occurred after the glutamate challenge was prevented and the impairment of MMP was abolished.

In summary, these findings depict a pivotal role for CypA and Pin1 in glutamate-induced cell death in HT22 cells upstream of mitochondrial demise. Since this model exhibits common features of neurological disorders the results obtained here may give a platform to investigate new neuroprotective strategies.

The second part of this thesis dealt with the impact of activated trypsin-like serine proteases on cell viability and mitochondrial function. Inhibition of serine proteases with TLCK resulted in increased cell viability in HT22 cells and in primary cortical neurons. Furthermore, this work revealed that activation of trypsin-like serine proteases occurred upstream of Bid activation and moreover, in a very initial phase of this PCD pathway in HT22 cells. Further, lipid peroxidation was blocked and mitochondrial morphology alterations were prevented. In addition, ATP depletion and the impairment of the MMP were preserved and the decrease in mitochondrial respiration after glutamate toxicity was abolished. Interestingly, the interaction of Drp1 and CypA was strengthened by TLCK. However, the release of Drp1 from the actin cytoskeleton and the following redistribution of Drp1 from the cytoplasm to the mitochondria were not prevented.

In conclusion, the second part of this thesis highlighted trypsin-like serine proteases as mediators of glutamate-induced cell death in HT22 cells. The initial activation in this PCD pathway is a promising target for therapeutic intervention strategies in neurological diseases.

6. Zusammenfassung

Mitochondrien gelten als „Kraftwerke“ der Zelle, da sie in Form von ATP die Energie bereitstellen, die für nahezu alle zellulären Prozesse benötigt wird. Zudem sind Mitochondrien an einer Vielzahl von biochemischen Mechanismen und Signalkaskaden beteiligt, wie z.B. der Aufrechterhaltung der intrazellulären Ca^{2+} Homöostase oder der kontrollierten Bildung reaktiver Sauerstoffspezies. Neben diesen Funktionen spielen Mitochondrien eine zentrale Rolle bei Alterungsprozessen von Zellen und bei intrinsischen Signalkaskaden des programmierten Zelltods. Mitochondrien stellen dabei hochdynamische Organellen dar, die morphologisch entweder lange miteinander verbundene Netzwerke ausbilden oder als kleine kugelförmige Organellen vorliegen. Es besteht ein hochreguliertes Gleichgewicht dieser morphologischen Zustände, das unter pathologischen Bedingungen gestört wird und so zur Dysfunktion der Organellen und zum Zelltod beitragen kann. Entsprechende mitochondriale Veränderungen sind beispielsweise in Neuronen bei altersbedingten neurodegenerativen Erkrankungen wie Morbus Alzheimer, Morbus Parkinson, sowie nach akuten Hirnschädigungen durch Schädel-Hirn-Trauma oder Schlaganfall nachgewiesen worden. Darüber hinaus wurden sie mit den strukturellen und funktionellen Schädigungen der Organellen und der betroffenen Neurone in Verbindung gebracht. Post-translationale Proteinmodifikationen, Isomerisierung von Proteinen oder Protein-Protein Interaktionen können u.a. der Grund für solche mitochondrialen Fehlfunktionen sein und zum Nervenzelltod beitragen.

Aus einer Vielzahl von Forschungsarbeiten ist bekannt, dass Mitochondrien eine zentrale Rolle in den intrinsischen Signalwegen des programmierten Zelltods in Neuronen einnehmen, der vor allem durch die Zerstörung der mitochondrialen Membranintegrität gekennzeichnet ist. Hierbei ist der wesentliche Schritt die Freisetzung des pro-apoptotischen Proteins AIF aus dem mitochondrialen Intermembranraum. Daher waren die Hauptziele der vorliegenden Arbeit, neue Regulatoren der Mitochondrienschädigung und der Freisetzung von AIF in Modellen des programmierten Zelltods zu charakterisieren und diese als mögliche Ziele therapeutischer Angriffspunkte zu definieren. In diesem Zusammenhang wurde die Beteiligung von zwei Peptidyl-prolyl cis-trans Isomerasen CypA und Pin1 sowie von Serinproteasen an mitochondrialen Schädigungsmechanismen untersucht.

Die Mehrzahl der Experimente wurde in einer hippokampalen neuronalen Mauszelllinie (HT22 Zellen) durchgeführt. Dabei handelt es sich um ein gut charakterisiertes Modellsystem für oxidativen Stress in Neuronen, das insbesondere für Untersuchungen mitochondrialer Prozesse bei intrinsischen Signalkaskaden des programmierten Zelltods hervorragend geeignet ist. Das bedeutendste Merkmal dieser Form des Zelltods ist die Freisetzung von AIF aus den Mitochondrien und die anschließende Translokation in den Zellkern, in dem AIF eine Schädigung der DNA hervorruft. Die Ergebnisse aus den HT22 Zellen wurden zudem in weiteren Experimenten im Modell der Glutamat-induzierten Exzitotoxizität in primären Neuronen verifiziert.

Der erste Teil dieser Arbeit zeigt, dass CypA in Neuronen eine wichtige Rolle im Glutamat-induzierten Zelltod und der mitochondrialen AIF Freisetzung spielt. Glutamattoxizität führt zu einer Translokation von CypA in den Zellkern, wo es mit AIF einen pro-apoptotischen Komplex bildet, der zur Schädigung der DNA führt. Die verminderte Expression von CypA schützt HT22 Zellen gegen Glutamattoxizität und zudem waren infolge der verminderten CypA-Spiegel die Mitochondrien geschützt. Eine Hemmung der CypA Expression verhindert ferner den Verlust des Mitochondrienmembranpotentials und die Fragmentierung der Organellen als typische morphologische Veränderung der geschädigten Mitochondrien sowie die Freisetzung von AIF aus dem mitochondrialen Intermembranraum. Weiterhin wurde die Lipidperoxidation in den Zellen deutlich abgeschwächt, die in der Spätphase der Glutamatschädigung durch mitochondriale Schäden gesteigert wird und die Endphase des Zelltods kennzeichnet.

Andere Untersuchungen dieser Arbeit zeigen, dass Pin1, eine weitere Peptidyl-prolyl cis-trans Isomerase, ebenfalls an neuronalen Zelltodmechanismen und mitochondrialen Veränderungen beteiligt ist. Der spezifische Pin1 Inhibitor Br57 führt zu einer verminderten Empfindlichkeit der HT22 Zellen gegenüber Glutamat. Die dadurch bedingte Zunahme der Zellviabilität ist mit mitochondrialen Veränderungen assoziiert. Die Applikation von Br57 alleine resultiert einerseits in einer zunehmenden Mitochondrienfragmentierung, kann andererseits allerdings die weitere Fragmentierung der Mitochondrien, die durch Glutamat hervorgerufen wird, verhindern. Die erhöhte Mitochondrienteilung war dabei mit einer leichten Reduktion der ATP Spiegel in Br57 behandelten Kontrollzellen verbunden. Jedoch wird der

deutliche Abfall der ATP Spiegel, der normalerweise nach Glutamatschädigung auftritt, verhindert. Des Weiteren wird der Glutamat-induzierte Zusammenbruch des Mitochondrienmembranpotentials durch die Pin1 Inhibition günstig beeinflusst.

Zusammenfassend zeigt der erste Teil dieser Arbeit, dass beide Peptidyl-prolyl cis-trans Isomerasen, CypA und Pin1, in den intrinsischen Signalkaskaden des neuronalen Zelltods eine besondere Funktion einnehmen. Dabei sind sie offenbar entscheidend an der Regulation der Mitochondrienintegrität und -funktion beteiligt, so dass diese PPIs vielversprechende Angriffspunkte für neue neuroprotektive Strategien darstellen.

Der zweite Teil dieser Dissertation befasst sich mit dem Einfluss von aktivierten Serinproteasen auf mitochondriale Funktionen und dem daraus resultierenden Zelltod. Die Hemmung von Serinproteasen mit TLCK, einem Serinproteaseinhibitor, konnte den durch Glutamat-induzierten Zelltod sowohl in HT22 Zellen als auch in primären kortikalen Neuronen verhindern. Weiterhin zeigt diese Arbeit, dass die Aktivierung von Serinproteasen zu einem sehr frühen Zeitpunkt in dieser Form des programmierten Zelltods in HT22 Zellen stattfindet, bereits bevor die Aktivierung des pro-apoptotischen Proteins Bid und die daraus folgende Schädigung der Mitochondrien einsetzen. Ferner vermindert der Serinproteaseinhibitor TLCK die Glutamat-induzierte Lipidperoxidation, pathologische und morphologische Veränderungen der Mitochondrien, ATP Depletion sowie die Verminderung des Mitochondrienmembranpotentials und den Abfall der mitochondrialen Atmung. Interessanterweise wird gleichzeitig durch TLCK die Interaktion zwischen Drp1 und CypA verstärkt. Allerdings werden die Freisetzung von Drp1 aus dem Aktinzytoskelett und die darauffolgende Translokation von Drp1 aus dem Zytoplasma zu den Mitochondrien nicht verhindert.

Zusammenfassend zeigt der zweite Teil dieser Arbeit, dass Serinproteasen vom Trypsintyp den Glutamat-induzierten oxidativen Zelltod in neuronalen HT22 Zellen vermitteln. Die initiale Aktivierung von Serinproteasen in diesem Modell des programmierten Zelltods ist ein möglicher therapeutischer Ansatzpunkt bei neurologischen Erkrankungen und Alterungsprozessen, bei denen oxidativer Stress und daraus folgende mitochondriale Schädigungsmechanismen wesentlich zur Fortschreitung der pathologischen Veränderungen in den Nervenzellen beitragen.

7. Abbreviations

Abbreviation	Full text
°C	Grad Celsius
µ	Micro
µM	Micromolar
AD	Alzheimer's disease
AIF	Apoptosis-inducing-factor
ALS	Amyotrophic lateral sclerosis
AMPA	2-amin-3-(3-hydroxy-5-methylisoxazol-4-yl) propionate
ANOVA	Analysis of variance
ANT	Adenine nucleotide translocator
Apaf1	Apoptosis-protease activating factor
APP	Amyloid precursor
ATP	Adenosinetriphosphate
AVPI	AnnexinV/propidium iodide
Bak	Bcl2 antagonist killer 1
Bax	Bcl2-associated x protein
BCA	Bicinchoninic acid
Bcl2	B-cell-lymphoma 2
Bid	Bcl2 interacting domain death agonist
Bim_{EL}	Bcl-2 interacting mediator of cell death
BODIPY	4,4-diflouro-5-(4-phenyl1,3-butadienyl)-4-bora-3a,4a-diaza-s-indacene-3-undecanoic acid
Bp	Base pare
Br57	Pin1 inhibitor
Ca^{2+}	Calcium
CAD	Caspase-activated deoxyribonuclease
CaMK	Calcium/calmodulin-dependent kinase
CARD	Caspase recruitment domain
CCCP	Carbonylcyanide-3-chlorophenylhydrazone
cFLIP	Cellular FLICE inhibitor protein
CHOP	CCAAT/enhancer-binding protein-homologous protein
CMT2A	Charcot-Marie-Tooth 2A
CNS	Central nervous system
CsA	Cyclosporine A

CSPs	Chymotrypsin-like serine proteases
CTL	Cytotoxic T lymphocytes
CypA	Cyclophilin A
CypA$^{-/-}$	CypA knock out
CypB	Cyclophilin B
CypD	Cyclophilin D
Cyps	Cyclophilins
Cytc	Cytochrom c
DAPI	4`, 6-diamidino-2-phenylindole dihydrochloride
DD	Death domain
DED	Death effector domain
DISC	Death-inducing signaling complex
DMEM	Dulbecco's modified eagle medium
DMSO	Dimethylsulfoxide
DNA	Deoxyribonucleic acid
DOA	Dominant optic atrophy
Drp1	Dynamin-related protein 1
DSB	Double strand breaks
DTT	DL-Dithiotreitol
EndoG	Endonuclease G
ER	Endoplasmatic reticulum
ERK	Extracellular signal-regulated kinase
ETC	Electron transport chain
FACS	Fluorescence-activated cell sorting
FADD	Fas-associated death domain
FASL	FAS ligand
FCS	Fetal calf serum
Fis1	Mitochondria fission 1 protein
FK506	Tacrolimus
FKBP	FK506-binding proteins
GAPDH	Glyceraldehyde-3-phosphate-dehydrogenase
GSH	Glutathione
h	Hour
H_2O_2	Hydrogen peroxide
HBSS	Hank`s balanced medium

HCl	Hydrochloric acid
HD	Huntington's disease
HI	Hypoxia-ischemia
Hq	Harlequin
HtrA2/Omi	High temperature acquired protein A2
IAP	Inhibitor of apoptosis
ICAD	Inhibitor of CAD
ICE	Interleukin 1β converting enzyme
IMS	Mitochondrial intermembrane space
IP	Immunoprecipitation
JNK	C-Jun N-terminal kinase
kDa	Kilo Dalton
MAPK	Mitogen-activated protein kinase
MCAO	Middle cerebral artery occlusion
MEM+	Eagle's minimum essential medium
Mfn	Mitofusin
MIM	Mitochondrial inner membrane
MLS	Mitochondrial localization sequence
mM	Millimolar
MMP	Mitochondrial membrane potential
MNNG	1-methyl-2-nitro-1-nitrosoguanidine
MOM	Mitochondrial outer membrane
mtDNA	Mitochondrial DNA
MTT	3-(4,5-Dimethylthiazol-2-yl)-2,5-diphenyltetrazolium bromide
$NaHCO_3$	Sodium hydrogen carbonate
NaOH	Sodium hydroxide
NCI	Normalized cell index
NK	Natural killer
nM	Nanomolar
NMDA	N-methyl-D-aspartic acid
OGD	Oxygen glucose deprivation
Opa1	Optical atrophy 1
Oxphos	Oxidative phosphorylation
PARP	Poly (ADP-Ribose) Polymerase
PBS	Phosphate buffered saline

PCD	Programmed cell death
PD	Parkinson's disease
PEI	Polyethylenimine
PFA	Paraformaldeyde
pH	Potentia hydrogenii
PI	Propidium iodide
Pin1	Protein interacting with NIMA (never in mitosis A)-1
PPIase	Peptidyl-prolyl cis-trans isomerase
PTP	Permeability transition pore
PVDF	Polyvinylidenfluorid
RNA	Ribonucleic acid
ROCK	Rho-associated kinase
ROS	Reactive oxygen species
RT	Room temperature
SD	Standard deviation
SDS	Sodium dodecyl sulfate
SDS-PAGE	Sodium dodecyl sulfate polyacrylamide gel electrophoresis
siRNA	Small interfering RNA
Smac/Diablo	Second mitochondria-derived activator of caspases
tAIF	Truncated AIF
TBI	Traumatic brain injury
tBid	Truncated Bid
TBS	Tris bufferd solution
TBST	Tris bufferd solution with Tween 20
TCA	Tricarboxylic acid cycle
TE	Trypsin-EDTA
TEMED	Tetramethylenethylendiamin
TLCK	Nα-Tosyl-L-lysine-chlormethyl ketone hydrochloride
TMRE	Tetramethylrhodamine ethyl ester
TNFR1	TNFα receptor 1
TNFα	Tumor necrosis factor α
TPCK	Np-Tosyl-L-phenylalanyl chloromethyl ketone
TRADD	TNF receptor-associated death domain
TRAIL	TNF-related apoptosis inducing ligand
TRAILR	TRAIL receptor

VDAC	Voltage-dependent anioin channel
XIAP	X-chromosomal linked inhibitor of apoptosis

8. References

1. Loo DT, Copani A, Pike CJ, et al. Apoptosis is induced by beta-amyloid in cultured central nervous system neurons. Proc. Natl. Acad. Sci. U.S.A. 1993;90:7951–55.
2. Mattson MP. Apoptosis in neurodegenerative disorders. Nat. Rev. Mol. Cell Biol. 2000;1:120–29.
3. Culmsee C, Landshamer S. Molecular insights into mechanisms of the cell death program: role in the progression of neurodegenerative disorders. Curr Alzheimer Res. 2006;3:269–83.
4. Galluzzi L, Vitale I, Abrams JM, et al. Molecular definitions of cell death subroutines: recommendations of the Nomenclature Committee on Cell Death 2012. Cell Death Differ. 2011;19:107–20.
5. Kerr JFR, Wyllie AH, Currie AR. Apoptosis: a basic biological phenomenon with wide-ranging implications in tissue kinetics. British journal of cancer. 1972;26:239.
6. Wajant H. The Fas signaling pathway: more than a paradigm. Science. 2002;296:1635–36.
7. Schütze S, Tchikov V, Schneider-Brachert W. Regulation of TNFR1 and CD95 signalling by receptor compartmentalization. Nature reviews Molecular cell biology. 2008;9:655–62.
8. Elmore S. Apoptosis: a review of programmed cell death. Toxicologic pathology. 2007;35:495–516.
9. Schulze-Osthoff K, Ferrari D, Los M, et al. Apoptosis signaling by death receptors. European Journal of Biochemistry. 1998;254:439–59.
10. Kischkel FC, Hellbardt S, Behrmann I, et al. Cytotoxicity-dependent APO-1 (Fas/CD95)-associated proteins form a death-inducing signaling complex (DISC) with the receptor. The EMBO journal. 1995;14:5579.
11. Muzio M, Chinnaiyan AM, Kischkel FC, et al. FLICE, a novel FADD-homologous ICE/CED-3–like protease, is recruited to the CD95 (Fas/APO-1) death-inducing signaling complex. Cell. 1996;85:817–27.
12. Enari M, Sakahira H, Yokoyama H, et al. A caspase-activated DNase that degrades DNA during apoptosis, and its inhibitor ICAD. Nature. 1998;391:43–50.

13. Kroemer G, Martin SJ. Caspase-independent cell death. Nature medicine. 2005;11:725–30.
14. Kitazumi I, Tsukahara M. Regulation of DNA fragmentation: the role of caspases and phosphorylation. FEBS J. 2011;278:427–41.
15. Schug ZT, Gonzalvez F, Houtkooper RH, et al. BID is cleaved by caspase-8 within a native complex on the mitochondrial membrane. Cell Death & Differentiation. 2011;18:538–48.
16. Cheung ECC, McBride HM, Slack RS. Mitochondrial dynamics in the regulation of neuronal cell death. Apoptosis. 2007;12:979–92.
17. Mattson MP, Gleichmann M, Cheng A. Mitochondria in neuroplasticity and neurological disorders. Neuron. 2008;60:748–66.
18. Kroemer G, Petit P, Zamzami N, et al. The biochemistry of programmed cell death. The FASEB Journal. 1995;9:1277–87.
19. Adrain C, Creagh EM, Martin SJ. Apoptosis-associated release of Smac/DIABLO from mitochondria requires active caspases and is blocked by Bcl-2. The EMBO journal. 2001;20:6627–36.
20. Suzuki Y, Imai Y, Nakayama H, et al. A serine protease, HtrA2, is released from the mitochondria and interacts with XIAP, inducing cell death. Molecular Cell. 2001;8:613–21.
21. Green DR. Apoptotic pathways: ten minutes to dead. Cell. 2005;121:671–74.
22. Mehta SL, Manhas N, Raghubir R. Molecular targets in cerebral ischemia for developing novel therapeutics. Brain research reviews. 2007;54:34–66.
23. Chipuk JE, Fisher JC, Dillon CP, et al. Mechanism of apoptosis induction by inhibition of the anti-apoptotic BCL-2 proteins. Proceedings of the National Academy of Sciences. 2008;105:20327–32.
24. Cregan SP, Fortin A, MacLaurin JG, et al. Apoptosis-inducing factor is involved in the regulation of caspase-independent neuronal cell death. The Journal of cell biology. 2002;158:507–17.
25. Stefanis L. Caspase-dependent and -independent neuronal death: two distinct pathways to neuronal injury. Neuroscientist. 2005;11:50–62.
26. Joza N, Pospisilik JA, Hangen E, et al. AIF: Not Just an Apoptosis-Inducing Factor. Annals of the New York Academy of Sciences. 2009;1171:2–11.
27. Dirnagl U, Iadecola C, Moskowitz MA. Pathobiology of ischaemic stroke: an integrated view. Trends in neurosciences. 1999;22:391–97.

28. Chan DC. Mitochondria: dynamic organelles in disease, aging, and development. Cell. 2006;125:1241–52.
29. Wallace DC. A mitochondrial paradigm of metabolic and degenerative diseases, aging, and cancer: a dawn for evolutionary medicine. Annual review of genetics. 2005;39:359.
30. Lin MT, Beal MF. Mitochondrial dysfunction and oxidative stress in neurodegenerative diseases. Nature. 2006;443:787–95.
31. McBride HM, Neuspiel M, Wasiak S. Mitochondria: more than just a powerhouse. Current Biology. 2006;16:R551-R560.
32. Liu Y, Fiskum G, Schubert D. Generation of reactive oxygen species by the mitochondrial electron transport chain. Journal of Neurochemistry. 2002;80:780–87.
33. Eckert A, Keil U, Marques CA, et al. Mitochondrial dysfunction, apoptotic cell death, and Alzheimer's disease. Biochemical pharmacology. 2003;66:1627–34.
34. Sies H. Oxidative stress: oxidants and antioxidants. Experimental physiology. 1997;82:291–95.
35. Wang X. The expanding role of mitochondria in apoptosis. Genes & Development. 2001;15:2922–33.
36. Martinou J, Youle RJ. Mitochondria in apoptosis: Bcl-2 family members and mitochondrial dynamics. Developmental cell. 2011;21:92–101.
37. Wei MC, Zong W, Cheng EH, et al. Proapoptotic BAX and BAK: a requisite gateway to mitochondrial dysfunction and death. Science. 2001;292:727–30.
38. Chipuk JE, Moldoveanu T, Llambi F, et al. The BCL-2 family reunion. Molecular Cell. 2010;37:299–310.
39. Billen LP, Shamas-Din A, Andrews DW. Bid: a Bax-like BH3 protein. Oncogene. 2008;27:S93-S104.
40. Orth M, Schapira AH. Mitochondria and degenerative disorders. American journal of medical genetics. 2001;106:27–36.
41. Mattson MP, Kroemer G. Mitochondria in cell death: novel targets for neuroprotection and cardioprotection. Trends in molecular medicine. 2003;9:196–205.
42. Bossy-Wetzel E, Barsoum MJ, Godzik A, et al. Mitochondrial fission in apoptosis, neurodegeneration and aging. Current opinion in cell biology. 2003;15:706–16.

43. Smirnova E, Griparic L, Shurland D, et al. Dynamin-related protein Drp1 is required for mitochondrial division in mammalian cells. Molecular Biology of the Cell. 2001;12:2245–56.
44. James DI, Parone PA, Mattenberger Y, et al. hFis1, a novel component of the mammalian mitochondrial fission machinery. Journal of Biological Chemistry. 2003;278:36373–79.
45. Cipolat S, de Brito, Olga Martins, Dal Zilio B, et al. OPA1 requires mitofusin 1 to promote mitochondrial fusion. Proceedings of the National Academy of Sciences of the United States of America. 2004;101:15927–32.
46. Lackner LL, Nunnari J. Small molecule inhibitors of mitochondrial division: tools that translate basic biological research into medicine. Chemistry & biology. 2010;17:578–83.
47. Rappaport L, Oliviero P, Samuel JL. Cytoskeleton and mitochondrial morphology and function. Mol Cell Biochem. 1998;184:101–05.
48. Drubin DG, Jones HD, Wertman KF. Actin structure and function: roles in mitochondrial organization and morphogenesis in budding yeast and identification of the phalloidin-binding site. Molecular Biology of the Cell. 1993;4:1277–94.
49. De Vos, Kurt J., Allan VJ, Grierson AJ, et al. Mitochondrial Function and Actin Regulate Dynamin-Related Protein 1-Dependent Mitochondrial Fission. Current Biology. 2005;15:678–83. Accessed March 13, 2014.
50. Taguchi N, Ishihara N, Jofuku A, et al. Mitotic phosphorylation of dynamin-related GTPase Drp1 participates in mitochondrial fission. Journal of Biological Chemistry. 2007;282:11521–29.
51. G. M. Cereghetti, A. Stangherlin, O. Martins de Brito, C. R. Chang, C. Blackstone, P. Bernardi, and L. Scorrano. Dephosphorylation by calcineurin regulates. PNAS;2008:15803–08. Accessed January 27, 2014.
52. Cribbs JT, Strack S. Reversible phosphorylation of Drp1 by cyclic AMP-dependent protein kinase and calcineurin regulates mitochondrial fission and cell death. EMBO reports. 2007;8:939–44.
53. Cereghetti GM, Costa V, Scorrano L. Inhibition of Drp1-dependent mitochondrial fragmentation and apoptosis by a polypeptide antagonist of calcineurin. Cell Death Differ. 2010;17:1785–94. Accessed January 27, 2014.

54. Susin SA, Lorenzo HK, Zamzami N, et al. Molecular characterization of mitochondrial apoptosis-inducing factor. Nature. 1999;397:441–46.
55. Candé C, Cohen I, Daugas E, et al. Apoptosis-inducing factor (AIF): a novel caspase-independent death effector released from mitochondria. Biochimie. 2002;84:215–22.
56. Otera H, Ohsakaya S, Nagaura Z, et al. Export of mitochondrial AIF in response to proapoptotic stimuli depends on processing at the intermembrane space. The EMBO journal. 2005;24:1375–86.
57. Sevrioukova IF. Apoptosis-inducing factor: structure, function, and redox regulation. ANTIOXIDANTS & REDOX SIGNALING. 2011;14:2545–79.
58. Daugas E, Nochy D, Ravagnan L, et al. Apoptosis-inducing factor (AIF): a ubiquitous mitochondrial oxidoreductase involved in apoptosis. FEBS Lett. 2000;476:118–23.
59. Ye H, Cande C, Stephanou NC, et al. DNA binding is required for the apoptogenic action of apoptosis inducing factor. Nat Struct Biol. 2002;9:680–84.
60. Susin SA, Daugas E, Ravagnan L, et al. Two distinct pathways leading to nuclear apoptosis. J Exp Med. 2000;192:571–80.
61. Montague JW, Gaido ML, Frye C, et al. A calcium-dependent nuclease from apoptotic rat thymocytes is homologous with cyclophilin. Recombinant cyclophilins A, B, and C have nuclease activity. J Biol Chem. 1994;269:18877–80.
62. Candé C, Vahsen N, Kouranti I, et al. AIF and cyclophilin A cooperate in apoptosis-associated chromatinolysis. Oncogene. 2004;23:1514–21. Accessed February 5, 2014.
63. Baritaud M, Boujrad H, Lorenzo HK, et al. Histone H2AX: The missing link in AIF-mediated caspase-independent programmed necrosis. Cell Cycle. 2010;9:3166–73.
64. Baritaud M, Cabon L, Delavallée L, et al. AIF-mediated caspase-independent necroptosis requires ATM and DNA-PK-induced histone H2AX Ser139 phosphorylation. Cell Death Dis. 2012;3:e390. Accessed January 27, 2014.
65. Arnoult D, Parone P, Martinou J, et al. Mitochondrial release of apoptosis-inducing factor occurs downstream of cytochrome c release in response to several proapoptotic stimuli. J Cell Biol. 2002;159:923–29.

66. Yu S, Wang H, Poitras MF, et al. Mediation of poly(ADP-ribose) polymerase-1-dependent cell death by apoptosis-inducing factor. Science. 2002;297:259–63.
67. Chiu L, Ho F, Shiah S, et al. Oxidative stress initiates DNA damager MNNG-induced poly (ADP-ribose) polymerase-1-dependent parthanatos cell death. Biochemical pharmacology. 2011;81:459–70.
68. Wang Y, Kim NS, Haince J, et al. Poly (ADP-ribose)(PAR) binding to apoptosis-inducing factor is critical for PAR polymerase-1-dependent cell death (parthanatos). Science signaling. 2011;4:ra20.
69. Polster BM, Basanez G, Etxebarria A, et al. Calpain I induces cleavage and release of apoptosis-inducing factor from isolated mitochondria. J Biol Chem. 2005;280:6447–54.
70. Landshamer S, Hoehn M, Barth N, et al. Bid-induced release of AIF from mitochondria causes immediate neuronal cell death. Cell Death Differ. 2008;15:1553–63.
71. Grohm J, Plesnila N, Culmsee C. Bid mediates fission, membrane permeabilization and peri-nuclear accumulation of mitochondria as a prerequisite for oxidative neuronal cell death. Brain, Behavior, and Immunity. 2010;24:831–38.
72. Tobaben S, Grohm J, Seiler A, et al. Bid-mediated mitochondrial damage is a key mechanism in glutamate-induced oxidative stress and AIF-dependent cell death in immortalized HT-22 hippocampal neurons. Cell Death Differ. 2011;18:282–92.
73. Blomgren K, Zhu C, Hallin U, et al. Mitochondria and ischemic reperfusion damage in the adult and in the developing brain. Biochem Biophys Res Commun. 2003;304:551–59.
74. Slemmer JE, Zhu C, Landshamer S, et al. Causal role of apoptosis-inducing factor for neuronal cell death following traumatic brain injury. Am J Pathol. 2008;173:1795–805.
75. Cheung, Eric C C, Melanson-Drapeau L, Cregan SP, et al. Apoptosis-inducing factor is a key factor in neuronal cell death propagated by BAX-dependent and BAX-independent mechanisms. J Neurosci. 2005;25:1324–34.
76. Plesnila N, Zhu C, Culmsee C, et al. Nuclear translocation of apoptosis-inducing factor after focal cerebral ischemia. J Cereb Blood Flow Metab. 2004;24:458–66.

77. Öxler E, Dolga A, Culmsee C. AIF depletion provides neuroprotection through a preconditioning effect. Apoptosis. 2012;17:1027–38.
78. Zhu C, Wang X, Huang Z, et al. Apoptosis-inducing factor is a major contributor to neuronal loss induced by neonatal cerebral hypoxia-ischemia. Cell Death Differ. 2007;14:775–84.
79. Culmsee C, Zhu C, Landshamer S, et al. Apoptosis-inducing factor triggered by poly(ADP-ribose) polymerase and Bid mediates neuronal cell death after oxygen-glucose deprivation and focal cerebral ischemia. J Neurosci. 2005;25:10262–72.
80. Thal SE, Zhu C, Thal SC, et al. Role of apoptosis inducing factor (AIF) for hippocampal neuronal cell death following global cerebral ischemia in mice. Neurosci Lett. 2011;499:1–3.
81. Hangen E, Blomgren K, Bénit P, et al. Life with or without AIF. Trends in biochemical sciences. 2010;35:278–87.
82. Klein JA, Longo-Guess CM, Rossmann MP, et al. The harlequin mouse mutation downregulates apoptosis-inducing factor. Nature. 2002;419:367–74.
83. Vahsen N, Cande C, Briere J, et al. AIF deficiency compromises oxidative phosphorylation. EMBO J. 2004;23:4679–89.
84. Apostolova N, Cervera AM, Victor VM, et al. Loss of apoptosis-inducing factor leads to an increase in reactive oxygen species, and an impairment of respiration that can be reversed by antioxidants. Cell Death Differ. 2006;13:354–57.
85. Madala PK, Tyndall JDA, Nall T, et al. Update 1 of: Proteases universally recognize beta strands in their active sites. Chemical reviews. 2011;110:PR1-PR31.
86. Stennicke HR, Salvesen GS. Biochemical characteristics of caspases-3,-6,-7, and-8. Journal of Biological Chemistry. 1997;272:25719–23.
87. Wolf BB, Green DR. Suicidal tendencies: apoptotic cell death by caspase family proteinases. Journal of Biological Chemistry. 1999;274:20049–52.
88. Sprick MR, Rieser E, Stahl H, et al. Caspase-10 is recruited to and activated at the native TRAIL and CD95 death-inducing signalling complexes in a FADD-dependent manner but can not functionally substitute caspase-8. The EMBO journal. 2002;21:4520–30.

89. Krueger A, Baumann S, Krammer PH, et al. FLICE-inhibitory proteins: regulators of death receptor-mediated apoptosis. Molecular and cellular biology. 2001;21:8247–54.
90. Boatright KM, Salvesen GS. Mechanisms of caspase activation. Current opinion in cell biology. 2003;15:725–31.
91. Troy CM, Rabacchi SA, Hohl JB, et al. Death in the balance: alternative participation of the caspase-2 and-9 pathways in neuronal death induced by nerve growth factor deprivation. The Journal of Neuroscience. 2001;21:5007–16.
92. Lassus P, Opitz-Araya X, Lazebnik Y. Requirement for caspase-2 in stress-induced apoptosis before mitochondrial permeabilization. Science. 2002;297:1352–54.
93. Lazebnik YA, Kaufmann SH, Desnoyers S, et al. Cleavage of poly (ADP-ribose) polymerase by a proteinase with properties like ICE. 1994.
94. Creagh EM, Martin SJ. Caspases: cellular demolition experts. Biochemical Society Transactions. 2001;29:696–702.
95. Jäättelä M. Programmed cell death: many ways for cells to die decently. Annals of medicine. 2002;34:480–88.
96. Suzuki K, Hata S, Kawabata Y, et al. Structure, activation, and biology of calpain. Diabetes. 2004;53:S12-S18.
97. Battaglia F, Trinchese F, Liu S, et al. Calpain inhibitors, a treatment for Alzheimer's disease. Journal of Molecular Neuroscience. 2003;20:357–62.
98. Ray SK, Hogan EL, Banik NL. Calpain in the pathophysiology of spinal cord injury: neuroprotection with calpain inhibitors. Brain research reviews. 2003;42:169–85.
99. Gao G, Dou QP. N-terminal cleavage of Bax by calpain generates a potent proapoptotic 18-kDa fragment that promotes Bcl-2-independent cytochrome C release and apoptotic cell death. Journal of cellular biochemistry. 2001;80:53–72.
100. Raynaud F, Marcilhac A. Implication of calpain in neuronal apoptosis. Febs Journal. 2006;273:3437–43.
101. Chwieralski CE, Welte T, Bühling F. Cathepsin-regulated apoptosis. Apoptosis. 2006;11:143–49.

102. Turk B, Turk D, Turk V. Lysosomal cysteine proteases: more than scavengers. Biochimica et Biophysica Acta (BBA)-Protein Structure and Molecular Enzymology. 2000;1477:98–111.
103. Stoka V, Turk V, Turk B. Lysosomal cysteine cathepsins: signaling pathways in apoptosis. Biological chemistry. 2007;388:555–60.
104. Zhao M, Brunk UT, Eaton JW. Delayed oxidant-induced cell death involves activation of phospholipase A2. FEBS letters. 2001;509:399–404.
105. Yamashima T, Oikawa S. The role of lysosomal rupture in neuronal death. Progress in neurobiology. 2009;89:343–58.
106. Guicciardi ME, Bronk SF, Werneburg NW, et al. Bid is upstream of lysosome-mediated caspase 2 activation in tumor necrosis factor alpha-induced hepatocyte apoptosis. Gastroenterology. 2005;129:269–84.
107. Stoka V, Turk B, Schendel SL, et al. Lysosomal protease pathways to apoptosis. Cleavage of bid, not pro-caspases, is the most likely route. J Biol Chem. 2001;276:3149–57.
108. Bidere N, Lorenzo HK, Carmona S, et al. Cathepsin D triggers Bax activation, resulting in selective apoptosis-inducing factor (AIF) relocation in T lymphocytes entering the early commitment phase to apoptosis. J Biol Chem. 2003;278:31401–11.
109. Ovaere P, Lippens S, Vandenabeele P, et al. The emerging roles of serine protease cascades in the epidermis. Trends in biochemical sciences. 2009;34:453–63.
110. Hedstrom L. An overview of serine proteases. Curr Protoc Protein Sci. 2002;Chapter 21:Unit 21.10.
111. Turgeon VL, Houenou LJ. The role of thrombin-like (serine) proteases in the development, plasticity and pathology of the nervous system. Brain Res Brain Res Rev. 1997;25:85–95.
112. Williams MS, Henkart PA. Apoptotic cell death induced by intracellular proteolysis. The Journal of Immunology. 1994;153:4247–55.
113. Bleackley RC, Heibein JA. Enzymatic control of apoptosis. Natural product reports. 2001;18:431–40.
114. Neumann H, Medana IM, Bauer J, et al. Cytotoxic T lymphocytes in autoimmune and degenerative CNS diseases. Trends in neurosciences. 2002;25:313–19.

115. Hurn PD, Subramanian S, Parker SM, et al. T- and B-cell-deficient mice with experimental stroke have reduced lesion size and inflammation. J Cereb Blood Flow Metab. 2007;27:1798–805.
116. Troost D, Van den Oord, JJ, Jong J de, et al. Lymphocytic infiltration in the spinal cord of patients with amyotrophic lateral sclerosis. Clinical neuropathology. 1989;8.
117. Trapani JA. Granzymes: a family of lymphocyte granule serine proteases. Genome Biol. 2001;2:3014.1-3014.7.
118. Chaitanya GV, Schwaninger M, Alexander JS, et al. Granzyme-b is involved in mediating post-ischemic neuronal death during focal cerebral ischemia in rat model. Neuroscience. 2010;165:1203–16.
119. Strauss KM, Martins LM, Plun-Favreau H, et al. Loss of function mutations in the gene encoding Omi/HtrA2 in Parkinson's disease. Human molecular genetics. 2005;14:2099–111.
120. Walle LV, Lamkanfi M, Vandenabeele P. The mitochondrial serine protease HtrA2/Omi: an overview. Cell Death & Differentiation. 2008;15:453–60.
121. van Loo G, van Gurp M, Depuydt B, et al. The serine protease Omi/HtrA2 is released from mitochondria during apoptosis. Omi interacts with caspase-inhibitor XIAP and induces enhanced caspase activity. Cell death and differentiation. 2002;9:20–26.
122. Yang Q, Church-Hajduk R, Ren J, et al. Omi/HtrA2 catalytic cleavage of inhibitor of apoptosis (IAP) irreversibly inactivates IAPs and facilitates caspase activity in apoptosis. Genes & Development. 2003;17:1487–96.
123. Blink E, Maianski NA, Alnemri ES, et al. Intramitochondrial serine protease activity of Omi/HtrA2 is required for caspase-independent cell death of human neutrophils. Cell Death & Differentiation. 2004;11:937–39.
124. Althaus J, Siegelin MD, Dehghani F, et al. The serine protease Omi/HtrA2 is involved in XIAP cleavage and in neuronal cell death following focal cerebral ischemia/reperfusion. Neurochemistry international. 2007;50:172–80.
125. Landshamer S. Role of Bid and AIF in Glutamate-induced Neuronal Cell Death; 2007.
126. Su D, Su Z, Wang J, et al. UCF-101, A Novel Omi/HtrA2 Inhibitor, Protects Against Cerebral Ischemia/Reperfusion Injury in Rats. The Anatomical Record. 2009;292:854–61.

127. Zhao K, Zhao X, Tu Y, et al. Lysosomal chymotrypsin B potentiates apoptosis via cleavage of Bid. Cell. Mol. Life Sci. 2010;67:2665–78. Accessed January 27, 2014.
128. Aoshiba K, Yasuda K, Yasui S, et al. Serine proteases increase oxidative stress in lung cells. Am J Physiol Lung Cell Mol Physiol. 2001;281:L556-64.
129. Hara A, Niwa M, Nakashima M, et al. Protective effect of apoptosis-inhibitory agent, N-tosyl-L-phenylalanyl chloromethyl ketone against ischemia-induced hippocampal neuronal damage. J Cereb Blood Flow Metab. 1998;18:819–23.
130. Mitsui C, Sakai K, Ninomiya T, et al. Involvement of TLCK-sensitive serine protease in colchicine-induced cell death of sympathetic neurons in culture. J Neurosci Res. 2001;66:601–11.
131. Gong B, Chen Q, Endlich B, et al. Ionizing radiation-induced, Bax-mediated cell death is dependent on activation of cysteine and serine proteases. Cell Growth Differ. 1999;10:491–502.
132. Available at: http://www.biochemj.org/bj/347/bj3470669.htm. Accessed February 22, 2014.
133. Moffitt KL, Martin SL, Walker B. The emerging role of serine proteases in apoptosis. Biochemical Society Transactions. 2007;35:559–60.
134. Agarwal ML, Taylor WR, Chernov MV, et al. The p53 network. Journal of Biological Chemistry. 1998;273:1–4.
135. Haupt S, Berger M, Goldberg Z, et al. Apoptosis-the p53 network. Journal of Cell Science. 2003;116:4077–85.
136. Renzing J, Hansen S, Lane DP. Oxidative stress is involved in the UV activation of p53. Journal of Cell Science. 1996;109:1105–12.
137. Rideout HJ, Zang E, Yeasmin M, et al. Inhibitors of trypsin-like serine proteases prevent DNA damage-induced neuronal death by acting upstream of the mitochondrial checkpoint and of p53 induction. Neuroscience. 2001;107:339–52.
138. Barbier S, Chatre L, Bras M, et al. Caspase-independent type III programmed cell death in chronic lymphocytic leukemia: the key role of the F-actin cytoskeleton. haematologica. 2009;94:507–17.
139. Göthel SF, Marahiel MA. Peptidyl-prolyl cis-trans isomerases, a superfamily of ubiquitous folding catalysts. Cellular and Molecular Life Sciences CMLS. 1999;55:423–36.

140. Schreiber SL. Chemistry and biology of the immunophilins and their immunosuppressive ligands. Science. 1991;251:283–87.
141. Davis TL, Walker JR, Campagna-Slater V, et al. Structural and biochemical characterization of the human cyclophilin family of peptidyl-prolyl isomerases. PLoS biology. 2010;8:e1000439.
142. Siekierka JJ, Hung SHY, Poe M, et al. A cytosolic binding protein for the immunosuppressant FK506 has peptidyl-prolyl isomerase activity but is distinct from cyclophilin. 1989.
143. Liu J, Farmer Jr, Jesse D, Lane WS, et al. Calcineurin is a common target of cyclophilin-cyclosporin A and FKBP-FK506 complexes. Cell. 1991;66:807–15.
144. Steiner JP, Dawson TM, Fotuhi M, et al. High brain densities of the immunophilin FKBP colocalized with calcineurin. Nature. 1992;358:584–87.
145. Dawson TM, Steiner JP, Dawson VL, et al. Immunosuppressant FK506 enhances phosphorylation of nitric oxide synthase and protects against glutamate neurotoxicity. Proc Natl Acad Sci U S A. 1993;90:9808–12.
146. Ide T, Morikawa E, Kirino T. An immunosuppressant, FK506, protects hippocampal neurons from forebrain ischemia in the mongolian gerbil. Neurosci Lett. 1996;204:157–60.
147. Arii T, Kamiya T, Arii K, et al. Neuroprotective effect of immunosuppressant FK506 in transient focal ischemia in rat: therapeutic time window for FK506 in transient focal ischemia. Neurol Res. 2001;23:755–60.
148. Klettner A, Herdegen T. FK506 and its analogs-therapeutic potential for neurological disorders. Current Drug Targets-CNS & Neurological Disorders. 2003;2:153–62.
149. Lu KP, Liou Y, Zhou XZ. Pinning down proline-directed phosphorylation signaling. Trends in cell biology. 2002;12:164–72.
150. Lippens G, Landrieu I, Smet C. Molecular mechanisms of the phospho-dependent prolyl cis/trans isomerase Pin1. Febs Journal. 2007;274:5211–22.
151. Butterfield DA, Abdul HM, Opii W, et al. REVIEW: Pin1 in Alzheimer's disease. Journal of Neurochemistry. 2006;98:1697–706.
152. Lu KP, Zhou XZ. The prolyl isomerase PIN1: a pivotal new twist in phosphorylation signalling and disease. Nature reviews Molecular cell biology. 2007;8:904–16.

153. Sultana R, Boyd-Kimball D, Poon HF, et al. Oxidative modification and down-regulation of Pin1 in Alzheimer's disease hippocampus: a redox proteomics analysis. Neurobiology of aging. 2006;27:918–25.
154. Putcha GV, Moulder KL, Golden JP, et al. Induction of BIM, a proapoptotic BH3-only BCL-2 family member, is critical for neuronal apoptosis. Neuron. 2001;29:615–28.
155. Becker, Esther B E, Howell J, Kodama Y, et al. Characterization of the c-Jun N-terminal kinase-BimEL signaling pathway in neuronal apoptosis. J Neurosci. 2004;24:8762–70.
156. Becker EBE, Bonni A. Pin1 mediates neural-specific activation of the mitochondrial apoptotic machinery. Neuron. 2006;49:655–62.
157. Wang P, Heitman J. The cyclophilins. Genome biology. 2005;6:226.
158. Galat A. Peptidylprolyl cis/trans isomerases (immunophilins): biological diversity-targets-functions. Current topics in medicinal chemistry. 2003;3:1315–47.
159. Kim J, Choi TG, Ding Y, et al. Overexpressed cyclophilin B suppresses apoptosis associated with ROS and Ca2+ homeostasis after ER stress. Journal of Cell Science. 2008;121:3636–48.
160. Jeong K, Kim H, Kim K, et al. Cyclophilin B is involved in p300-mediated degradation of CHOP in tumor cell adaptation to hypoxia. Cell Death & Differentiation. 2013.
161. Crompton M, Virji S, Ward JM. Cyclophilin-D binds strongly to complexes of the voltage-dependent anion channel and the adenine nucleotide translocase to form the permeability transition pore. Eur J Biochem. 1998;258:729–35.
162. Schinzel AC, Takeuchi O, Huang Z, et al. Cyclophilin D is a component of mitochondrial permeability transition and mediates neuronal cell death after focal cerebral ischemia. Proceedings of the National Academy of Sciences of the United States of America. 2005;102:12005–10.
163. Baum N, Schiene-Fischer C, Frost M, et al. The prolyl cis/trans isomerase cyclophilin 18 interacts with the tumor suppressor p53 and modifies its functions in cell cycle regulation and apoptosis. Oncogene. 2009;28:3915–25.
164. Vousden KH, Lane DP. p53 in health and disease. Nature reviews Molecular cell biology. 2007;8:275–83.

165. Handschumacher RE, Harding MW, Rice J, et al. Cyclophilin: a specific cytosolic binding protein for cyclosporin A. Science. 1984;226:544–47.
166. Göldner FM, Patrick JW. Neuronal localization of the cyclophilin A protein in the adult rat brain. Journal of Comparative Neurology. 1996;372:283–93.
167. Capano M, Virji S, Crompton M. Cyclophilin-A is involved in excitotoxin-induced caspase activation in rat neuronal B50 cells. Biochem. J. 2002;363:29–36.
168. Zhu C, Wang X, Deinum J, et al. Cyclophilin A participates in the nuclear translocation of apoptosis-inducing factor in neurons after cerebral hypoxia-ischemia. The Journal of experimental medicine. 2007;204:1741–48.
169. Tanaka H, Shimazaki H, Kimura M, et al. Apoptosis-Inducing Factor and Cyclophilin A Cotranslocate to the Motor Neuronal Nuclei in Amyotrophic Lateral Sclerosis Model Mice. CNS neuroscience & therapeutics. 2011;17:294–304.
170. Morimoto BH, Koshland, D E Jr. Excitatory amino acid uptake and N-methyl-D-aspartate-mediated secretion in a neural cell line. Proc Natl Acad Sci U S A. 1990;87:3518–21.
171. Murphy TH, Miyamoto M, Sastre A, et al. Glutamate toxicity in a neuronal cell line involves inhibition of cystine transport leading to oxidative stress. Neuron. 1989;2:1547–58.
172. Tan S, Sagara Y, Liu Y, et al. The regulation of reactive oxygen species production during programmed cell death. The Journal of cell biology. 1998;141:1423–32.
173. Grohm J, Kim S, Mamrak U, et al. Inhibition of Drp1 provides neuroprotection in vitro and in vivo. Cell Death Differ. 2012;19:1446–58.
174. Daum S, Erdmann F, Fischer G, et al. Aryl Indanyl Ketones: Efficient Inhibitors of the Human Peptidyl Prolylcis/trans Isomerase Pin1. Angew. Chem. Int. Ed. 2006;45:7454–58. Accessed January 27, 2014.
175. Kazhdan I, Long L, Montellano R, et al. Targeted gene therapy for breast cancer with truncated Bid. Cancer Gene Ther. 2006;13:141–49.
176. Liu Y, Peterson DA, Kimura H, et al. Mechanism of cellular 3-(4,5-dimethylthiazol-2-yl)-2,5-diphenyltetrazolium bromide (MTT) reduction. J Neurochem. 1997;69:581–93.
177. Diemert S, Dolga AM, Tobaben S, et al. Impedance measurement for real time detection of neuronal cell death. J Neurosci Methods. 2012;203:69–77.

178. Walker JM. The bicinchoninic acid (BCA) assay for protein quantitation. Methods Mol Biol. 1994;32:5–8.
179. Chen J, Jin K, Chen M, et al. Early detection of DNA strand breaks in the brain after transient focal ischemia: implications for the role of DNA damage in apoptosis and neuronal cell death. Journal of Neurochemistry. 1997;69:232–45.
180. Kroemer G. The proto-oncogene Bcl-2 and its role in regulating apoptosis. Nature medicine. 1997;3:614–20.
181. Vander Heiden, Matthew G, Chandel NS, Williamson EK, et al. Bcl-x< sub> L Regulates the Membrane Potential and Volume Homeostasis of Mitochondria. Cell. 1997;91:627–37.
182. Green DR, Reed JC. Mitochondria and apoptosis. Science-AAAS-Weekly Paper Edition. 1998;281:1309–11.
183. Fukui M, Song J, Choi J, et al. Mechanism of glutamate-induced neurotoxicity in HT22 mouse hippocampal cells. European journal of pharmacology. 2009;617:1–11.
184. Martinou J, Green DR. Breaking the mitochondrial barrier. Nature reviews Molecular cell biology. 2001;2:63–67.
185. Desagher S, Martinou J. Mitochondria as the central control point of apoptosis. Trends in cell biology. 2000;10:369–77.
186. Karbowski M, Youle RJ. Dynamics of mitochondrial morphology in healthy cells and during apoptosis. Cell Death & Differentiation. 2003;10:870–80.
187. Frank S. Dysregulation of mitochondrial fusion and fission: an emerging concept in neurodegeneration. Acta neuropathologica. 2006;111:93–100.
188. Knott AB, Perkins G, Schwarzenbacher R, et al. Mitochondrial fragmentation in neurodegeneration. Nature Reviews Neuroscience. 2008;9:505–18.
189. Semba S, Huebner K. Protein expression profiling identifies cyclophilin A as a molecular target in Fhit-mediated tumor suppression. Mol Cancer Res. 2006;4:529–38.
190. Becker EBE, Bonni A. Pin1 in neuronal apoptosis. Cell cycle (Georgetown, Tex.). 2007;6:1332.
191. Gohil VM, Sheth SA, Nilsson R, et al. Nutrient-sensitized screening for drugs that shift energy metabolism from mitochondrial respiration to glycolysis. Nat Biotechnol. 2010;28:249–55.

192. Ricci JE, Waterhouse N, Green. Mitochondrial functions during cell death, a complex (IV) dilemma. Cell Death & Differentiation. 2003;10.
193. Rodriguez J, Lazebnik Y. Caspase-9 and APAF-1 form an active holoenzyme. Genes Dev. 1999;13:3179–84.
194. Zou H. An APAF-1 Cytochrome c Multimeric Complex Is a Functional Apoptosome That Activates Procaspase-9. Journal of Biological Chemistry. 1999;274:11549–56.
195. Ferri KF, Kroemer G. Organelle-specific initiation of cell death pathways. Nat Cell Biol. 2001;3:E255-63.
196. Roberg K. Relocalization of cathepsin D and cytochrome c early in apoptosis revealed by immunoelectron microscopy. Lab Invest. 2001;81:149–58.
197. Rousalova I, Krepela E. Granzyme B-induced apoptosis in cancer cells and its regulation (review). Int J Oncol. 2010;37:1361–78.
198. Gorman JJ. Inhibition of human thrombin assessed with different substrates and inhibitors. Characterization of fibrinopeptide binding interaction. Biochim Biophys Acta. 1975;412:273–82.
199. Kupfer A, Gani V, Jimenez JS, et al. Affinity labeling of the catalytic subunit of cyclic AMP-dependent protein kinase by N alpha-tosyl-L-lysine chloromethyl ketone. Proceedings of the National Academy of Sciences. 1979;76:3073–77.
200. Kinzel V, Konig N. Interaction of protease inhibitors with the catalytic subunit of cAMP-dependent protein kinase. Biochem Biophys Res Commun. 1980;93:349–53.
201. Solomon DH, O'Brian CA, Weinstein IB. N-alpha-Tosyl-L-lysine chloromethyl ketone and N-alpha-tosyl-L-phenylalanine chloromethyl ketone inhibit protein kinase C. FEBS Lett. 1985;190:342–44.
202. KOSTKA V, CARPENTER FH. INHIBITION OF CHYMOTRYPSIN ACTIVITY IN CRYSTALLINE TRYPSIN PREPARATIONS. J Biol Chem. 1964;239:1799–803.
203. Barry M, Heibein JA, Pinkoski MJ, et al. Granzyme B short-circuits the need for caspase 8 activity during granule-mediated cytotoxic T-lymphocyte killing by directly cleaving Bid. Mol Cell Biol. 2000;20:3781–94.
204. Takahashi K. Antioxidative action of N-?-tosyl-L-lysine chloromethyl ketone prevents death of glutathione-depleted cardiomyocytes induced by hydrogen peroxide. JBPC. 2010;01:164–71. Accessed January 27, 2014.

205. Heggeness MH, Simon M, Singer SJ. Association of mitochondria with microtubules in cultured cells. Proceedings of the National Academy of Sciences. 1978;75:3863–66.
206. Frank S, Gaume B, Bergmann-Leitner ES, et al. The role of dynamin-related protein 1, a mediator of mitochondrial fission, in apoptosis. Dev Cell. 2001;1:515–25.
207. Asai A, Qiu J, Narita Y, et al. High level calcineurin activity predisposes neuronal cells to apoptosis. Journal of Biological Chemistry. 1999;274:34450–58.
208. Artus C, Boujrad H, Bouharrour A, et al. AIF promotes chromatinolysis and caspase-independent programmed necrosis by interacting with histone H2AX. The EMBO journal. 2010;29:1585–99.
209. Doti N, Reuther C, Scognamiglio PL, et al. Inhibition of the AIF/CypA complex protects against intrinsic death pathways induced by oxidative stress. Cell Death Dis. 2014;5:e993.
210. Wulf G, Ryo A, Liou Y, et al. The prolyl isomerase Pin1 in breast development and cancer. Breast Cancer Research. 2003;5:76–88.
211. Barone MC, Desouza LA, Freeman RS. Pin1 promotes cell death in NGF-dependent neurons through a mechanism requiring c-Jun activity. Journal of Neurochemistry. 2008;106:734–45.
212. Lu P, Zhou XZ, Liou Y, et al. Critical role of WW domain phosphorylation in regulating phosphoserine binding activity and Pin1 function. Journal of Biological Chemistry. 2002;277:2381–84.
213. Youle RJ, Van Der Bliek, Alexander M. Mitochondrial fission, fusion, and stress. Science. 2012;337:1062–65.
214. Chan DC. Fusion and fission: interlinked processes critical for mitochondrial health. Annu Rev Genet. 2012;46:265–87.
215. Leist M, Jäättelä M. Triggering of apoptosis by cathepsins. Cell death and differentiation. 2001;8:324–26.
216. Abraham MC, Shaham S. Death without caspases, caspases without death. Trends Cell Biol. 2004;14:184–93.
217. Guicciardi ME, Leist M, Gores GJ. Lysosomes in cell death. Oncogene. 2004;23:2881–90.

218. Miao Q, Sun Y, Wei T, et al. Chymotrypsin B Cached in Rat Liver Lysosomes and Involved in Apoptotic Regulation through a Mitochondrial Pathway. Journal of Biological Chemistry. 2008;283:8218–28. Accessed January 27, 2014.
219. Ding X, Patel M, Shen D, et al. Enhanced HtrA2/Omi Expression in Oxidative Injury to Retinal Pigment Epithelial Cells and Murine Models of Neurodegeneration. Investigative Ophthalmology & Visual Science. 2009;50:4957–66.
220. Egger L, Schneider J, Rheme C, et al. Serine proteases mediate apoptosis-like cell death and phagocytosis under caspase-inhibiting conditions. Cell Death & Differentiation. 2003;10:1188–203.
221. Hu Y, Huang M, Wang P, et al. Ucf-101 protects against cerebral oxidative injury and cognitive impairment in septic rat. International Immunopharmacology. 2013;16:108–13.
222. Martins LM, Morrison A, Klupsch K, et al. Neuroprotective role of the Reaper-related serine protease HtrA2/Omi revealed by targeted deletion in mice. Molecular and cellular biology. 2004;24:9848–62.
223. Movsesyan VA, Yakovlev AG, Fan L, et al. Effect of Serine Protease Inhibitors on Posttraumatic Brain Injury and Neuronal Apoptosis. Experimental Neurology. 2001;167:366–75. Accessed January 27, 2014.
224. Saldeen J, Welsh N. Interleukin-1β Induced Activation of NF-κB in Insulin-Producing RINm5F Cells Is Prevented by the Protease Inhibitor Nα-< i> p-Tosyl-L-Lysine Chloromethylketone. Biochemical and Biophysical Research Communications. 1994;203:149–55.
225. Kim H, Lee HS, Chang KT, et al. Chloromethyl ketones block induction of nitric oxide synthase in murine macrophages by preventing activation of nuclear factor-kappa B. J Immunol. 1995;154:4741–48.
226. Zhou Q, Salvesen G. Activation of pro-caspase-7 by serine proteases includes a non-canonical specificity. Biochem. J. 1997;324:361–64.
227. Frydrych I, Mlejnek P. Serine protease inhibitors N-alpha-tosyl-L-lysinyl-chloromethylketone (TLCK) and N-tosyl-L-phenylalaninyl-chloromethylketone (TPCK) are potent inhibitors of activated caspase proteases. J Cell Biochem. 2008;103:1646–56.

228. Anesti V, Scorrano L. The relationship between mitochondrial shape and function and the cytoskeleton. Biochimica et Biophysica Acta (BBA)-Bioenergetics. 2006;1757:692–99.
229. Li J, Li Q, Xie C, et al. β-actin is required for mitochondria clustering and ROS generation in TNF-induced, caspase-independent cell death. Journal of Cell Science. 2004;117:4673–80.
230. Diemert S. The role of p53 and CYLD in mitochondrial death pathways and mechanisms of neuronal necroptosis; 2011

9. Publications

9.1. Original papers

C Reuther, GK Ganjam, AM Dolga and C Culmsee, Serine proteases mediate intrinsic death pathways in neurons upstream of mitochondrial demise, Apoptosis, submitted

S Diemert, GK Ganjam, **C Reuther**, N Plesnila, C Culmsee, CYLD mediates necroptotic cell death induced by oxidative stress, Apoptosis, 2013, in revision

N Doti, **C Reuther**, PL Scognamiglio, AM Dolga, N Plesnila, M Ruvo and C Culmsee, Inhibition of the AIF/CypA complex protects against intrinsic death pathways induced by oxidative stress, Cell Death and Disease, 2014

9.2. Poster presentations

2013

C Reuther, N Doti, M Ruvo, N Plesnila and C Culmsee, The role of Cyclophilin A in neuronal cell death and mitochondrial damage, 21st Euroconference on Apoptosis of the European Cell Death Organization (ECDO), Paris, France, 25.09.2014-28.09.2014

2012

C Reuther, S Oppermann, EM Öxler, AM Dolga and C Culmsee, Schädigungsmechanismen in Mitochondrien als neue therapeutische Ansatzpunkte der Neuroprotektion, Infotag der Pharmazie, Philipps-Universität Marburg, 24.02.2012

C Reuther, N Doti, M Ruvo, N Plesnila and C Culmsee, Cyclophilin A siRNA provides mitoprotection and prevents AIF-dependent neuronal cell death, ID: 682, Jahrestagung der Deutschen Gesellschaft für Experimentelle und Klinische Pharmakologie und Toxikologie (DGPT) Dresden, Germany, 19.03.2012-22.03.2012

C Reuther, N Doti, M Ruvo, N Plesnila and C Culmsee, Cyclophilin A plays a crucial role in mitochondrial damage and glutamate-induced cell death in HT22 neurons, 7th international Symposium on Neuroprotection and Neurorepair, Potsdam, Germany, 02.05.2012-05.05.2012

2011

N Doti, **C Reuther**, PL Scognamiglio, AM Dolga, N Plesnila, M Ruvo and C Culmsee, Peptide-mediated inhibition of AIF/CypA interaction: a new strategy for neuroprotection, N.: 367.23/II6, Society for Neuroscience Annual Meeting, Neuroscience 2011, Washington, USA, 12.11.2011-16.11.2011

9.3. Oral presentations

C Reuther, Cyclophilin A and serine proteases – Neuroprotective targets upstream of mitochondria, talk at the Institute of Stroke and Dementia Research (ISD), Ludwig-Maximilians Universität München (LMU), N. Plesnila, Munich, Germany, 17.02.2014

10. Acknowledgements

Die Danksagung enthält persönliche Angaben und ist nicht Bestandteil der elektronischen Ausgabe.

11. Danksagung

Die Danksagung enthält persönliche Angaben und ist nicht Bestandteil der elektronischen Ausgabe.

12. Curriculum vitae

CV enthält persönliche Angaben und ist nicht Bestandteil der elektronischen Ausgabe.